University of Alberta

Modeling Light for Regeneration Planning in Mixed-Species Boreal Forests

by

Kenneth John Stadt ©

A thesis submitted to the Faculty of Graduate Studies and Research in partial fulfillment of the requirements for the degree of Doctor of Philosophy

in

Forest Biology and Management

Department of Renewable Resources

Edmonton, Alberta

Fall 2002

National Library of Canada
Acquisitions and Bibliographic Services
395 Wellington Street
Ottawa ON K1A 0N4
Canada

Bibliothèque nationale du Canada
Acquisitions et services bibliographiques
395, rue Wellington
Ottawa ON K1A 0N4
Canada

Your file Votre référence

Our file Notre référence

The author has granted a non-exclusive licence allowing the National Library of Canada to reproduce, loan, distribute or sell copies of this thesis in microform, paper or electronic formats.

L'auteur a accordé une licence non exclusive permettant à la Bibliothèque nationale du Canada de reproduire, prêter, distribuer ou vendre des copies de cette thèse sous la forme de microfiche/film, de reproduction sur papier ou sur format électronique.

The author retains ownership of the copyright in this thesis. Neither the thesis nor substantial extracts from it may be printed or otherwise reproduced without the author's permission.

L'auteur conserve la propriété du droit d'auteur qui protège cette thèse. Ni la thèse ni des extraits substantiels de celle-ci ne doivent être imprimés ou autrement reproduits sans son autorisation.

0-612-81269-3

Canada

University of Alberta

Library Release Form

Name of Author: Kenneth John Stadt

Title of Thesis: Modeling Light for Regeneration Planning in Mixed-Species Boreal Forests

Degree: Doctor of Philosophy

Year this Degree Granted: 2002

Permission is hereby granted to the University of Alberta Library to reproduce single copies of this thesis and to lend or sell such copies for private, scholarly or scientific research purposes only.

The author reserves all other publication and other rights in association with the copyright in the thesis, and except as herein before provided, neither the thesis nor any substantial portion thereof may be printed or otherwise reproduced in any material form whatever without the author's prior written permission.

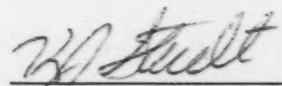

#3, 9311 – 87 Avenue,
Edmonton, Alberta
T6C 1K3

October 1, 2002

University of Alberta

Faculty of Graduate Studies and Research

The undersigned certify that they have read, and recommend to the Faculty of Graduate Studies and Research for acceptance, a thesis entitled "Modeling Light for Regeneration Planning in Mixed-Species Boreal Forests" submitted by Kenneth John Stadt in partial fulfillment of the requirements for the degree of Doctor of Philosophy in Forest Biology and Management.

Dr. Victor J. Lieffers

Dr. Ronald J. Hall

Dr. Stephen J. Titus

Dr. G. Peter Kershaw

Dr. Y. Feng

Dr. Jing M. Chen

October 1, 2002

Dedication

To my mother who taught me the names of the trees, my father who taught me their value, and my wife who enjoys the forest with me.

Abstract

Resource based models of forest regeneration offer a promising alternative to competition index-based approaches. Since light is frequently the key resource for regenerating trees, the focus of this thesis was to develop and test models for predicting light conditions beneath mixed species boreal forest canopies.

A two-scale model for the transmission of photosynthetically active radiation (PAR) through overstory trees was developed using a ray-tracing approach. For microsite predictions, trees were represented as geometric shapes containing leaf area properties typical of the species. For stand predictions, leaf area was distributed across the stand volume. Point penetration theory was applied to calculate the PAR transmission along each ray as it passed through the stand volume or through individual crowns. The rays were weighted by the diffuse and direct radiance of the sky region they originated, and summed to give the overall transmission. This model was validated at the stand level using instantaneous PAR transmission data measured in 17 stands.

The additional effect of understory vegetation on PAR transmission was modeled using a series of empirical and physical models based on leaf area and cover data. The empirical models were most effective; however the physical models also provided reasonable predictions when the effects of leaf inclination, clumping, transmissivity and reflectivity were included.

Combined overstory and cover-based understory models predicted daily and seasonal PAR transmission to 75 microsites in two large, stem-mapped stands, one in eastern Canada and one in the west. In addition, height growth of understory trees in these stands was correlated to seasonal transmission.

Tree morphology changes in response to shifts in light quality, particularly in the red (660 nm) and far-red (730 nm) wavelengths, so a model for predicting the red:far-red ratio was also tested. This model was effective, but only when transmissivity and reflectivity were estimated at the crown rather than the leaf level, due to the high density of opaque wood area within the crowns of spruce trees.

The effectiveness of these light quantity and quality models demonstrate that a light resource approach should be effective for modeling mixed species growth dynamics in the boreal forest.

Acknowledgement

Many people assisted on this project. I'd particularly like to thank my supervisor, Dr. Victor Lieffers, for his support, encouragement, occasional forbearance, and his infectious enthusiasm for forest biology. Dr. Ronald Hall helped me through the very difficult mapping stage of this work with considerable finesse. Dr. Christian Messier hosted my visit to Quebec and provided sites, field assistants, technical information and new ideas on boreal forest succession. Rick Hurdle gave me invaluable assistance in developing the instrumentation used in this project. Brigitte Grover and Alberta-Pacific Forest Industries supported this project, particularly the validation site selection and mapping. Darin Leadley of Weyerhauser Canada Drayton Valley Division and Kent Macdonald of Foothills Model Forest were helpful in selecting sites for calibrating the models. My wife, Sandra Stone, heard out my ideas with thoughtful patience and assisted in the field numerous times. Dr. Glen VanBrummelen helped me get started in the mathematics. Other able assistance was provided by Susan Hayduk, David Kelsberg, Brad Pinno, Sarah Lieffers, Ben Seaman, Paula Bartemucci, Wei Liu, Nicolette Kircher, Carolyn Huston, and Fidji Gendron. Thanks also to Dr. Stephen Titus, Dr. Peter Kershaw, Dr. Simon Landhausser, Dr. Uldis Silins, Dr. Philip Comeau, and my fellow students in Renewable Resources for their input, support and sense of humour.

The research was supported by grants from Manning Diversified Research Trust Fund, the Sustainable Forest Management Network of Centres of Excellence, and Alberta-Pacific Forest Industries. Integrated Mapping Technologies (Vancouver, B.C.) provided substantial in-kind support for the aerial photo mapping. I am grateful for personal support from a Natural Sciences and Engineering Research Council Postgraduate Scholarship, a University of Alberta Dissertation Fellowship, a Desmond I. Crossley Memorial Scholarship, the Andrew Stewart Memorial Graduate Prize, and a Margaret Brown Award in Environmental Studies and Wildlife Resources.

Table of Contents

Chapter 1. General Introduction 1

Radiation Terminology 2

Modeling Background 3

An Overview of Light Modeling Approaches 4

Linking Light Availability and Tree Growth 12

Thesis Overview 13

Literature Cited 14

Chapter 2. MIXLIGHT: A Flexible Light Transmission Model for Mixed-Species Stands 21

Introduction 21

Methods 24

Overview 24

Study area 26

Model Calibration 27

The MIXLIGHT Model 31

Stand Level Validation 35

Model Sensitivity and Foliage Inclination 36

Results 37

Calibration 37

Validation 38

Model Sensitivity and Foliage Inclination 39

Discussion 39

Literature Cited 44

Appendix 2A. Analytical Solutions for Determining the Intersection Points of a Ray with Regular Three-Dimensional Geometric Objects 54

Light ray equation 54

Crown and stem shape equations and intersections with light rays 54

Chapter 3. A Comparison of Light Modeling Approaches Applied to Understory Vegetation in Boreal Forests of Western North America 57

Introduction 57

Methods 59

Light and Foliage Measurements 59

Light Prediction Models and Analysis 61

Height Profiles 70

Summary and Model Evaluation 70

Results 72
Light and Foliage Measurements 72

Light Prediction Models 74

Discussion 75

Literature Cited 81

Chapter 4. Spatial modeling of light transmission and growth of *Picea glauca* and *Abies balsamea* in boreal forests of Alberta and Quebec 94

Introduction 94

Methods 96
Site Information and Stem Mapping 96

Light measurements 98

Light Transmission Modeling 100

Tree Growth Measurements 102

Statistical Analysis 102

Results 102
Partitioning of Total PPFD to Direct and Diffuse PPFD 102

Light Predictions 103

Tree Height Growth 103

Discussion 104
Light Simulations 104

Tree Growth 106

Conclusions 107

Literature Cited 109

Appendix 4A. Tree Crown Mapping with Large Scale Digital Stereo Aerial Photography 115

Chapter 5. Modeling Light Quality in Boreal Forest Stands 119

Introduction 119

Methods 120
Physical Models 120

Leaf Data 125

Field Sites 128

Light Measurements 129

Results and Discussion 130

Literature Cited 134

Chapter 6. General Discussion 140

Literature Cited 143

Appendix 6A: An Overview of the MIXLIGHT Forest Light Simulator 145

List of Tables

Table 2-1. Calibration trees' stem and crown parameters.....48

Table 3-1. Foliage measurements and parameters for western North American boreal understory species..85

Table 3-2. Theoretical light transmission models, parameters, and fit statistics for understory vegetation. .86

Table 3-3. Empirical light transmission models, parameters, and fit statistics for understory vegetation. ...87

Table 5-1. Leaf level and crown level reflectivity (ρ) and transmissivity (τ) data for boreal forest species at red (660 nm) and far red (730 nm) wavelengths.....136

List of Figures

Figure 1-1. Pictorial representation of the light transmission models.....20

Figure 2-1. Overview of MIXLIGHT's ray tracing approach to light modeling.....49

Figure 2-2. Calibration of foliage area density and foliage inclination parameters in the shadow of individual trees.....50

Figure 2-3. MIXLIGHT stand-level validation for 17 sites measured and modeled under various weather conditions and seasons.....51

Figure 2-4. Sensitivity analysis of the foliage area density, foliage inclination, crown radius and crown length parameters of MIXLIGHT for three stands.....52

Figure 2-5. MIXLIGHT stand-level validation with the foliage inclination parameter (χ) set to 1 for all species.....53

Figure 3-1. The angular distribution of light above the understory.....88

Figure 3-2. Comparison of visual percent cover estimates with the percentage of vertical pins which contacted vegetation.....89

Figure 3-3. Ground-level light transmission (fraction of above-understory light) as a function of (A) percent cover, (B) projected leaf area index (PLAI) and (C) leaf area index (LAI) for weeded calibration plots of nine common species of the western boreal forest.....90

Figure 3-4. Predicted light transmission (fraction of above-understory light) at ground-level *vs.* transmission measurements in undisturbed validation plots.....91

Figure 3-5. Vertical distribution of relative understory PLAI (PLAI above the current height / total ground-level PLAI) with relative height (measurement height / species' top height) for the nine understory species.....92

Figure 3-6. Light transmission fraction predicted using the point-frame estimate of total PLAI, vertical foliage area distribution functions for each species and average species' top heights, *vs.* measured light transmission.....93

Figure 4-1. Hourly diffuse fraction of total PPFD at Calling Lake, Alberta vs. the clearness index.....111

Figure 4-2. Simulated seasonal vs. measured PPFD transmission from June 27 to July 28 and August 22 to September 15, 2000 at five microsites at Calling Lake, Alberta.....112

Figure 4-3. Simulated vs. measured daily PPFD transmission.....113

Figure 4-4. Annual leader growth (g) as a function of predicted seasonal light transmission and tree height (H).....114

Figure 4A-1. Comparison of stereo digital aerial photographs and ground measurements for A) tree height, and B) crown radius, for △white spruce, and O trembling aspen.....118

Figure 5-1. A recently dead white spruce crown that has shed its needles next to two healthy crowns.....137

Figure 5-2. Outside canopy R:FR ratio vs. solar zenith angle and the diffuse fraction of total PPFD.....138

Figure 5-3. Predicted vs. measured R:FR ratio at 40 microsites in an aspen – black spruce – balsam fir – mountain maple stand on Lac Duparquet, Quebec, and 11 microsites in an aspen – white spruce transition site near Calling Lake, Alberta.....139

Chapter 1. General Introduction[1]

New paradigms of forest management in the boreal mixedwoods of Canada are emerging with the increased industrial utilization of hardwood species. Rather than regenerate conifer forests after conifer stands are cut, and hardwood forests after cutting hardwood, a "semi-natural" scheme has been proposed where the natural succession pattern of shade tolerant conifers developing beneath an early successional hardwood canopy is recognized as a method of increasing forest productivity and reducing the cost of regeneration (Lieffers and Beck 1994).

It is rare that pure, late successional conifer stands develop immediately following a disturbance such as fire or harvest. More frequently, fast–growing species such as trembling aspen (*Populus tremuloides*) dominate the site initially, leaving slower-growing spruce or fir in the understory. These understory trees may have established at the same time as the overstory, or establishment may be delayed or prolonged, depending on seed supply and the presence of suitable substrate (Lieffers et al. 1996). In western trembling aspen – white spruce (*Picea glauca*) mixedwoods, the aspen canopy begins to open after about 90 years and the spruce emerge into the canopy. In eastern mixedwoods, the success of balsam fir (*Abies balsamea*) is additionally regulated by periodic outbreaks of spruce budworm, which selectively removes canopy firs (Kneeshaw and Bergeron 1999).

There are a considerable number of management options for implementing such a "semi-natural" paradigm. Under-planting and understory scarification, followed by stand-tending or harvesting with understory protection, are some early to mid rotation options for establishing conifers. Shelterwood harvesting offers a late rotation alternative for conifer establishment, particularly for suppressing competing vegetation (Lieffers and Stadt 1994).

---

[1] Much of the "Overview of Light Modeling" section of this chapter has been published in the "Models for Prediction of Light in Stands" section of Lieffers, V.J., C.M. Messier, K.J. Stadt, F. Gendron, and P. Comeau. 1999. Predicting and managing light in the understory of boreal forests. Canadian Journal of Forest Research 29: 796-811.

The timing of management interventions and harvest designs should be based on the autecological characteristics of the trees and the manager's ability to alter the understory environment. The critical factor in the survival and growth of understory conifers has been shown to be light, specifically photosynthetically active radiation (PAR) (Klinka et al. 1992, Comeau et al. 1993, Lieffers and Stadt 1994). White spruce, for example, grows poorly in the deep shade cast beneath dense spruce canopy trees and responds positively to increasing understory light up to the levels encountered under older aspen canopies, (Lieffers and Stadt 1994). The survival and rate of spruce accession into the overstory canopy can thus be controlled by manipulation of the overstory through partial cutting. Scarification or planting can also be timed to take advantage of windows of increased light during the development of the mixedwood canopy (Lieffers et al. 1999).

Another emerging factor in forest dynamics is the effect of the quality of light on plant development. Gilbert et al. (2001) and others (e.g. Morgan et al. 1983) have shown marked effects of different red: far red photon flux density (R:FR) ratios on the rate of height growth of trees, even when the total PAR remains similar. The pigment phytochrome mediates this response, as well as numerous other light-sensitive plant processes (Smith 2001). Other light quality effects are related to the amount of blue light (Combes et al. 2000). Light quality can be regulated by changing the density and species composition of the surrounding trees.

Radiation Terminology

There is still some confusion in the literature about radiation nomenclature. Pearcy's (1989) recommendations were followed here. "Radiation" is used as a general term for electromagnetic radiation. "Light" was used colloquially, usually referring to photosynthetically active radiation (PAR) of the 400-700 nm waveband, but occasionally including far red "light" at 730 nm as well. Radiation and PAR can refer to either the flux density of energy ($J\ m^{-2}\ s^{-1} = W\ m^{-2}$) or quanta ($\mu mol\ m^{-2}\ s^{-1}$). Where the distinction was important, "irradiance" (I) was used for energy, and "photon flux density" (PFD) for quanta. Photosynthetic photon flux density (PPFD) is thus different in units, though not in waveband, from photosynthetic irradiance (PI). "Shortwave irradiance" (S) is used in

the sky radiation partitioning models for direct-beam vs. diffuse light, and refers to radiation from 300-1000 nm, measured in energy units. "Radiance" is the incoming radiant flux density per unit solid angle. "Relative quantum radiance" is my own term for the normalized angular distribution of radiance measured in quantum units ($\mu mol\ m^{-2}\ s^{-1}$ $steradian^{-1}$) before normalization (after which it is unit-less). "Near-infrared radiation" (NIR) refers to the 700-1300 nm waveband. It should be noted that the light simulation models described here that assume that the leaves are opaque (*i.e.* optically black) or with fixed transmissivity and reflectivity would function identically for energy or quantum units since they allow for no spectral shift.

Modeling Background

Many models of boreal forest dynamics have taken a direct empirical approach, relating growth and mortality to competition indices, chiefly the basal area of competitors (*e.g.* Huang and Titus 1999). Resource-based models represent an alternative approach. In these, the driving variables are levels of critical resources rather than competition indices. In a sense the resource levels are an ideal competition index.

There is a tremendous variety of resource based models with various time steps and degrees of physical and physiological detail. This review focuses on forest management oriented models which function primarily with annual or longer time steps. Kimmins et al. (1990) developed a series of non-spatial resource models (FORECAST/FORCEE), which track nitrogen and phosphorous levels and PAR availability for coastal forests. The spatial model, SORTIE, tracks the PAR resource and has been applied in New England hardwood forests (Pacala et al.1993) and northern British Columbia interior forests (Canham et al. 1999, Kobe et al. 1997, Wright et al. 1998). Korol et al. (1995) adapted the ecosystem process model FOREST-BGC (Running and Coughlan 1988) to model the growth of Douglas-fir at different densities. Bartelink (2000) developed a light driven forest growth model for mixed Douglas-fir - beech forests in the Netherlands. Kull and Tulva (2000) applied a light driven model to European aspen (*Populus tremula*) plantations in Estonia. A model of forest dynamics for the Canadian boreal forest, in which competition is primarily light-driven, is currently under development. One of the

objectives of this dissertation was to provide light prediction data and approaches for this larger boreal project.

Resource-based modeling has a number of advantages over competition index-based approaches. Chief among these is that resource modeling makes competition mechanisms explicit. Competition indexes approximate the effects of competition on growth by careful mathematical formulation. Tracking the resources that plants actually compete for, on the other hand, gives measurable state variables besides yield or survival, and makes it simpler to test hypotheses about the mechanisms of forest development. Another advantage is that the models are unaffected by the choice of management system. If the resource tracking is done well, the response to any range of silvicultural systems, from clearcut and plant to single-tree selection, can be modeled.

The obvious disadvantage of resource-based models is their complexity. Natural systems can be extremely complex, and no model can track all the resources and interactions. Typically one or two resources that are key to the system are modeled. These simplifications make the model less flexible. For example, white spruce growth in boreal mixedwood stands appears to be strongly dependent on light. However, some conditions which increase light, such as creating gaps, also increase the likelihood of frost damage (Groot and Carlson 1996). Thus, resource based models may be subject to restrictions on their use to some degree as well. Data requirements are another issue. Some models require extensive calibration and may need extremely detailed information on tree architecture to operate, or for their initial validation. However, the initial effort required to set up a resource-based model may not be that much greater than what is needed to maintain the network of permanent sample plots necessary for calibrating competition index models.

An Overview of Light Modeling Approaches

Approaches to modeling light beneath forest canopies attempt to link measurements of canopy density and structure to a light transmission probability for each microsite or

canopy position. The simplest and most widely used approach in agricultural and forestry applications is the Beer-Lambert Law. Its original form is

[1-1] $I/I_o = e^{-a\,b\,c}$

where I is the PAR measure at the detector, I_o is the light incident on the absorbing region (I/I_o is the fractional transmission), a is the absorptivity of the objects in the region (dimensionless), b is the path length of the beam through the absorbing region (e.g. in m), and c is a measure of the 'concentration' of the objects (for trees this could be leaf or wood area density, *LAD*, *WAD* in $m^2\ m^{-3}$). The product $a\ b\ c$ is the absorbance for the region (Swinehart 1962). In ecological applications, some of these absorption parameters are often combined. Key assumptions of the Beer-Lambert Law are that the objects in the absorbing region are randomly distributed in vertical and horizontal space and that the light rays are parallel. Given the same assumptions, Oker-Blom (1986) demonstrated that the Beer-Lambert Law can be derived from a Poisson process.

The Beer-Lambert Law is applied at various scales depending on the information available. The simplest models treat the entire canopy as the light-absorbing region (Figure 1-1a) with an extinction coefficient, k, derived from a calibration of light vs. leaf area index (*LAI*, m^2m^{-2}), i.e.

[1-2] $I/I_o = e^{-k\,LAI}$

Note that Equation 1-2 embeds the light path length (b). Here c = *LAD* = *LAI*/canopy height, and canopy height = $b \cos Z$, where Z is the light source angle from vertical (zenith). Since k is the absorptivity corrected for its projection on a horizontal plane, i.e. $k=a/\cos Z$, Equation 1-2 is consistent with Equation 1-1. This application of the Beer-Lambert Law was introduced by Monsi and Saeki (1953) and has been widely used. In forestry, its most frequent application is to estimate *LAI*, rather than predict light (Pierce and Running 1988, Dufrêne and Bréda 1995), but the inverse can also be effective. Using an independent estimate of *LAI*, Pierce and Running (1988), for example, found that Equation 1-2 accurately predicted light transmission in seven conifer stands at two solar angles ($r^2 \geq 0.94$).

Because Equation 1-2 is relatively simple, an extinction coefficient may be required for each stand type. Jarvis and Leverenz (1983) report a range of values of k from 0.28 to 0.65, determined empirically by inversion of Equation 1-2 for pure stands of various species. However, the extinction coefficient is known to be affected by the angle of incident light and the leaf angle distribution of the foliage (Campbell 1986, Lang 1987, Black et al. 1991, Equation 1-5 below) making it difficult to generalize k for other solar angles and species mixtures. LAI must also be determined, either directly, which is time consuming, or by estimation from relationships between leaf area and sapwood area, which must be established first (Waring and Schlesinger 1985). Most forests are mixtures of species and therefore k and LAI should be determined for each species and combined additively in the model (Equation 1-3) (Cannell and Grace 1993).

[1-3] $$I/I_o = e^{-\sum_{species} k_{species} LAI_{species}}$$

Further, equations 1-2 and 1-3 are strictly valid only if the effects of boles, branches and beam enrichment are ignored, the leaves are randomly positioned in space, and either the leaves are horizontal (i.e. not inclined) or the light originates from one direction (Oker-Blom 1986). Bole and branch wood plays a significant role in light attenuation (Cermák 1989, Chen 1996), but can be accounted for by basing the extinction coefficient on plant area index (PAI = LAI + wood area index, WAI) or adding WAI as another term in the model (cf. Equation 1-3). WAI can be measured directly (Sampson and Smith 1993) or estimated by light-interception techniques (Dufrêne and Bréda 1995), although for light predictions the latter results in a somewhat circular process. To account for non-random leaf distribution and leaf inclination requires more effort (see below). The parallel light assumption can be met instead by limiting predictions to clear days when the sun acts as an approximate point source of most of the incident light, or by treating the sun and sky as many small sources of light and integrating transmission along numerous paths.

Sampson and Smith (1993) suggested a model that reflected the change in the extinction coefficient, k with the solar zenith angle (Z, Figure 1-1b):

[1-4] $$I/I_o = e^{-G/\cos Z \cdot LAI}$$

where

[1-5] $$G = a = k \cos Z$$

This formulation extends direct sunlight transmission predictions to all solar angles for predictions at any time of day or season. However, these authors found that G was not independent of LAI in 19 lodgepole pine stands, and thus Equation 1-4 predicted light transmission poorly.

A further refinement is to define the absorptivity, a, as a separately measurable foliage projection parameter, conventionally symbolized as G (Nilson 1971). G and k are interconvertible using Equation 1-5, and recent studies use either. If the foliage area is inclined according to some distribution and the shadow of this distribution is projected onto a surface perpendicular to the direction of the light source, G is the ratio of the shadow area to the upper surface area of the distribution (Campbell 1986, Oker-Blom 1986). A random azimuth orientation is usually assumed, so that only the inclination from horizontal needs to be considered. Values of G for known distributions are given by Nilson (1971), Campbell (1986) and Oker-Blom (1986), and usually vary with the zenith angle of the light source. When G is ignored, a spherical distribution is implicitly applied, which has a constant G value of 0.5 for all source directions. The highly flexible beta distribution (Goel and Strebel 1984) has also been used to model forest foliage inclination (Wang and Jarvis 1990), but requires numerical techniques to approximate G. Of course leaf angle is nearly impossible to measure directly on trees, but Norman and Campbell (1989) have developed an iterative inversion process which can parameterize k and LAI (or G and LAD, with appropriate modifications) given a number of measurements of direct sunlight transmission taken at different solar angles.

To extend light predictions to cloudy days or over long periods, the Beer-Lambert Law can be applied to the probability of transmitting a single beam of diffuse light through the canopy from each region of the sky (Equation 1-6, Figure 1-1c, d, e):

[1-6] $$i = i_o(Z, \alpha) \cdot \cos Z \cdot e^{-G(Z) \cdot b \cdot LAD}$$

where i is the light reaching a horizontal plane at the measurement point, i_o is the light originating from the sky at a given zenith (Z) and azimuth (α), the cosine of the zenith corrects i_o to light relative to the horizontal, G again is a function of the leaf inclination distribution and the zenith (cf. Oker-Blom 1986), and b and LAD are as above. Equation

1-6 is integrated numerically over the upper hemisphere. Complex functions of the distribution of diffuse sky brightness (i_o) with zenith and azimuth are available (Oker-Blom 1986), but the degree of cloudiness makes the actual distribution uncertain, so it is often assumed that all areas of sky are equally bright (Canham et al. 1994, Ter Mikaelian et al. 1997). Several studies (Canham et al. 1994, Ter Mikaelian et al. 1997) have developed a "seasonal sky" which has sectors whose brightness or radiance is the product of the time the solar track passes through the sector, the direct beam radiation flux when the sun is at that zenith, and the proportion of sunlit (vs. cloudy) hours per day. Diffuse light could also be incorporated into the i_o values for these sectors, so that integration of Equation 1-6 over these sectors would give the total seasonal light.

The effects of non-random distribution of foliage horizontally and vertically within the canopy has been addressed by a number of simulation studies (Sampson and Smith 1993, Larsen and Kershaw 1996) and found to be the next most important factor after *LAI* in predicting light transmission. An attempt to include between-crown gaps in a Beer-Lambert Law model was not fruitful (Sampson and Smith 1993). Positive and negative binomial distributions or Markov models (Nilson 1971, Sinclair and Knoerr 1982, Oker-Blom 1986) have been suggested as alternatives to the Beer-Lambert Law for nonrandom foliage distributions, but estimating these models' parameters is not straightforward. Wang and Jarvis (1990), Pukkala et al. (1993), Canham et al. (1994, 1999), Cescatti (1997), and Bartelink (1998) took another approach, and used spatially-mapped tree crowns, modeled as cylinders or ellipsoids, as multiple light-absorbing regions (Figure 1-1d). Other workers have divided the canopy into small volumes or voxels and assigned the leaf area from the nearest tree to each voxel (Comeau et al. 1998, Brunner 1998, Combes et al. 2000, Sinoquet et al. 2001, Figure 1-1d). Both the geometric and the voxel approach account for gaps and the horizontal aggregation of foliage into crowns, allowing some degree of spatial prediction.

In these models, light transmission depends on the sum of the path lengths within the crowns through which light beams pass on their way from the sky to the measurement point. Pukkala's pure Scots pine model used allometrically-determined projected leaf

area density (*pLAD* = the projected leaf area per tree divided by crown volume), equivalent to $G \times LAD$, to convert within crown length (b) into absorption (Equation 1-7):

[1-7] $$i = i_o(Z,\alpha) \cdot \cos Z \cdot e^{-\sum_{species}\sum_{tree} pLAD_{species,tree} \cdot b_{species,tree}}$$

(Pukkala et al. (1993) multiplied transmission values rather than added absorbances; these are equivalent). The absolute path length variant of Canham et al.'s (1994) mixedwood model also combines foliage projection and *LAD* into species-specific extinction coefficients equivalent to projected leaf area density (*pLAD*), except these were determined by maximum likelihood regression of the sum of the path lengths through crowns of each species on canopy openness as determined by hemispherical photography. The predictions of Pukkala et al.'s (1993) model were correlated with measured light transmission ($r \geq 0.69$) and showed a similar spatial distribution; seedling growth correlated with predicted light as well. For Canham et al.'s (1994) model, predictive accuracy is harder to evaluate. Openness calculated by the model appears to be correlated with the estimate determined from hemispherical photographs, but no independent validation was performed.

Korzukhin and Ter Mikaelian (1995) also developed a spatially-explicit model where individual trees or shrubs are represented by vertical or horizontal planar screens of appropriate shape that are semi-transparent to light. The model estimates the amount of light passing through the screens and between the trees to specific ground positions. It is similar in approach to the "hits" variant of Canham et al.'s (1994, 1999) model. For species with long crowns and multiple layers, Ter Mikaelin et al. (1997) refined the model to use multiple horizontal screens, each representing a single uniform layer of leaves with the correct horizontal size and approximate vertical position (Figure 1-1e). The issue of within-crown foliage distribution can then be addressed as well, particularly for species with tiered, whorled branch structure. With good estimation of leaf area and extinction coefficients for the screens, estimation error was less than 8% of the measured light.

Several other attempts have been made to model within-crown foliage distribution. Norman and Welles (1983) applied the Beer-Lambert Law to nested subcrown regions of different leaf area density. Individual tree crowns were modeled as nested ellipses, and transmission was calculated as the sum of the subcrown absorbances (projected *LAD*×path length through each subcrown region)

[1-8] $$i = i_o(Z,\alpha)\cdot\cos Z\cdot e^{-\sum_{tree}\sum_{subcrown} pLAD_{tree,subcrown}\cdot b_{tree,subcrown}}$$

Norman and Jarvis (1975) grouped single cohort shoots into flat, circular whorls positioned along a stem. The proportion of the horizontal area occupied by these whorls when projected toward the light source, the probability of hitting a shoot within a whorl at this angle, the transmission through the shoot cylinder, as well as the contribution of reflection and through-leaf transmission were used to calculate light flux through successive canopy layers (see below). In single tree crowns, Wang and Jarvis (1990) distributed leaves vertically through the live crown and horizontally from the stem according to density functions fit to harvested trees. Transmission through these trees was calculated as with Norman and Welles (1983). Oker-Blom et al. (1991) developed a hierarchical model of light transmission, in which light can be absorbed by individual leaves, shoots, or crowns, to determine the relative importance of leaf size, area and inclination, shoot area and distribution, and stem distribution in the stand on model predictions. *LAI* was poorly estimated, confounding the analysis, but this paper laid the groundwork for modeling light transmission at any of these levels. The crown-absorption variant of this model produced estimates of light transmission within 8% transmission of the measured value for four pure lodgepole pine and one Engelmann spruce stand (Oker-Blom et al. 1991).

The contribution of light scattering through the reflection and through-leaf transmission of direct sunlight and diffuse light from leaf surfaces is the most difficult aspect to model. Canham et al. (1994) estimated the effects of direct sunlight scattering as the difference between diffuse light predicted by their model and measured light at times when the sun was shining but not striking the measurement sensor. From this estimate, they suggested that scattering could account for 14-41% of the understory radiation. Norman and Jarvis

(1975) modeled scattering by measuring leaf reflection and through-leaf transmission values, converting these, and the leaf distribution information (see above) to vertical upward and downward transmission/reflection coefficients for thin horizontal layers of canopy. To model the entire light environment, an iterative approach was taken. First, upward and downward reflection was evaluated layer by layer from the ground, starting with the soil reflectivity, to the top of the canopy. This yielded a starting ratio of diffuse light tending upward to diffuse light tending downward at each layer. Transmission, reflection, and absorption of diffuse skylight was then evaluated layer by layer from above the canopy to the ground. The process was iterated several more times, but with both direct-sunlight and diffuse light fluxes considered, until the upward- and downward-tending light estimates at each layer were stable (Figure 1-1f). By accounting for leaf transmission and reflection, the direct and diffuse light scattered by each layer could contribute to the layer's estimate of total diffuse flux. The predictive accuracy of this model appears to be good. The stand-average transmission at four heights was predicted closely by the model (Norman and Jarvis 1975). Using a modeling approach that combined the Norman and Jarvis (1975) radiative transfer approach with a geometric individual tree crown model, Wang and Jarvis (1990) found the difference between predicted and measured transmission for Sitka spruce and radiata pine stands was less than 10%. Cescatti (1997) and Bartelink (1998) have similarly combined Norman and Jarvis' (1975) model with their individual crown ray-tracing to account for scattering. However, in addition to the required information on the leaf area density, spatial distribution, and inclination angle distribution, information on transmission and reflectivity of leaves and stems must also be obtained for each species involved.

Most of these approaches (except for Combes et al. 2000 and Sinoquet et al. 2001) to modeling light use ray-tracing techniques to search for crowns, gaps and leaves. In graphics rendering software, ray-tracing can also incorporate reflections and refractions to trace the paths from the viewing location (i.e. simulation microsite) to the radiation sources. For plant canopies, refraction is only an issue at the cellular scale (as light passes in and out of hydrated cells) and its only relevance to modeling at these scales is through its effect on scattering radiation in leaf reflectance and transmittance. Leaves are far too

numerous to deal with as individual objects causing refractions and reflections, so these components of ray-tracing are not used here.

Another rendering approach in computer graphics is radiosity. This is a very time-intensive iterative approach, which calculates the illumination (e.g. PAR) of small sections of every object in the scene by all other objects viewed from the section. Iteration allows multiple reflections to occur, and processing continues until the illumination of each small section of the scene becomes stable. Sinoquet et al. (2001) and Combes et al. (2000) used a radiosity approach for modeling the flux and quality of light in a single walnut (*Juglans regia*) crown.

Since the primary interest in forest light modeling is for predicting PAR, where light scattering is a relatively small component, I elected to use the ray-tracing approach. For modeling PAR transmission in small, closed-canopy plots and for dealing with edge effects, the horizontally-infinite layer approach was used. For modeling PAR in larger, crown mapped plots, the individual crown approach was used. To model the changing light quality, particularly the red: far red ratio, Norman and Welles' (1983) semi-spatial approach was adopted.

Linking Light Availability and Tree Growth

The PAR vs. tree growth relationship was formalized by Monteith (1977), who suggested that radiation use efficiency (RUE), the ratio of an individual plant's net primary productivity (NPP) to absorbed photosynthetically active radiation (APAR), was a constant when other factors were not limiting. Limitations in nutrients and water, high temperatures and increased CO_2 concentration may affect RUE. Brunner and Nigh (2000) found that RUE in suppressed trees was higher than that in canopy trees, and may be non-linear. Foliar nitrogen has been suggested as a useful parameter for adjusting RUE (Medlyn 1996). However, Raulier et al. (2000) found little temperature effect on RUE in sugar maple (*Acer saccharum*). Grace et al. (1987) showed that RUE was constant for annual APAR and above-ground biomass growth of *Pinus radiata*. Korol et al. (1995) found this RUE approach effective for modeling growth of Douglas fir (*Pseudotsuga*

menziesii) at different densities. Bartelink et al. (1997) also applied this approach to mixed stands of Douglas fir and beech. To be effective, the RUE approach requires both a light simulation model, to calculate PAR availability and absorption, and an NPP partitioning model, to allocate carbon to various tree organs. Pacala et al. (1993), and Wright et al. (1998) took a more direct approach, and developed non-linear relationships between PAR availability and tree diameter or height growth. This latter approach was followed in this study.

Thesis Overview

The main focus of this dissertation is quantifying light in the understory of boreal mixedwoods. There is also a preliminary study relating the effects of light to white spruce and balsam fir growth. There are four research chapters. Chapter 2 describes the structure of the crown and canopy scale overstory light transmission models, their calibration, and their testing at the canopy scale. Chapter 3 describes a series of models we tested to include the effects of competing understory vegetation on light. Chapter 4 describes a test of the crown scale overstory model coupled with an understory model for determining the spatial distribution of light and the growth of understory trees across two large heterogeneous forest sites, one in western Canada and one in eastern Canada. Chapter 5 contains the description and test of a model for predicting light quality, specifically the red: far-red ratio, and its implications for forest dynamics.

Literature Cited

Bartelink, H.H. 1998. Radiation interception by forest trees: a simulation study on effects of stand density and foliage clustering on absorption and transmission. Ecological Modelling 105: 213-225.

Bartelink, H.H. 2000. Effects of stand composition and thinning in mixed-species forests: a modeling approach applied to Douglas-fir and beech. Tree Physiology 20: 399-406.

Bartelink, H.H., Kramer, K., Mohren, G.M.J. 1997. Applicability of the radiation-use efficiency concept for simulating growth of forest stands. Agricultural and Forest Meteorology 88: 169-179.

Black, T.A., J.M. Chen, X. Lee, and R.M. Sagar. 1991. Characteristics of shortwave and longwave irradiances under a Douglas-fir forest stand. Canadian Journal of Forest Research 21:1020-1028.

Brunner, A. 1998. A light model for spatially explicit forest stand models. Forest Ecology and Management 107: 19-46.

Brunner, A. and G. Nigh. 2000. Light absorption and bole volume growth in individual Douglas-fir trees. Tree Physiology 20:323-332.

Campbell, G.S. 1986. Extinction coefficients for radiation in plant canopies calculated using an ellipsoidal inclination angle distribution. Agricultural and Forest Meteorology 36: 317-321.

Campbell, G.S. and J.M. Norman. 1989. The description and measurement of plant community structure. In Plant canopies: their growth, form, and function (G. Russell, B. Marshall and P.G. Jarvis, eds) - Society for Experimental Biology Seminar Series 31, pp. 1-19.

Canham, C.D., K.D. Coates, P. Bartemucci and S. Quaglia. 1999. Measurement and modeling of spatially explicit variation in light transmission through interior cedar-hemlock forests of British Columbia. Canadian Journal of Forest Research 29: 1775-1783.

Canham, C.D., A.C. Finzi, S.W. Pacala, and D.H. Burbank. 1994. Causes and consequences of resource heterogeneity in forests: interspecific variation in light transmission by canopy trees. Canadian Journal of Forest Research 24: 337-349.

Cannell, M.G.R. and J. Grace. 1993. Competition for light: detection, measurement, and quantification. Canadian Journal of Forest Research 23: 1969-1979.

Cermák, J. 1989. Solar equivalent leaf area: an efficient biometrical parameter of individual leaves, trees and stands. Tree Physiology 5: 269-289.

Cescatti, A. 1997. Modelling the radiative transfer in discontinuous canopies of asymmetric crowns. II. Model testing and application in a Norway spruce stand. Ecological Modelling 101: 275-284.

Chen, J.M. 1996. Optically-based methods for measuring seasonal variation of leaf area index in boreal conifer stands. Agricultural and Forest Meteorology 80: 135-163.

Combes, D., Sinoquet, H., and Varlet-Grancher, C. 2000. Preliminary measurement and simulation of the spatial distribution of the Morphogenetically Active Radiation (MAR) within an isolated tree canopy. Annals of Forest Science 57: 497-511.

Comeau, P., R. Macdonald, R. Bryce and B. Groves. 1998. Lite: a model for estimating light interception through forest canopies, users manual and program documentation. Research Branch, Ministry of Forests, Victoria, B.C. Working Paper 35.

Comeau, P.G., T.F. Braumandl, C.-Y. Xie. 1993. Effects of overtopping vegetation on light availability and growth of Engelmann spruce (*Picea engelmannii*) seedlings. Canadian Journal of Forest Research 23:2044-2048.

Dufrêne, E. and N. Bréda. 1995. Estimation of deciduous forest leaf area index using direct and indirect methods. Oecologia 104: 156-162.

Gilbert, I.R., P.G. Jarvis, H. Smith. 2001 Proximity signal and shade avoidance differences between early and late successional trees. Nature 411: 792-795.

Goel, N.S. and D.E. Strebel. 1984. Simple beta distribution representation of leaf orientation in vegetation canopies. Agronomy Journal 76: 200-202.

Grace, J.C., P.G. Jarvis, and J.M. Norman. 1987. Modelling the interception of solar radiant energy in intensively managed stands. New Zealand Journal of Forestry Science 17: 193-209.

Groot, A. and D.W. Carlson. 1996. Influence of shelter on night temperatures, frost damage and bud break of white spruce seedlings. Canadian Journal of Forest Research 26: 1531-1538.

Huang, S. and S.J. Titus. 1999. Estimating a system of nonlinear simultaneous individual tree models for white spruce in boreal mixed-species forests. Canadian Journal of Forest Research 29: 1805-1811.

Jarvis, P.G. and J.W. Leverenz. 1983. Productivity of temperate deciduous and evergreen forests. In O.L. Lange, P.S. Nobel, C.B. Osmond and H. Ziegler, Eds.

Physiological Plant Ecology IV. Ecosystem Processes: Mineral Cycling, Productivity and Man's Influence. Encyclopedia of Plant Physiology, New Series, Vol. 12D. Springer-Verlag, Berlin, pp. 233-280.

Kimmins, J.P., C. Caza, C. Messier, J. Karakatsoulis, K.A. Scoullar, M.J. Apps. 1990. FORCYTE and FORECAST: ecosystem-level management models with which to examine the yield, economic, energy and wildlife implication of vegetation management as a component of rotation-length silvicultural systems. FRDA Report, Canadian Forestry Service 109: 107-108.

Klinka, K., Q. Wang, G.J. Kayahara and R.E. Carter. 1992. Light-growth response relationships in Pacific silver fir (*Abies amabilis*) and subalpine fir (*Abies lasiocarpa*). Canadian Journal of Botany 70: 1919-1930.

Kneeshaw, D.D. and Y. Bergeron. 1999. Spatial and temporal patterns of seedling and sapling recruitment within canopy gaps caused by spruce budworm. Ecoscience 6: 214-222.

Kobe, R.K. and K.D. Coates. 1997. Models of sapling mortality as a function of growth to characterize interspecific variation in shade tolerance of eight tree species of northwestern British Columbia. Canadian Journal of Forest Research 27: 227-236.

Korol, R.L., S.W. Running, K.S. Milner. 1995. Incorporating intertree competition into an ecosystem model. Canadian Journal of Forest Research 25:413-424.

Korzukhin, M.D. and M.T. Ter-Mikaelian. 1995. An individual tree-based model of competition for light. Ecological Modelling 79: 221-229.

Kull, O. and I. Tulva. 2000. Modelling canopy growth and steady-state leaf area index in an aspen stand. Annals of Forest Science 57: 611-621.

Lang, A.R.G. 1987. Simplified estimate of leaf area index from transmittance of the sun's beam. Agricultural and Forest Meteorology 41: 179-186.

Larsen, D.R. and J.A. Kershaw, Jr. 1996. Influence of canopy structure assumptions on predictions from Beer's law. A comparison of deterministics and stochastic simulations. Agricultural and Forest Meteorology 81: 61-77.

Lieffers, V.J. and J.A. Beck, Jr. 1994. A semi-natural approach to mixedwood management in the prairie provinces. The Forestry Chronicle 70: 260-264.

Lieffers, V.J., C.M. Messier, K.J. Stadt, F. Gendron, and P. Comeau. 1999. Predicting and managing light in the understory of boreal forests. Canadian Journal of Forest Research 29: 796-811.

Lieffers, V.J., B.D. Pinno, and K.J. Stadt. 2002. Light dynamics and free-to-grow standards in aspen-dominated mixedwood forests. Forestry Chronicle 78: 137-145.

Lieffers, V.J. and K.J. Stadt. 1994. Growth of understory *Picea glauca*, *Calamagrostis canadensis*, and *Epilobium angustifolium* in relation to overstory light transmission. Canadian Journal of Forest Research 24: 1193-1198.

Lieffers, V.J., K.J. Stadt, and S. Navratil. 1996. Age structure and growth of understory white spruce under aspen. Canadian Journal of Forest Research 26: 1002-1007.

Medlyn, B.E. 1998. Physiological basis of the light use efficiency model. Tree Physiology 18:167-176.

Monsi, M. and Saeki, T., 1953. Über den Lichtfactor in den Pflanzengesellschaften und seine bedeutung für die stoffproduktion. Japan Journal of Botany 14, 22-52.

Monteith, J.L. 1977. Climate and efficiency of crop production in Britain. Philosophical Transactions of the Royal Society of London, Series B, pp.277-294.

Morgan, D.C., D.A. Rook, I.J. Warrington and H.L. Turnbull. 1983. Growth and development of *Pinus radiata* D. Don: the effect of light quality. Plant, Cell and Environment 6: 691-701.

Nilson, T. 1971. A theoretical analysis of the frequency of gaps in plant stands. Agricultural and Forest Meteorology 8: 25-38.

Norman, J.M. and Campbell. 1989. Canopy structure. In R.W. Pearcy, J. Ehleringer, H.A. Mooney and P.W. Rundel, eds. Plant Physiological Ecology: Field Methods and Instrumentation. Chapman and Hall, New York, pp. 301-325.

Norman, J.M. and J.M. Welles. 1983. Radiative transfer in an array of canopies. Agronomy Journal 75: 481-488.

Norman, J.M. and P.G. Jarvis. 1975. Photosynthesis in Sitka spruce (*Picea sitchensis* (Bong.) Carr.) V. Radiation penetration theory and a test case. Journal of Applied Ecology 12: 839-878.

Oker-Blom, P. 1986. Photosynthetic radiation regime and canopy structure in modeled forest stands. Acta Forestalia Fennica 197: 1-44.

Oker-Blom, P., M.R. Kaufmann, and M.G. Ryan. 1991. Performance of a canopy light interception model for conifer shoots, trees and stands. Tree Physiology 9: 227-243.

Pacala, S.W., C.D. Canham and J.A. Silander. 1993. Forest models defined by field measurements: I. The design of a northeastern forest simulator. Canadian Journal of Forest Research 23: 1980-1988.

Pearcy, R.W. 1989. Radiation and light measurements. In R.W. Pearcy, J. Ehleringer, H.A. Mooney and P.W. Rundel, eds. Plant Physiological Ecology: Field Methods and Instrumentation. Chapman and Hall, New York, pp. 97-116.

Pierce, L.L. and S.W. Running. 1988. Rapid estimation of coniferous forest leaf area index using a portable integrating radiometer. Ecology 69: 1762-1767.

Pukkala, T., T. Kuuluvainen, and P. Stenberg. 1993. Below-canopy distribution of photosynthetically active radiation and its relation to seedling growth in a boreal Pinus sylvestris stand: a simulation approach. Scandinavian Journal of Forest Research 8: 313-325.

Raulier, F., P.Y. Bernier and C.H. Ung. 2000. Modeling the influence of temperature on monthly gross primary productivity of sugar maple stands. Tree Physiology 20:333-345.

Running, S.W. and J. Coughlan. 1988. A general model of forest ecosystem processes for regional applications. I. Hydrologic balance, canopy gas exchange, and primary production processes. Ecological Monographs 42: 125-154.

Sinclair, T.R. and K.R. Knoerr. 1982. Distribution of photosynthetically active radiation in the canopy of a loblolly pine plantation. Journal of Applied Ecology 19: 183-191.

Sinoquet, H., X. Le-Roux, B. Adam, T. Ameglio, F.A. Daudet. 2001. RATP: a model for simulating the spatial distribution of radiation absorption, transpiration and photosynthesis within canopies: application to an isolated tree crown. Plant, Cell, and Environment 24:395-406.

Smith, H. 2001. Phytochromes and light signal perception by plants – an emerging synthesis. Nature 407: 585-591.

Stadt, K.J. and V.J. Lieffers. 2000. MIXLIGHT: A flexible light transmission model for mixed-species forest stands. Agricultural and Forest Meteorology 102:235-252.

Swinehart, D.F. 1962. The Beer-Lambert Law. Journal of Chemical Education 39: 333-335.

Ter Mikaelian, M.T. and R.G. Wagner. 1997. Distance-independent models for predicting photosynthetically active radiation transmission through young forest plant canopies. Canadian Journal of Forest Research 27: 127-130.

Wang, Y.P. and P.G. Jarvis. 1990. Influence of crown structural properties on PAR absorption, photosynthesis, and transpiration in Sitka spruce: application of a model (MAESTRO). Tree Physiology 7: 297-316.

Waring, R.H. and Schlesinger, W.H., 1985. Forest Ecosystems: Concepts and Management. Academic Press, New York.

Sampson, D.A. and F.W. Smith. 1993. Influence of canopy architecture on light penetration in lodgepole pine (Pinus contorta var. latifolia) forests. Agricultural and Forest Meteorology 64: 63-79.

Wright. E.F., K.D. Coates, C.D. Canham, and P. Bartemucci. 1998. Species variability in growth response to light across a climatic in northwestern British Columbia. Canadian Journal of Forest Research 28: 871-886.

Figure 1-1. Pictorial representation of the light transmission models. The actual canopy structure is shown in light gray. The medium gray area in each frame is the light-absorbing region for modeling purposes, which can be (a, b) stand canopy, (c) a voxel of canopy space, (d) tree crown, (e) crown layer, or (f) canopy layer. The sources of light are shown above each canopy: the sun (globe) and skylight (stippled bar). Paths taken by light rays from these sources through the canopy are shown by arrows: the wide arrow is the path of direct sunlight and the narrow arrows are the paths of diffuse skylight. Arrows are black where they pass through the modeled canopy or crown structures. Z is the solar zenith angle.

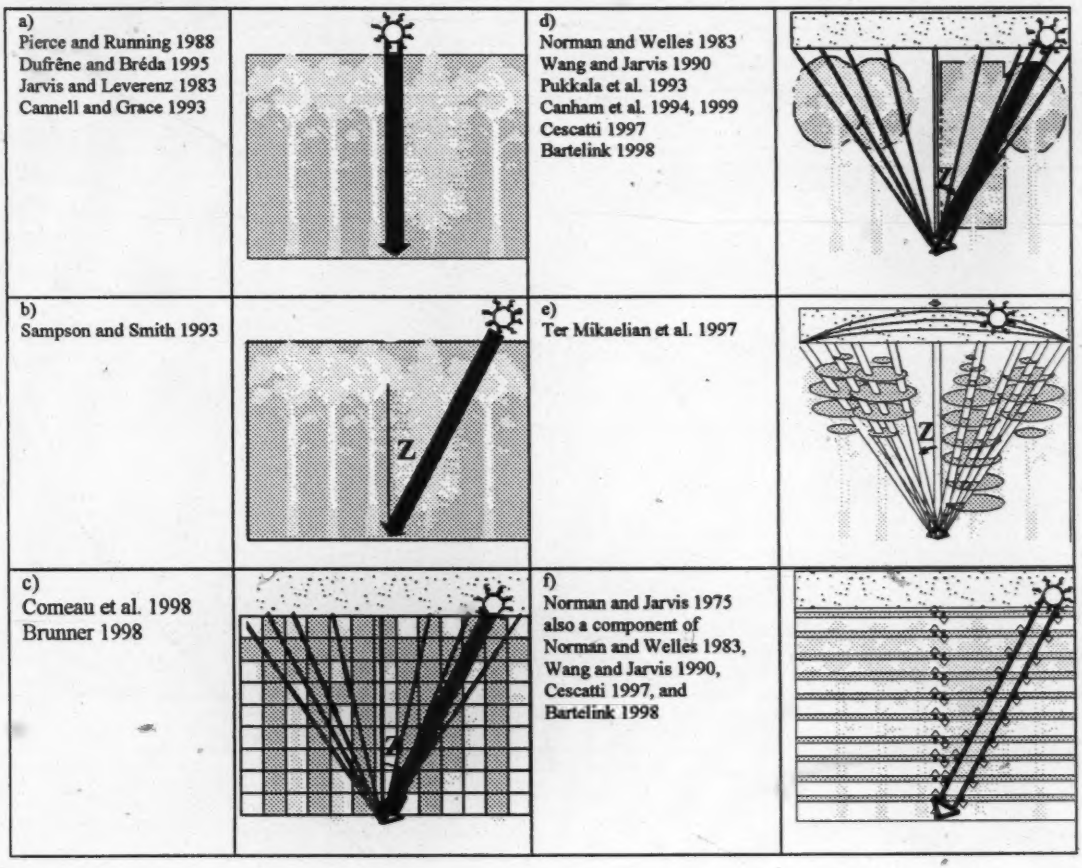

Chapter 2. MIXLIGHT: A Flexible Light Transmission Model for Mixed-Species Forests[2]

Introduction

The characterization of light in forests has been a key focus of work on forest community dynamics and regeneration. Numerous studies have established the dependence of tree and understory growth on available light in stands (Messier et al., 1989; Lieffers and Stadt, 1994) and microsites (Poulson and Platt, 1989; Alaback and Tappeiner 1991; Klinka et al. 1992; McLure and Lee 1993; Poage and Peart 1993; Runkle et al. 1995). However, adequate measurement of light is time-consuming due to the heterogeneity in the arrangement and composition of the canopy, diurnal and seasonal changes in solar position and cloudiness, and leaf-on and off cycles. A number of authors have shown that it is possible to use the well-described laws of solar geometry and information about the canopy structure to predict light regimes in forests at the stand (Norman and Jarvis 1975) and the microsite level (Grace et al. 1987; Wang and Jarvis 1990; Pukkala et al. 1993; Canham et al. 1994; Cescatti 1997b; Ter-Mikaelian et al. 1997; Bartelink 1998; Brunner 1998).

Forest tenures often cover large areas of mixed composition and have various types of inventory data available for management decisions. These inventories may vary considerably, but are frequently based on tree species, diameter and height measurements and may include crown length and width, and stem spatial location (Vanclay 1994). There is also a considerable range of stand-tending and harvesting options which have implications for the light regime and vegetation response. However, light models are driven by parameters that are seldom measured in working forests, and may be poorly structured for simulating the effects of silivicultural treatment. What is required is an easily-calibrated, multi-species model of light availability that is flexible enough to be driven by existing forestry data and produce accurate understory light predictions on a scale appropriate to the data and management goals. Such a model would be of

---

[2] A version of this chapter has been published as Stadt, K.J. and V.J. Lieffers. 2000. MIXLIGHT: A flexible light transmission model for mixed-species forest stands. Agricultural and Forest Meteorology 102:235-252.

considerable help in studying, planning and managing regeneration in working and research forests (Lieffers et al. 1999).

Light availability models developed for forests vary considerably in approach and complexity. The simplest fit the Beer-Lambert Law empirically, calculating light transmission based on the overlying leaf area index and an extinction coefficient (Monsi and Saeki 1953; Pierce and Running 1988). These produce reasonable predictions only for a restricted range of solar angles and are limited to stands which are similar to those in which their extinction coefficients were calibrated (Lieffers et al. 1999). Another approach has been to model the forest canopy as a number of horizontally homogeneous layers of grouped foliage, each with an appropriate fraction of the canopy leaf area and layer transmission and reflection coefficients. Such a model predicted the light profile well in a pure Sitka spruce plantation (Norman and Jarvis 1975), but a considerable amount of data was required to generate the model parameters. These models require leaf-area measurements of various complexity, but leaf area is seldom available in forestry data. They are also limited to stand-level predictions of light only, and do not account for the horizontal spatial variation of light at microsites throughout the stand.

Spatial approaches group foliage into identifiable objects such as individual rows, crowns, crown layers or shoots which are described geometrically as cylinders, ellipsoids, quarter ellipsoids or disks with measurements to locate these objects in three-dimensional space. Light penetration through these objects is modeled spatially and temporally, given the solar geometry for that latitude and time, and the position and size parameters of the geometric shapes. Pukkala et al. (1993) tested a crown model of this type in a pure Scots pine stand, Bartelink (1998) and Brunner (1998) tested somewhat similar models in pure Douglas-fir and beech stands, and Canham et al. (1994) and Ter-Mikaelian et al. (1997) developed models for mixed-species stands. These use size- or species-specific estimates of the projected leaf area density within the crown or similar extinction coefficients to compute through-crown light transmission. They do not account for light reflection, but are able to predict the spatial distribution of light at microsites throughout the stand with reasonable accuracy. Lastly, a number of models combine the spatial features of the

geometric approach with a homogeneous layer model to deal with light reflection (Grace et al. 1987; Wang and Jarvis 1990; Cescatti 1997a). These have shown good spatial accuracy in pure stands, but require a suite of detailed input data.

Tools for modeling light are thus well-developed. Applications, however, have been limited by model inflexibility or the quantity and type of data required. Calibration (estimating model parameters) has been particularly difficult. In MIXLIGHT, we aimed to build a flexible, accessible simulator which would allow light penetration theory to be applied to existing forest inventory data with minimal calibration and make light availability predictions for a wide range of stands. We designed our model to operate at either the microsite or stand scale to fit the data available and the spatial precision required. MIXLIGHT can generate light predictions from either a complete tree list or a minimal list of tree species and stem diameters. The complete list includes species, diameter, height, height to the base of the live crown, crown radius, and tree location coordinates. Where some of the crown size information is missing, regressions are used to determine these parameters. A separate table of foliage area density, foliage inclination parameters and the crown shape for each species and/or each crown-class is required. These can be obtained following the calibration described here or from other sources. To account for exposure effects, stand slope and aspect are also required. Dates for deciduous leaf-on and leaf-off, and start / end-dates of the growing season can be added to simulate the seasonal light regime. This is critical for accounting for the leaf-off shoulder seasons in the spring and fall which are important for carbon fixation in wintergreen, evergreen and ephemeral species (Hutchison and Matt 1977; Man and Lieffers 1997). In large inventoried plots with stem location data available, light modeling can be carried out at the microsite scale. When the stem position data are missing, the inventoried stand is small and dominated by edge effects, or if only a stand-level estimate of light is required, MIXLIGHT will operate at the stand scale, using generalized canopy parameters calculated from the tree list. Since canopy parameters can also be obtained from remote-sensing or canopy analysis instruments, the capability to predict stand-level light directly from canopy leaf area index and inclination information is also possible.

In this paper, we present the structure of MIXLIGHT, describe a simple method of calibrating the foliage area density and inclination coefficients, and validate its stand-level predictions across a wide range of stand types in the boreal mixedwood forest of central Alberta, Canada. The importance of the key parameters of MIXLIGHT for stand-level estimation are evaluated in a sensitivity analysis. A microsite-level validation, using the individual tree crown geometry modeling features of MIXLIGHT is presented in Chapter 4.

Methods

Overview

An ideal forest light transmission model would integrate the light-attenuating effect of all foliage positioned between the sky and the measurement point. Since this is seldom possible, a common modeling approach is to sample the intervening foliage by tracing numerous rays from starting points scattered across the sky hemisphere to the measurement point (P_0) within the stand (Figure 2-1A, Canham et al. 1994; Bartelink 1998; Brunner 1998). MIXLIGHT takes this approach, and uses the light penetration function (Equation 2-1) to calculate transmission along each of these rays based on the density of the foliage through which the ray passed, the degree to which this foliage area is oriented toward the light source, and the length of the ray's path (S) through individual tree crowns (Figure 2-1B) or the stand canopy (Figure 2-1C). These ray transmission values are weighted by the strength of the light source and averaged to give an estimate of the integrated light transmission (the ratio of below to above canopy light) at the measurement point. The individual crown approach (Figure 2-1B) accounts for horizontal variation in overstory foliage and produces microsite light predictions, while the canopy scale approach (Figure 2-1C) distributes foliage randomly throughout the canopy and produces stand-level predictions. Calibration of the foliage area density and foliage projection parameters is accomplished by inverting the modeling process for the simple case of sunlight shining through the crown of an isolated tree (Figure 2-2). This is repeated at several times of day at different sun angles, so that the foliage area density and foliage projection parameters can be determined. Simulations are then carried out

using these species-specific foliage parameters with the tree lists from the sites of interest.

Theory

MIXLIGHT models the transmission of photosynthetically active radiation (PAR: 400-700 nm). We use 'light' as a synonym for PAR, though visible light is a slightly wider waveband. Foliage is taken to include leaves, branches and stem that are contained within the crown or canopy volume since these all attenuate light. Each fragment of foliage area is assumed to transmit and reflect no light so that a thin ray of light incident on the forest is either completely absorbed or completely transmitted, depending on whether it hits or misses foliage. If the foliage is randomly distributed within the crown or canopy region, the probability that the ray will not be intercepted ($P(0)$) is given by the Poisson distribution as shown in Equation 2-1.

$$[2\text{-}1] \quad P(0) = T = \frac{q[Z,\alpha]}{q_0[Z,\alpha]} = e^{-\sum_{j=1}^{n} G[Z,\chi_j] S_j F_j}$$

$$[2\text{-}2] \quad q[Z,\alpha] = q_0[Z,\alpha] e^{-\sum_{j=1}^{n} G[Z,\chi_j] S_j F_j}$$

Equation 2-2 is rearranged to yield light flux density ($q[Z,\alpha]$) rather than transmission (T), which is a more convenient form for modeling the diffuse and seasonal light flux (see Equation 2-4). In Eqs. 1 and 2, $q[Z,\alpha]$ is the flux density (μmol m^{-2} s^{-1}) of a ray of light through a surface perpendicular to the ray direction, originating from a distant point source defined by its zenith (Z, angle from vertical) and azimuth (α, compass orientation), $q_0[Z,\alpha]$ is the light flux density (μmol m^{-2} s^{-1}) incident on the canopy from the same source, $G[Z,\chi_j]$ (unit-less) is the projection of one unit of foliage area perpendicular to the direction of the light source, χ_j is a parameter describing the foliage area inclination (see below), S_j is the path length (m) through the light-absorbing region, and F_j is the foliage area density (in m^2m^{-3}). By analogy with the Beer-Lambert Law (Swinehart 1955), we consider the product $G[Z,\chi_j]S_jF_j$ (=-ln T) as the absorbance for the region j. Since absorbances are additive, the summation in Eqs. 1 and 2 deals with any

number of light absorbing regions (n) that intersect the light path, from a single canopy (n = 1, Figure 2-1C) to an array of individual crowns (n = number of trees, Figure 2-1B).

[2-3] $$T_{direct} = \frac{Q_{direct}}{Q_{0,direct}} = \frac{\cos Z_s \, q[Z_s, \alpha_s]}{\cos Z_s \, q_0[Z_s, \alpha_s]}$$

[2-4]

$$T_{diffuseor\ seasonal} = \frac{Q_{diffuseor\ seasonal}}{Q_{0,\ diffuseor\ seasonal}} = \frac{\int_{\cos Z=1}^{0} \int_{\alpha=0}^{360} \cos Z \, q[Z,\alpha] \, d\alpha \, d\cos Z}{\int_{\cos Z=1}^{0} \int_{\alpha=0}^{360} \cos Z \, q_0[Z,\alpha] \, d\alpha \, d\cos Z} \cong \frac{\sum_{c=1}^{nc} \sum_{a=1}^{na} (\cos Z_c \, q[Z_c, \alpha_a])}{\sum_{c=1}^{nc} \sum_{a=1}^{na} (\cos Z_c \, q_0[Z_c, \alpha_a])}$$

For instantaneous estimates of light transmission, Equation 2-2 is applied once for direct-beam radiation transmission (T_{direct}) using the sun's position angles (Z_s, α_s; Equation 2-3), and multiple times using angles identifying the centers of equal-area sectors of the sky (*i.e.* sky-elements of equal solid angle) for integrating the transmission of diffuse or seasonal skylight (Equation 2-4). (Note that Equation 2-3 simplifies to Equation 2-1 since only one ray is traced). In Equation 2-4, c=1..nc is the index for the zenith angles (Z_c) which are divided into nc equal increments of the cosine of the zenith from 1 (Z_c=0) to 0 (Z_c=90°) to achieve equal-area sampling of the sky, and a=1..na is the index for the azimuth angles (α_a) which are divided into na equal increments from 0 to 360°. The flux densities of all rays are cosine-corrected to the flux density through a horizontal surface. For daily or seasonal transmission, we followed the example of Canham et al. (1994) and generated a "seasonal sky matrix," which adds to the diffuse skylight the flux density of the sun while it passes through each sky sector and is not obscured by cloud. Equation 2-4 is then applied, using the Z, α coordinates of each of these sectors and the incident seasonal light flux density ($q_0[Z,\alpha]$) calculated for the sector. With this approach, light availability can be calculated seasonally or for specific times of the year and day, and for various weather conditions.

Study area

Calibration and validation of MIXLIGHT were performed in a number of stands across west-central Alberta (53°30' - 54°10' N, 114°50' - 118° W). Mean annual temperature in

this region is 0.9 - 2.6°C, and precipitation is 530 - 560 mm a^{-1}, approximately 60% of it falling during the growing season (May - August) (Anon. 1982a, 1982b). All stands were upland sites with submesotrophic to mesotrophic nutrient status and mesic to hygric ecological moisture regime (Anon. 1994)

Model Calibration

Foliage area density

The foliage area density of various tree species was determined on newly-isolated residual trees on clearcut edges and in partial-cut stands. We visited 10 cutblocks from late June to August in 1996 and 1997 for leaf-on calibration, and in April 1997 for leaf-off measurements. Before cutting, the sites were dominated by either aspen (*Populus tremuloides* Michx.), white spruce (*Picea glauca* (Moench) Voss) or mixtures of these, balsam fir (*Abies balsamea* (L.) Mill.), balsam poplar (*Populus balsamifera* L.), and white birch (*Betula papyrifera* Marsh.). Trees were measured as soon after logging as possible (1 week to 3 months) so they still retained most of the leaf and shape characteristics they had while growing in the stand.

Light measurements were taken with an 80 sensor linear radiometer (Model SF-80, Decagon Devices, Inc., Pullman, WA) which measures PAR in quantum units (μmol m^{-2} s^{-1}) . Measurements were made during periods of direct sun when the trees cast a clearly delineated shadow on the ground. At each sample tree, crown width, total shadow length (h_t', stem base to shadow apex), length to the base of the shadow's live-crown (h_{lc}') and time of measurement were recorded first for crown size determination (Figure 2-2A). The light sampling strategy depended on the crown shape. Parallel transects at 1-2 m spacing (wider spacing for larger crowns) perpendicular to the central axis of the crown (see Figure 2-2A) were used for longer crowns. Radial transects at 45° intervals originating from the center of the crown shadow were used to sample ellipsoidal crowns (Figure 2-2B). To compensate for the horizontal movement of the sun (0.25° min^{-1}), the origin of each transect was aligned with the central axis of the shadow before commencing each transect. Vertical changes in the sun's position (<0.1° min^{-1}) were small enough to be ignored during the sampling period. Where necessary, ground slope and aspect were

measured to later transform the transect positions to horizontal coordinates. Every 50 cm from the transect origin, the radiometer wand has held at right angles to the transect (Figure 2-2C), six light measurements taken over six seconds and the average recorded. Sampling extended 100-150 cm past the edge of the shadow to provide at least one unshaded light measure (Q_0) for that transect. Length from the transect origin to the shadow edge (d, Figure 2-2C) was recorded for crown size determination. Total (Q_0) and diffuse light ($Q_{diffuse}$) were measured in unshaded sunlight adjacent to the crown shadow immediately before and after sampling each tree by exposing then shading a single sensor of the radiometer with a small disk at 2 m distance, and recording the output from that sensor. Sampling time depended on tree size, but was usually less than 20 minutes per tree.

An appropriate geometric shape (ellipsoid, paraboloid, cone, cylinder, or rocket (a cone of 25% of the crown length perched on a cylinder 75% of the crown length)) was chosen for the crown of each species (Table 2-1). To obtain the dimensions of these shapes (crown length (tree height minus live-crown height) and radius), actual height and live-crown height measurements were adjusted for the solar zenith angle at the time of measurement (Equation 2-5).

[2-5] $$actual\ length = \frac{shadow\ length}{\tan Z_s}$$

We assumed the crowns were circular in cross-section so that their crown radius was not affected by solar angle. The solar zenith and azimuth at the time, day, latitude and longitude of measurement were obtained using Iqbal's (1983) formulae.

The transmission of direct beam light (T_{direct}) was calculated by subtracting the diffuse component ($Q_{diffuse}$) from the light measured (Q) at the point and from the light measured outside the crown shadow (Q_0), then taking the ratio of these two (Equation 2-6).

[2-6] $$T_{direct} = (Q - Q_{diffuse})/(Q_0 - Q_{diffuse})$$

The diffuse light actually decreases for measurements nearer the tree since its stem and crown capture more of the diffuse light. The effect on direct-beam transmission and the resulting increase in the foliage density estimate that results from this is small, however,

because the direct-beam flux is so much greater (>4×) than the diffuse. The path length of the sun through the crown (S, Figure 2-2B) was estimated by solving for the intersection of the ray vector described by the measurement point and the sun angle with the geometric crown. Equations for determining the two intersection points ($P_1(x_1, y_1, z_1)$ and $P_2(x_2, y_2, z_2)$) for a ray passing through the various crown shapes are presented in Appendix 2 A. The distance formula (Equation 2-7) was then applied to the intersection points to obtain the path length.

[2-7] $$S = \sqrt{(x_2 - x_1)^2 + (y_2 - y_1)^2 + (z_2 - z_1)^2}$$

The projection of a unit of foliage area in the sun's direction ($G[Z_s, \chi_j]$) was calculated using Equation 2-9, as described below. Lastly, the foliage area density (F_j) was calculated from these variables by inverting Equation 2-1 (Equation 2-8).

[2-8] $$F_j = \frac{-\ln T_{direct}}{G[Z_s, \chi_j]S}$$

Foliage densities were averaged over all measurement points within each tree's shadow. Trees were then averaged within a species to yield that species' average foliage area density. Estimates calculated from radial transects were weighted by the length from the transect origin to the measurement point to even out the area sampling rate.

Foliage inclination and projection

Since the foliage area is not perpendicular to every angle it is viewed from, nor to each light source, it is necessary to correct the apparent projected area to actual (one-sided) surface area. Campbell and Norman (1989) demonstrated that a simple and effective method of modeling the inclination of many leaves is to assume the foliage is oriented as if it was spread over the surface of an ellipsoid. If the orientation with regard to azimuth is assumed to be random, the ellipsoidal inclination distribution can be modeled with one parameter, the ratio of vertical to horizontal projections, χ_j. When χ_j=1, the foliage inclines as if covering a sphere: smaller values indicate mostly vertical foliage area orientation, larger χ_j indicate mostly horizontal foliage. The projection of an ellipsoid, having a surface area of 1, perpendicular to the light source zenith is given by Equation 2-9 (Campbell and Norman 1989).

$$[2\text{-}9] \quad G[Z,\chi_j] = \frac{\sqrt{\chi_j^2 \cos^2 Z + \sin^2 Z}}{(\chi_j + 1.774(\chi_j + 1.182)^{-0.733})}$$

Campbell and Norman (1989) also demonstrated how the inclination (χ_j) parameter can be obtained by measuring the gap fraction at a number of zenith angles (Z), then solving for foliage area and foliage inclination using inversion techniques. We used direct sunlight transmission as a measure of gap fraction in individual crowns then corrected for any change in the path length (S) with solar zenith angle (Z_s) to yield the dependent variable $-\ln(T_{direct})/S$. We found the inclination and foliage area density (F_j) parameters that offered the best fit to Equation 2-10 by nonlinear regression of $-\ln(T_{direct})/S$ on the independent variable Z_s.

$$[2\text{-}10] \quad -\ln T_{direct}/S = G[Z_s, \chi_j]F_j$$

A similar approach suing sunlight transmission approach to obtaining G for particular solar angles when F is known is demonstrated by Oker-Blom et al. (1991).

Direct-beam light transmission data taken at a number of solar angles were obtained from a study by Constabel (1995). She sampled 10 aspen, 10 overstory white spruce and 10 understory white spruce trees on June 22, 1994 in a partially-cut mixed forest in central Alberta (53°40' N, 116°40' W). Each crown was sufficiently isolated that it cast a distinct shadow through most of the day. Shadows were sampled during five one-hour periods with mean solar zenith angles of 30.7°, 32.9°, 35.7°, 51.2° and 65.3°. At each sampling time, nine light measurements (Q) were taken in the crown shadow of each tree, with the 80 cm radiometer wand held parallel to the stem. Three measurements were taken at random positions in the upper third of the crown, three in the middle, and three in the lower third, then averaged for each tree. Total (Q_0) and diffuse flux density ($Q_{diffuse}$) were measured in full sun adjacent to the crown shadow immediately before and after sampling each tree as outlined for the foliage area density measurements above. Tree height, h_t, live-crown height, h_{lc}, and crown width, cw, were determined with a clinometer and measuring tape.

With this data, we calculated direct sunlight transmission through the whole crown by subtracting the diffuse component as above (Equation 2-6). Since the measurement points were not mapped spatially (to speed sampling), we had to simplify the crown shape. We first determined the volume of each crown as either an ellipsoid (aspen) or a rocket (white spruce) using the crown length and width to establish the axis lengths. We then redefined the crowns as rectangular solids with one side facing the sun, one crown length deep and of equal length and width such that they contained the same volume as the original shape.

$$[2\text{-}11] \quad S = \frac{w}{\sin Z_s}$$

The path length of light through the crown (S) at the solar zenith (Z_s) was calculated using the width (w) of the rectangle (Equation 2-11). The negative logarithm of direct sunlight transmission was then divided by S, to yield the dependent variable in Equation 2-10. We used the derivative-free nonlinear regression method available in SAS release 6.12 (PROC NLIN METHOD=DUD, SAS Institute, Cary, NC) to regress $-\ln(T_{direct})/S$ on Z_s (Equation 2-10) and obtain χ_l and F_l. These parameters were calculated for each tree, then averaged for the species. Since the measurement points were not well -mapped, only the inclination parameter (χ_l) was used.

The MIXLIGHT Model

Crown-scale modeling

The light transmission model was adapted from previous models developed in Scandinavia (Pukkala et al. 1993) and New England (Canham et al. 1994). The trees were projected mathematically in 3-dimensional (x, y, z) space with stems modeled as paraboloids truncated at the base of the crown and crowns of the shape appropriate to the species (ellipsoids, paraboloids, cylinders, cones or rockets). The elevations of the stems and crowns were adjusted for the stand slope and aspect.

At each measurement point, diffuse skylight transmission was calculated by averaging the transmission along at least 480 light paths (Equation 2-4: na=24 equally spaced azimuths from 0 to 360°, and ne=20 zeniths, spaced by equal increments of the cosine of

the zenith from 1 (0°) to 0 (90°)). Each path was checked for slope, stem and crown hits. If the light source was obscured by the sloping ground (Equation 2-12), a value of 0% light transmission was returned for that path.

[2-12] $\cos(\Delta s) = \cos\beta\cos Z + \sin\beta\cos(\alpha - \Omega)$

Here, $\cos(\Delta s)$ is the cosine of the angle between a line perpendicular to the slope and the light source, β is the slope inclination, and Ω the slope aspect. If $\cos(\Delta s)<0$, the source is obscured by the slope. Stem hits were determined by checking the paraboloid stems for an intersection with the light path using the simultaneous solution to the ray and paraboloid equation (Appendix 2A). Any stem hit caused 0% transmission to be returned for that path.

In the absence of these, ray transmission was determined by the length the light ray passed through each crown of the various trees between the simulation point and the sky. Again, the simultaneous solution to the ray and geometric crown equation (Appendix 2A) was used to determine intersection points, and Equation 2-7 applied to obtain the length of the ray between these points (S). This ray length was multiplied by the foliage projection and foliage area density for the appropriate species to give an absorbance ($A_j = G[Z,\chi_j]S_jF_j$), which was summed for all crowns encountered on the path. The sum of these absorbance values along each light path was then converted back to a flux density ($q[Z,\alpha]$), as shown in Equation 2-2. We used the uniform overcast sky (UOC) assumption for diffuse light, *i.e.* light incident from all equal-area sectors of the sky was assumed to have equal flux density.

Direct sunlight absorbance was obtained in a similar way, but for only one light path using the solar zenith and azimuth angle at the date, time and location of measurement. The proportions of direct and diffuse light at the time of measurement were applied to the output to give the integrated light transmission prediction.

Canopy-scale modeling

To avoid excessive edge effects, crown scale modeling requires a large area of inventoried trees surrounding a much smaller central area in which predictions are made.

This allows ray-tracing to proceed to wide zenith angles without encountering the plot edge. For example, in a 50 × 50 m flat inventory plot with 20 m tall trees and with the measurement point at plot center, 51° is the widest possible zenith angle that will still avoid the plot edge. Although the light ray transmission values are weighted by the cosine of their zenith angle, nearly 40% of the weight of the diffuse light measurement would be obtained from zenith angles larger than 51° since there is so much sky area beneath this angle. Light transmission is low at large zenith angles owing to the long path through the canopy, so ignoring these angles would inflate the transmission estimate.

A stand-level light modeling scale can be used when edge effects are large or when the input data lack a stem map. This scale assumes the foliage is carried randomly within the horizontal space above the entire stand. It is therefore important to restrict the use of the stand-level approach to situations where random foliage across the canopy is reasonable. Gap edges and stands populated with well-spaced trees having dense crowns (i.e. northern conifer forests) have highly nonrandom leaf area distributions which must be accounted for either by the crown-scale modeling (as above) or by other techniques (e.g. Kucharik et al. 1999). Leaf area index (LAI) - measuring devices such as the plant canopy analyzer (LAI-2000, LI-COR Inc., Lincoln, Nebraska) use this model scale to calculate LAI and the mean inclination angle of the leaves from measurements of transmitted diffuse light. MIXLIGHT provides a provision to input plant canopy analyzer measurements directly.

However, since LAI measurements are seldom obtained in forest inventories, MIXLIGHT can also estimate the leaf area contained within the trees in the inventory list. Our measurements of foliage area density (F, see Results below) did not suggest a change in F_f with tree size: trees of the same species maintained a similar foliage area density regardless of their crown volume. We therefore calculated stand-level foliage area density (F_{canopy}) as the sum of the foliage area contained in each tree crown (the product of crown volume, V_j, and crown foliage density, F_j) plus one half the surface area of each stem (B_j), divided by the canopy volume (V_{canopy} = plot length × plot width × average canopy tree height × cos β, where β is the slope inclination) (Equation 2-13).

$$[2\text{-}13]\quad F_{canopy} = \frac{\sum_{j=1}^{ntrees}\left(V_j F_j + \frac{1}{2}B_i\right)}{V_{canopy}}$$

Half the stem surface area is used since the light rays can only hit one side of the stem at a time. The volume of the geometric crowns and the surface area of the paraboloid stems (B_j) were calculated using standard equations (Glover 1996).

The projection of the foliage for stand-level modeling was treated differently than for individual crowns. In order to incorporate the effect of the below-crown stems (which we treated as truncated paraboloids) the projection of a unit of canopy foliage ($G_{canopy}[Z]$) was determined separately for every zenith angle used in ray tracing (the angles used in Equations 2-3 and 2-4). Again, the foliage projection was assumed constant with respect to the azimuth.

$$[2\text{-}14]\quad G_{canopy}[\mathrm{Z}] = \frac{\sum_{j=1}^{ntrees}(V_j F_j G[\mathrm{Z}, \chi_j] + \frac{4}{3} r_j h_j \sin \mathrm{Z})}{F_{canopy}}$$

The projection fraction for each zenith angle ($G_{canopy}[Z]$, Equation 2-14), is the sum of the projected area of the crown foliage at this angle (crown volume × crown foliage area density × crown foliage projection) plus the projected area at the same angle of the below-crown stem of each tree, divided by the total one-sided foliage and stem surface area (F_{canopy}, Equation 2-13). For simplicity, we treated the stem projection as the projection of a parabola with one face to the light source, which underestimates the projected area significantly only for very small zenith angles. In Equation 2-14, r_j is the radius at the base of the paraboloid stem and h_j is the tree height.

Light transmission is calculated as for the crown-scale model, except that there is only one object (n=1 in Equation 2-2) and the path length through the canopy is simpler to determine.

If the canopy is the height of an average canopy tree (h_{canopy}) and extends 'horizontally' (or following a constant ground slope) to infinity, the path length of a ray through the canopy (S_{canopy}, Figure 2-1C) is given by Equation 2-15, where z_o is the height of the

measurement point, Z and α are the zenith and azimuth of the light ray, ϕ is the apparent slope in the α direction, and β and Ω are the slope inclination and aspect, respectively.

[2-15] $$S_{canopy} = \frac{(h_{canopy} - z_o)\cos\phi}{\cos(Z - \phi)}, \quad \phi = \arctan[\tan\beta\cos(\alpha - \Omega)]$$

Stand Level Validation

Alberta Forest Service Permanent Sample Plots (PSPs) were used to apply and test the instantaneous predictions of MIXLIGHT on a stand level. We selected 17 upland PSPs, with species compositions ranging from dominance by pure aspen, white spruce, or lodgepole pine, to mixtures of these and balsam poplar, white birch and balsam fir. These PSPs were square plots, 900 to 1600 m^2 in area, with stem densities of 335 to 1420 stems ha^{-1}, and stand age (all sites were fire-initiated) from 69 to 159 years. We sampled 16 plots during the deciduous leaf-on period (mid June - early September) in 1996 and 1997, and remeasured 8, plus 1 new one, in the leaf-off period (April 1997). Light measurements were made with the same linear radiometer as the calibration measurements, either during mostly cloudy (no direct sunlight) or mostly clear (>80% of light from the sun) periods. Light was sampled above shrub height (~1.5 m) for 36-49 points following a 5 × 5 m grid pattern. At each point, 12 light readings were taken at 30° increments while sweeping the radiometer wand around a horizontal circle at arm's length: the mean of these 12 flux density measurements was recorded. These values were expressed as a percentage of the above-canopy light averaged for five minutes before and five minutes after the within canopy value was taken. Above-canopy light was measured by a point quantum sensor (LI-190SA, Li-Cor, Lincoln, NB) and datalogger (CR21X, Campbell Scientific, Logan, UT) in a nearby clearing. These 36-49 transmission measurements were then averaged to give the stand-level light transmission value.

On sunny days, the proportion of diffuse light was determined by sampling a single radiometer sensor outside the stand with and without a shade disk before and after the plot measurements. Trees were tallied to check for new mortality or ingrowth since the last forest service inventory, and measurements were taken of height, live-crown height, crown radius and breast-height diameter (DBH) for 8-12 trees in the plot. A polynomial

regression between these crown parameters *vs.* DBH, overstory species density and composition was developed for each species (all regressions had $R^2>0.76$). For each PSP we then created a complete list of all the trees, containing species, stem position (x and y coordinates), DBH, and estimated height, height-to-live-crown, and crown radius for each tree. The tree lists were loaded into the model along with the appropriate site information (latitude, longitude, slope, aspect, plot dimensions, date and time of measurement, percentage of diffuse light at time of measurement) and the species-specific parameters (crown shape, crown foliage area density and crown foliage inclination). Canopy-scale model predictions were then compared to the measured values of light transmission on a stand-average basis.

Model Sensitivity and Foliage Inclination

The model was evaluated for the sensitivity of its light transmission predictions to the inputs on a stand level. This sensitivity analysis was performed using tree lists from 3 stand types: deciduous-dominated, mixed conifer-deciduous with some large (80 m^2) gaps, and a conifer stand. For each sensitivity run, we altered one of four key parameters across all species. These parameters were the species-specific foliage area density (F) and ellipsoidal leaf inclination parameter (χ_l), the crown radius (cr), and the crown length (cl). Note that this was a test of the sensitivity of MIXLIGHT's stand-level predictions, so varying the crown size parameters altered the model predictions through their effect on the calculated canopy foliage area and projection. They were included nonetheless, since the model is driven by these individual tree measurements. The other parameters not tested are measured with a much higher degree of accuracy (latitude, longitude, slope, aspect, plot dimensions, date and time of measurement, percentage of diffuse light at time of measurement, tree coordinates). The tested parameters were varied one at a time through a set of logarithmic multiples over seven runs: 2^{-2}, 2^{-1}, $2^{-0.5}$, 2^{0}, $2^{0.5}$, 2^{1}, and 2^{2} (25, 50, 71, 100, 141, 200, and 400% of the original value). Instantaneous light transmission predictions on cloudy (100% diffuse light) and sunny (90% direct sunlight) days were compared.

Since other models have not attempted to account for the effects of foliage inclination (Grace et al. 1987; Pukkala et al. 1993; Canham et al. 1994, Brunner 1998), and some effort is required to calibrate this parameter, we also tested MIXLIGHT on the validation sites with the foliage inclination parameter set to spherical (χ_l=1) for all species. This required small corrections to the foliage area density estimates, since they were adjusted for projection during calibration (Equation 2-8).

Results

Calibration

Calibration trees were sampled in 10 harvested areas. Generally, each species was sampled in at least at two different sites, except for lodgepole pine for which only one suitable partial-cut site was available. Tree size spanned the range of sizes which might be expected in mature stands (Table 2-1). Selection of the appropriate geometric crown shape was straightforward. Early self-pruning and die-back of the lower branches made an ellipsoid shape appropriate for the deciduous and pine crowns. Continuous branch growth with the development of a slight sag made a paraboloid fit the fir crowns well, and the rocket (cone over cylinder) shape was superior for white spruce because of the increasingly pronounced branch sag from the mid to lower crown.

Individual fir crowns transmitted the least light, followed by overstory white spruce, understory spruce, pine, and leaf-on birch, aspen, and balsam poplar (Table 2-1). During the leaf-off season, light transmission through deciduous crowns was roughly doubled. In 50 of the 57 trees sampled, and without apparent bias as to species or size, the light absorption value calculated at each measurement point within the crown shadow was significantly correlated with the calculated path length of the sun ray through the geometric crown to that point ($P<0.05$), indicating that path length can account for at least some of the variation in transmitted light. Regression analysis indicated that the effect of path length on light absorbance (-ln T) was linear, so Equation 2-8 should provide appropriate estimates of foliage area density.

Crown foliage area densities generally followed similar patterns as crown light transmission: species that transmitted little light through their crowns had the highest foliage density (Table 2-1). That this is not necessarily so is shown by birch, which, owing to the short light path through its narrow crown, transmitted more light than aspen, yet had more foliage per unit crown volume. There was no effect of stem diameter or crown volume on the foliage density within each species (data not shown); this parameter appears to be constant within the size range of trees measured. Foliage inclination, measured in leaf-on aspen and white spruce only, tended from mostly vertical for overstory spruce (χ_l=0.10 as much straight-down as sideways projection) to half as much horizontal projection as vertical (0.53) for understory spruce, to close to spherical (0.82) for aspen (Table 2-1).

Validation

MIXLIGHT predictions of instantaneous stand-level light transmission were well-correlated with measured light transmission (Figure 2-3, Pearson's r=0.86, n=25, P<0.0001). The slope of the predicted *vs.* measured relationship (1.03) for a regression constrained to pass through the origin was not significantly different from the ideal slope of 1 (P=0.5606). For some medium-light sites, MIXLIGHT predicted higher light levels than were actually measured by as much as 22% absolute transmission (44% transmission predicted for a site with 22% measured light). There was also a tendency to underestimate transmission to high-light sites (which were measured under leaf-off conditions): the worst was 48% transmission predicted for a site in which 64% was measured. The residual plot suggests a curvilinear relationship (Figure 2-2B). Indeed, a quadratic equation with intercept had a better fit (adjusted R^2=0.81) than the linear, zero-intercept equation (adjusted R^2=0.69). Analysis of the residuals from a 1:1 relationship also showed that the deviations were negatively correlated with increasing site moisture class: overstory light transmission tended to be overestimated in wetter sites and underestimated in drier sites (P=0.0065). No effect of site nutrient status was detectable (P=0.6194).

Model Sensitivity and Foliage Inclination

Results of the sensitivity analysis of MIXLIGHT at the canopy level were similar under sunny and cloudy conditions. Only the overcast day results, which had slightly more variation, are shown (Figure 2-4). Predictions were most responsive to foliage area density and crown radius. Doubling or halving the species' foliage densities (the range indicated by the calibration data, see Table 2-1) caused a change in the light prediction of about half the original transmission value in the aspen and mixedwood stands, and slightly more in the spruce stand. Crown radius had an effect on transmission roughly similar in magnitude to foliage density, but more asymmetric. An increase in radius tended to have a greater effect than a decrease, except in the spruce stand. The effect of varying the tree crown length was smaller than the effect of varying foliage density or crown radius. Changes in the foliage inclination parameter caused the least effect: even extreme (0.25-4×) variations (*e.g.* $\chi_l = 0.026$ - 0.42 for canopy spruce, and $\chi_l = 0.20$ - 3.3 for aspen) caused a change in the predicted transmission of only a relative 20% from the original transmission value.

The results of assuming the foliage inclination was spherical for all species are shown in Figure 2-5. Light in all sites was underestimated, but the relative error was particularly high for the low-light sites. Model predictions are still precise and capture slightly more of the site-to-site variation (adjusted R^2=0.82 when the spherical assumption was used, *vs.* 0.69 with the measured foliage inclination parameters), but consistently predict lower values.

Discussion

Models for predicting forest light regimes are well-developed, ranging from relatively simple stand models to complex microsite models which rely on detailed measurements of individual-crown or shoot architecture (Cescatti,1997; Brunner 1998). To our knowledge, none of these models have been extensively tested in numerous stands, a necessary prerequisite for applying a light model to track forest regeneration and stand development. This is likely due to model inflexibility or the quantity and complexity of the data required to drive these models. MIXLIGHT, on the other hand, is designed to

apply existing theory to the data presently available to a forest manager, and make understory light predictions at a scale appropriate to the data and the goals of the manager.

On the stand scale, MIXLIGHT predicts light transmission very well for a wide range of forest types during both the leaf-on and leaf-off season and under sunny and cloudy conditions (Figure 2-3A). Validation stands varied from highly structured mixtures of tree species in patches with gaps to closed, single-species, single-strata canopies. It appears that MIXLIGHT can capture much of the site-to-site variation in light transmission based on inventory data and the two species-specific foliage parameters. It should thus be an effective modeling tool for managing understory regeneration and vegetation in extensive forest areas.

For canopy-scale modeling, MIXLIGHT requires only a list of the trees, with species, stem diameter, height and crown dimensions (length and width), which are often available in standard forest inventory data, plus species-specific foliage area and inclination parameters. Stem diameter to height functions are available for tree species in many forest districts; we were also able to develop reasonable diameter to live-crown height relationships based on stand characteristics. A predictive function for crown width or radius has proved more elusive. This parameter is affected by crown abrasion from snow and wind (Grier 1988), as well as by stand density and composition. Good within-stand relationships were obtained using only stem diameter and species as predictive variables, but we are currently collecting more extensive data on crown width in hopes of developing a site-independent equation. In principle, these relationships could reduce MIXLIGHT data requirements to the two foliage parameters, site attributes (plot location and size, slope, and aspect) and a list of species with their stem diameter. The equations we used to calculate tree height, crown length, and crown radius are summarized in Appendix 6A, at the end of this thesis.

Leaf area is the most critical driving variable in light transmission modeling (Sampson and Smith 1993), but is also a difficult parameter to measure. Allometric equations are

commonly used to relate leaf area to stem diameter or sapwood area (Pierce and Running 1988; Oker-Blom et al. 1991; Pukkala et al. 1993) but require considerable effort to calibrate. Branch and stem area must be also be estimated, as these also extinguish light. Light interception techniques (Welles and Cohen 1996) provide a simpler method to estimate shading leaf, branch and stem area. Generally these techniques are applied to entire canopies, but Lang and McMurtrie (1992), Acock et al. (1994) and Villalobos et al. (1995) have demonstrated how these methods can be applied to individual plants. For small plants, particularly where the foliage distribution is non-random, this method may underestimate foliage area (Lang and McMurtrie 1992). Villalobos et al. (1995), however, found reasonable estimates of single-tree foliage area using light interception methods with larger olive trees. Our calibration trees had large (>2 m long) crowns and all species demonstrated a linear relationship between the negative logarithm of direct-beam light transmission and path length, which suggests a random foliage distribution. We did not independently verify our foliage density estimates, but our data do meet the theoretical requirements for effective estimation by the light interception technique.

Our leaf-on foliage area estimates are slightly higher than values reported for similar species. One-sided lodgepole pine needle area density, calculated from the data of Oker-Blom et al. (1991), was 0.4 - 1.8 m^2m^{-3}, which includes a lower limit than we found in our data for trees of similar crown volume. Engelmann spruce (*Picea engelmannii* Parry ex Engelm.), in the same study, had a needle area density of 0.6 - 1.9 m^2m^{-3}, while our white spruce (which are similar in profile), had a foliage area density of 0.8 - 2.6 m^2m^{-3}. Our estimates include within-crown branch and stem area, which largely accounts for the differences (Oker-Blom et al. (1991) assumed the branch area was 15% of the needle area). An interesting contrast is with the New England forest species studied by Canham et al. (1994). They report 'absolute path length extinction coefficients' which are mathematically equivalent to projected foliage area density. This parameter can be obtained from our calibration data by dividing the negative logarithm of direct-beam light transmission by path length and assuming the projection (G) remains a constant for all light source angles (a spherical distribution of foliage inclination angles). The range of projected leaf area density was 0.07 m^2m^{-3} for red oak (*Quercus rubra* L.) to 0.32 m^2m^{-3}

for white pine (*Pinus strobus* L.) while the range for our boreal species was 0.20 m^2m^{-3} for balsam poplar to 0.99 m^2m^{-3} for balsam fir. Boreal trees appear to have more compact, denser crowns.

In several validation sites, MIXLIGHT's prediction error for stand-level light transmission was nearly half the measured value. This error may be important where the goal is to determine critical light levels for the survival of particular species. Fortunately, errors of this magnitude occurred for medium to high-light sites (>14% transmission) rather than low-light sites where the relative error would be greater and where the light compensation points of boreal tree and understory species occur (*e.g.* Greenway 1994, Man and Lieffers 1997). The sensitivity analysis indicated that the prediction range corresponding to the absolute variation found in the foliage area density (0.5 - 2 times the average value, Table 2-1) was similar in magnitude to the largest prediction error for the validation (Figure 2-4). No trends were found between foliage area density and tree size or site nutrient status; however, deviations from the measured values were correlated with site moisture index. Since leaf area for aspen in particular appears to be limited by moisture (Waring and Schlesinger 1985; Messier et al. 1998), it is not surprising that wetter sites transmit less light than was predicted using the foliage area density of an 'average' tree. Fine-tuning improvements to MIXLIGHT could be made by further calibration of the species' foliage area densities for sites of different moisture index.

Light scattering may provide another source of error in the estimation of foliage area and subsequent simulation of light transmission. We assumed that the foliage elements transmit and reflect no light, but clearly this is not the case. For simulating light penetration through crowns or a canopy, neglecting light scattering should result in underestimation of the actual light transmission. In calibration, scattering would cause an underestimate of foliage area density. These effects may cancel each other; however, scattering depends on the species mix, leaf age, and leaf area as well as the solar angle (Norman and Jarvis 1975; Hutchison and Matt 1976), so its effects are complex. Hutchison and Matt (1976) suggested the contribution of beam enrichment (foliage-scattered sunlight), should be highest at high solar elevations in fully-leafed canopies (*i.e.*

at midsummer), and lowest in winter, but there is little evidence of such a trend in our data (Figure 2-3). Light scattering appears to be a relatively small component of the understory radiation in our high latitude forests.

Although canopy-scale modeling is more rapid and does not require a stem map, the assumption of random foliage distribution throughout the canopy volume is one which may not be met. The most obvious level of foliage grouping is into crowns. In quite open stands, as might occur following partial-cutting, more light would penetrate the canopy than would be predicted by a model that spreads the foliage randomly throughout the site. The concave-downward trend in our validation data (Figure 2-3) may be caused by foliage grouping in the high-light (*i.e.* open) stands. Crown-scale modeling may be more appropriate for these situations.

The sensitivity analysis illustrates the behavior of MIXLIGHT under systematic changes to its key parameters. It is clear that foliage area density and crown radius should be estimated with the most care. Crown length and foliage inclination are less critical, particularly if only a relative site-to-site comparison is required. If accurate predictions are required, however, it is clear that even foliage inclination should be measured, since setting the foliage inclination to spherical for the validation sites created a downward bias in the predictions (Figure 2-5).

MIXLIGHT provides a flexible predictive light transmission model, which predicts instantaneous stand-level light well for a wide range of stand conditions. Calibration of species' foliage area density and inclination parameters can be quickly accomplished by direct sunlight transmission measurements on isolated trees. Since so many forest processes are driven by light, we believe MIXLIGHT will provide a useful tool for evaluating stand tending and regeneration options in forests of diverse structure with limited inventory data. Work is currently under way to evaluate the microsite-level predictions of MIXLIGHT on instantaneous and long-term bases. Copies of BASIC and VisualBasic code for MIXLIGHT are available from the authors.

Literature Cited

Acock, M.C., Daughtry, C.S.T., Beinhart, G., Hirschmann, E. and Acock, B. 1994. Estimating leaf mass from light interception measurements on isolated plants of *Erythroxylum* species. Agronomy Journal 86: 570-574.

Alaback, P.B. and Tappeiner, J.C. II. 1991. Response of western hemlock (*Tsuga heterophylla*) and early huckleberry (*Vaccinium ovalifolium*) seedlings to forest windthrow. Canadian Journal of Forest Research 21: 534-539.

Anonymous 1982a. Canadian Climate Normals, Vol. 2, Temperature. Environment Canada, Atmospheric Environment Service, Downsview, Ontario.

Anonymous 1982b. Canadian Climate Normals, Vol. 3, Precipitation. Environment Canada, Atmospheric Environment Service, Downsview, Ontario.

Anonymous 1994. Ecological Land Survey Site Description Manual. Alberta Environmental Protection, Edmonton, Alberta.

Bartelink, H.H. 1998. Radiation interception by forest trees: a simulation study on effects of stand density and foliage clustering on absorption and transmission. Ecological Modelling105: 213-225.

Brunner, A. 1998. A light model for spatially explicit forest stand models. Forest Ecology and Management 107: 19-46.

Campbell, G.S. and Norman, J.M. 1989. The description and measurement of plant community structure. In: Plant Canopies: Their Growth, Form, and Function (eds G. Russell, B. Marshall and P.G. Jarvis), Society of Experimental Biology Seminar Series 31: 1-19.

Canham, C.D., Finzi, A.C., Pacala, S.W. and Burbank, D.H. 1994. Causes and consequences of resource heterogeneity in forests: interspecific variation in light transmission by canopy trees. Canadian Journal of Forest Research 24: 337-349.

Cescatti, A. 1997a. Modeling the radiative transfer in discontinuous canopies of asymmetric crowns. I. Model structure and algorithms. Ecological Modelling101: 263-274.

Cescatti, A. 1997b. Modeling the radiative transfer in discontinuous canopies of asymmetric crowns. II. Model testing and application in a Norway spruce stand. Ecological Modelling101: 275-284.

Constabel. A.C. 1995. Light Transmission Through Boreal Mixedwood Stands. MSc Thesis, University of Alberta.

Glover, T.J. 1996. Pocket Ref. Sequoia, Littleton, CO.

Grace, J.C., Jarvis, P.G. and Norman, J.M. 1987. Modeling the interception of solar radiant energy in intensively managed stands. New Zealand Journal of Forestry Science 17: 193-209.

Greenway, K.J. 1994. Plant Adaptations to Light Variability in the Boreal Mixed-wood Forest. PhD Thesis, University of Alberta.

Grier, C.C. 1988. Foliage loss due to snow, wind, and winter drying damage: its effects on leaf biomass of some western conifers. Canadian Journal of Forest Research 18: 1097-1102.

Hutchison, B.A. and D.R. Matt. 1976. Beam enrichment of diffuse radiation in a deciduous forest. Agricultural Meteorology 17: 93-100.

Hutchison, B.A. and D.R. Matt. 1977. The annual cycle of solar radiation in a deciduous forest. Agricultural Meteorology 18: 255-265.

Iqbal, M. 1983. An Introduction to Solar Radiation. Academic Press, New York.

Klinka, K., Wang, Q., Kayahara, G.J. and Carter, R.E. 1992. Light-growth response relationships in Pacific silver fir (Abies amabilis) and subalpine fir (*Abies lasiocarpa*). Canadian Journal Botany 70:1919-1930.

Kucharik, C.J., J.M. Norman, and S.T. Gower. 1999. Characterization of radiation regimes in nonrandom forest canopies: theory, measurements, and a simplified modeling approach. Tree Physiology 19: 695-706.

Lang, A.R.G. and McMurtrie, R.E., 1992. Total leaf areas of single trees of *Eucalyptus grandis* estimated from transmittance of the sun's beam. Agricultural and Forest Meteorology 58: 79-92.

Lieffers, V.J., Messier, C., Stadt, K.J., Gendron, F., and Comeau, P.G., 1999. Predicting and managing light in the understory of boreal forests. Canadian Journal of Forest Research 29: 796-811.

Lieffers, V.J. and Stadt, K.J., 1994. Growth of understory *Picea glauca*, *Calamagrostis canadensis*, and *Epilobium angustifolium* in relation to overstory light transmission. Canadian Journal of Forest Research 24: 1193-1198.

Man, R. and Lieffers, V.J., 1997. Seasonal photosynthesis responses to light and temperature in white spruce (*Picea glauca*) seedlings planted under an aspen (*Populus tremuloides*) canopy and in the open. Tree Physiology 17: 437-444.

McLure, J.W. and Lee, T.D., 1993. Small-scale disturbance in a northern hardwoods forest: effects on tree species abundance and distribution. Canadian Journal of Forest Research 23: 1347-1360.

Messier, C., Honer, T.W. and Kimmins, J.P., 1989. Photosynthetic photon flux density, red:far-red ratio, and minimum light requirement for survival of *Gaultheria shallon* in western red cedar - western hemlock stands in coastal British Columbia. Canadian Journal of Forest Research 19: 1470-1477.

Messier, C., Parent, S. and Bergeron, Y., 1998. Characterization of understory light environment in closed mixed boreal forests: effects of overstory and understory vegetation. Journal of Vegetation Science 9: 511-520.

Monsi, M. and Saeki, T., 1953. Über den Lichtfactor in den Pflanzengesellschaften und seine bedeutung für die stoffproduktion. Japan Journal of Botany 14: 22-52.

Norman, J.M. and Jarvis, P.G., 1975. Photosynthesis in Sitka spruce (*Picea sitchensis* (Bong.) Carr.) V. Radiation penetration theory and a test case. Journal of Applied Ecology 9: 747-766.

Oker-Blom, P., Kaufmann, M.R. and Ryan, M.G., 1991. Performance of a canopy light interception model for conifer shoots, trees and stands. Tree Physiology 9: 227-243.

Pierce, L.L. and Running, S.W., 1988. Rapid estimation of coniferous forest leaf area index using a portable integrating radiometer. Ecology 69: 1762-1767.

Poage, N.J. and Peart, D.R., 1993. The radial growth of American beech (*Fagus grandifolia*) to small canopy gaps in northern hardwood forest. Bulletin of the Torrey Botanical Club 120: 45-48.

Poulson, T.L. and Platt, W.J., 1989. Gap light regimes influence canopy tree diversity. Ecology 70: 553-555.

Pukkala, T., Kuuluvainen, T. and Stenberg, P., 1993. Below-canopy distribution of photosynthetically active radiation and its relation to seedling growth in a boreal *Pinus sylvestris* stand: a simulation approach. Scandinavian Journal of Forest Research 8: 313-325.

Runkle, J.R., Stewart, G.H. and Veblen, T.T., 1995. Sapling diameter growth in gaps for two *Nothofagus* species in New Zealand. Ecology 76: 2107-2117.

Sampson, D.A. and Smith, F.W., 1993. Influence of canopy architecture on light penetration in lodgepole pine (*Pinus contorta* var. *latifolia*) forests. Agricultural and Forest Meteorology 64: 63-79.

Swinehart, D.F., 1962. The Beer-Lambert Law. J. Chem. Educ. 39: 333-335.

Ter-Mikaelian, M.T., Wagner, R.G., Shropshire, C., Bell, F.W. and Swanton, C.J., 1997. Using a mechanistic model to evaluate sampling designs for light transmission through forest canopies. Canadian Journal of Forest Research 27: 117-126.

Vanclay, J.K., 1994. Modelling Forest Growth and Yield. Applications to mixed tropical forest. CAB International, Wallingford, UK.

Villalobos, F.J., Orgaz, F. and Mateos, L., 1995. Non-destructive measurement of leaf area in olive (*Olea europaea* L.) trees using a gap inversion method. Agricultural and Forest Meteorology 73: 29-42.

Wang, Y.P. and Jarvis, P.G., 1990. Description and validation of an array model - MAESTRO. Agricultural and Forest Meteorology 51: 237-280.

Waring, R.H. and Schlesinger, W.H., 1985. Forest Ecosystems: Concepts and Management. Academic Press, New York.

Welles, J.M and Cohen, S., 1996. Canopy structure measurement by gap fraction analysis using commercial instrumentation. Journal of Experimental Botany 47, 1335-1342.

Table 2-1. Calibration trees' stem and crown parameters. Data shown are minimum-maximum (mean).

					Crown characteristics					
Season	Species	# of trees	DBH[1] (cm)	Height (m)	Length (m)	Radius (m)	Shape	T_{direct}[2] (%)	Foliage area density (m^2m^{-3})	Foliage Inclination (χ_l)[3]
Leaf-on	Balsam fir	3	12-23 (17)	8.7-15.5 (11.6)	3.6-7.8 (5.6)	1.5-2.1 (1.8)	parabol-oid	9-14 (12)	1.90-2.06 (1.98)	1
	Overstory white spruce	5	39-67 (48)	20.1-28.9 (26.0)	5.9-12.1 (9.7)	1.2-2.2 (1.7)	rocket	5-28 (19)	1.32-2.56 (1.88)	0.00-0.63 (0.10)
	Understory white spruce	5	13-20 (16)	6.7-11.8 (9.4)	3.4-5.9 (4.6)	1.4-2.1 (1.7)	rocket	6-45 (24)	0.81-2.62 (1.80)	0.00-0.81 (0.53)
	Lodgepole pine	6	18-28 (23)	18.2-23.7 (20.9)	2.1-4.5 (3.3)	0.7-1.5 (1.2)	ellipsoid	23-33 (27)	1.03-1.86 (1.39)	1
	Aspen	11	25-62 (43)	21.3-28.5 (24.0)	3.4-8.9 (6.5)	1.5-4.1 (3.0)	ellipsoid	22-53 (36)	0.25-0.68 (0.44)	0.32-1.08 (0.82)
	Birch	7	8-31 (15)	9.1-24.0 (13.2)	2.8-10.3 (5.8)	1.2-3.5 (2.0)	ellipsoid	20-55 (39)	0.31-1.77 (0.80)	1
	Balsam poplar	6	12-47 (39)	8.5-27.1 (21.8)	2.9-10.0 (6.3)	1.2-3.1 (2.3)	ellipsoid	40-59 (52)	0.17-0.64 (0.30)	1
Leaf-off	Aspen	6	25-48 (36)	22.3-26.3 (23.6)	2.5-6.5 (5.2)	1.6-3.3 (2.6)	ellipsoid	66-87 (74)	0.09-0.19 (0.14)	1
	Birch	5	7-31 (20)	8.2-23.6 (14.9)	3.2-9.3 (5.7)	1.9-3.5 (2.4)	ellipsoid	70-93 (78)	0.04-0.22 (0.124)	1
	Balsam poplar	3	12-47 (31)	9.8-24.8 (18.5)	2.7-5.0 (4.1)	0.8-3.0 (2.0)	ellipsoid	74-84 (77)	0.12-0.23 (0.170)	1

[1]Diameter at breast height (1.3m).
[2]Transmission of sunlight through the crown averaged across the crown shadow.
[3]Parameter describing the relative projection of leaf area in the vertical *vs.* the horizontal direction assuming the leaves follow an ellipsoidal inclination distribution (Campbell and Norman 1989). Calibrated for the dominant trees, aspen (leaf-on, n=10), overstory (n=10) and understory white spruce (n=10), only using the data of Constabel (1995); all other species are assigned a value of 1 (foliage area inclined as if covering the surface of a sphere).

Figure 2-1. Overview of MIXLIGHT's ray tracing approach to light modeling. A) View of light rays extending from the sun and points scattered across the sky through a stand of trees to the measurement point (P_0). For clarity, only 30 rays are shown (a typical simulation uses 480). B) Transmission of a ray of light through individual crowns for microsite-level modeling, C) or through the entire canopy for stand-level modeling. The ray extends from a point in the sky to the measurement point (P_0) following zenith angle Z. Regions (crowns or canopy) that absorb light and contain a random spatial distribution of foliage area are shown in gray. The intersection points between the ray and crowns (P_{j1}, P_{j2}) are shown and the path length through each crown (S_j) or canopy (S_{canopy}) is highlighted in white. β is the slope inclination.

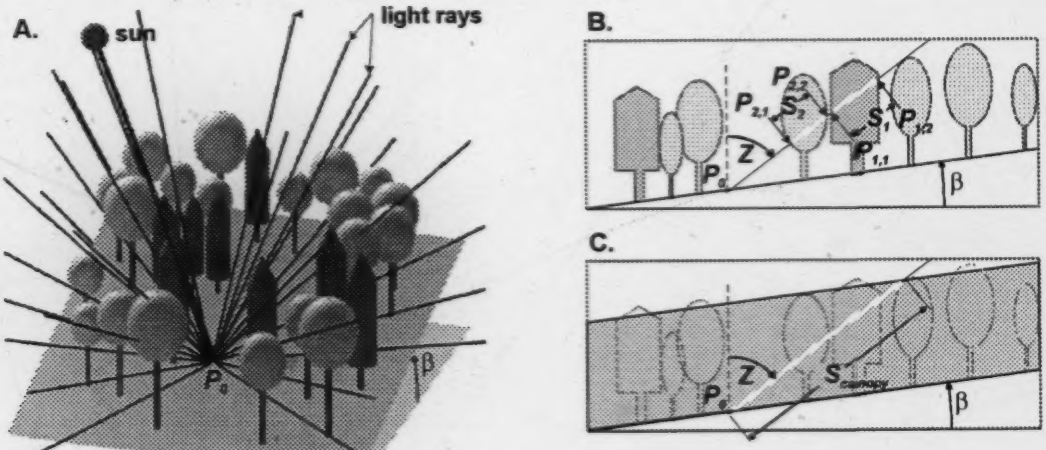

Figure 2-2. Calibration of foliage area density and foliage inclination parameters in the shadow of individual trees. A) Transect layout for rocket (shown), cylindrical, paraboloid and conical crowns. Transects originate at the central axis of the shadow and extend perpendicularly (one in each direction to the shadow edge). Measurements of shadow 'height' (h_t'), transect 'height' (h') and shadow height to live-crown (h_{lc}'), all with respect to the base of the stem, are shown. B) Transect layout for ellipsoidal crowns. Transects originate in the center of the crown shadow and extend to the shadow edge. A ray of sunlight passing through the crown to one of the transects is shown: Z is the solar zenith angle, P_1 and P_2 are the intersection points of the ray with the crown, and S is the path length of the ray through the crown. C) Detail of a single transect showing a light measurement with the radiometer wand held at right angles to the transect. θ is the angle made by the transect and the central axis of the shadow and d is the distance from the transect origin to the shadow edge.

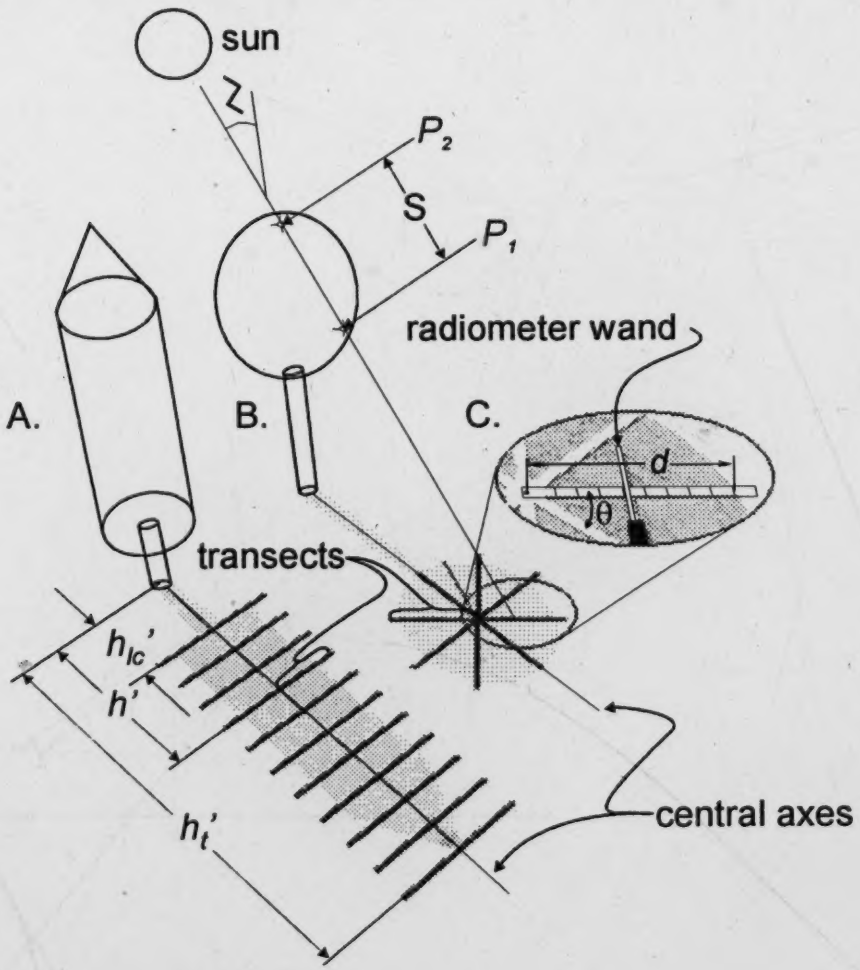

Figure 2-3. MIXLIGHT stand-level validation for 17 sites measured and modeled under various weather conditions and seasons: ○leaf-off on a sunny-day, □leaf-off on a cloudy day, ●leaf-on on a sunny day, ■leaf-on on a cloudy day. Since some sites were measured under several conditions (sun/cloud, leaf-on/leaf-off) there are 25 data points. A) Predicted instantaneous light transmission (% of above-canopy light) is compared to measured light transmission averaged across the stand. The numbers refer to the group and plot number assigned to these sites by the Alberta Forest Service. B) Residuals from a 1:1 relationship between predicted and measured light transmission.

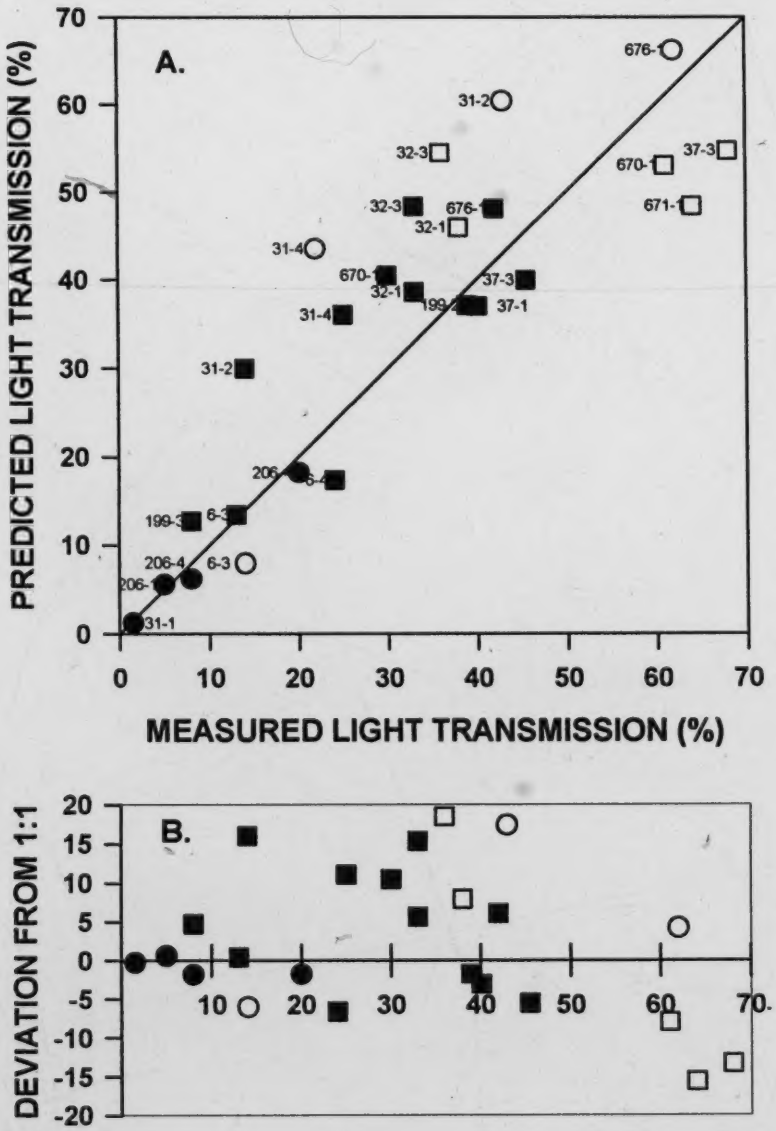

Figure 2-4. Sensitivity analysis of the (▲) foliage area density, (◆) foliage inclination, (●) crown radius and (■) crown length parameters of MIXLIGHT for three stands: A) aspen dominated, B) white spruce / aspen mixedwood with gaps, C) white spruce dominated. Parameters were multiplied by the percentage shown. Light transmission predictions are instantaneous stand-level predictions for a cloudy day during the leaf-on season.

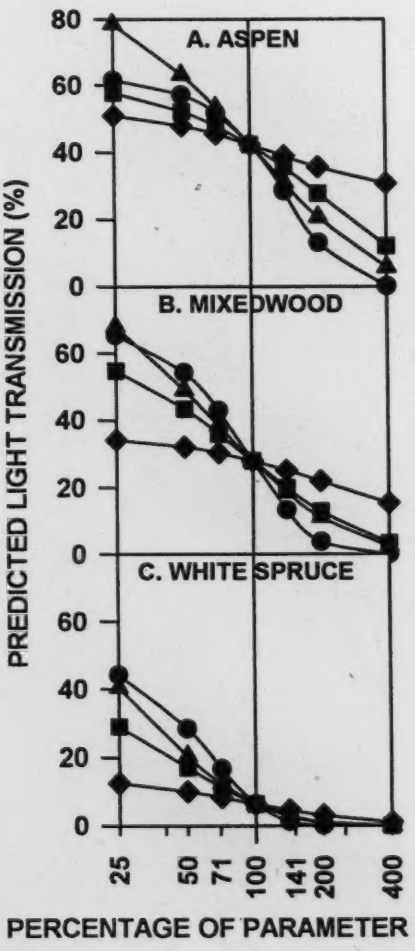

Figure 2-5. MIXLIGHT stand-level validation with the foliage inclination parameter (χ_l) set to 1 for all species. Same 17 sites as Figure 2-3, measured and modeled under various weather conditions and seasons: ○leaf-off on a sunny-day, □leaf-off on a cloudy day, ●leaf-on on a sunny day, ■leaf-on on a cloudy day. Predicted instantaneous light transmission (% of above-canopy light) is compared to measured light transmission averaged across the stand. The dotted line is the 1:1 relationship.

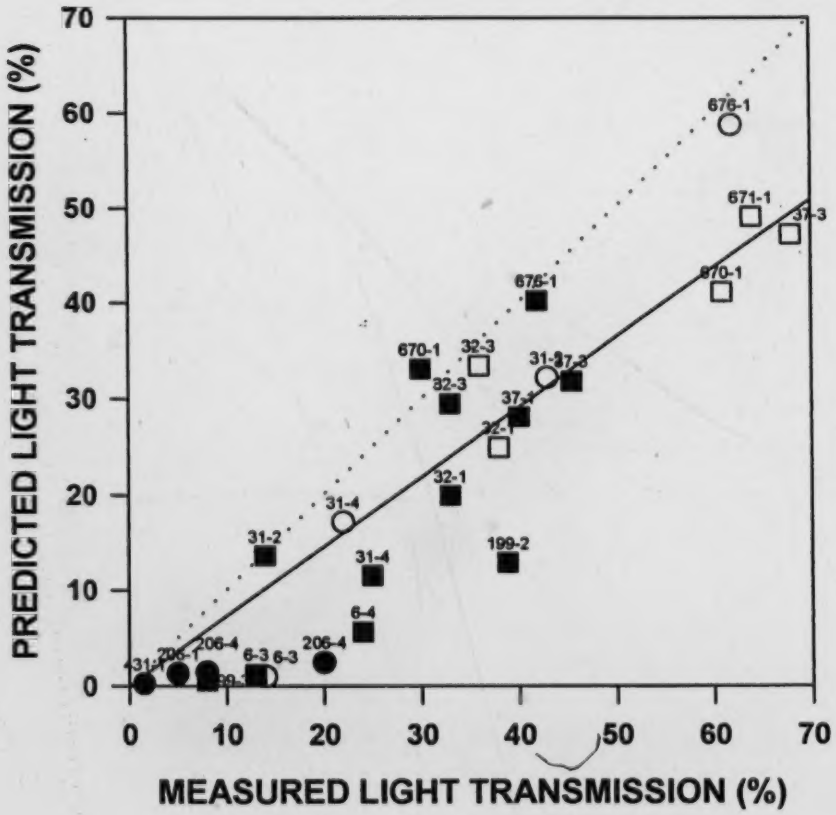

Appendix 2A. Analytical Solutions for Determining the Intersection Points of a Ray with Regular Three-Dimensional Geometric Objects

Light ray equation

The equation of a line containing the light measurement point $P_0 = (x_0, y_0, z_0)$, with vertical (zenith) angle, Z, and orientation with respect to north (azimuth), α, is given by Equation 2A-1:

$$\text{[2A-1]} \quad \begin{aligned} x &= x_o + at \\ y &= y_o + bt \\ z &= z_o + ct \end{aligned}$$

where $a = \sin \alpha$, $b = \cos \alpha$, $c = \cot Z$, and t is any real number. The y-axis increases northward, the x-axis westerly, and the z-axis upward.

Crown and stem shape equations and intersections with light rays

Conical, paraboloid, cylindrical and rocket shaped crowns are truncated at the base of the live-crown (tree base elevation plus the live-crown height ($z_b + h_{lc}$)) and the at the top of the tree (base elevation plus tree height ($z_b + h_t$), the apex of the cone or paraboloid). Crown centers (with respect to the crown length and width coordinates, not the center of mass) are at the point (u, v, w) where u and v are the x- and y-coordinates of the tree base (x_b, y_b), and $w = z_b + h_{lc} + \frac{1}{2}cl$, $cl = h_t - h_{lc}$. Stems are truncated at the tree base elevation (z_b) at the bottom and the live crown height ($z_b + h_{lc}$) at the top. To simplify calibration of the foliage area density and inclination parameters for each tree, the origin (0, 0, 0) was set to the center of the crown shadow (*i.e.* midway along the crown shadow length and midway across the crown shadow width). For predicting light in a stand, the origin was set to the center of the stand.

Functions describing the intersection between the light ray and each of the geometric shapes were generated by substituting the three elements of Equation 2A-1 into each of the shape equations (*i.e.* substitute $x_0 + t\,a$ for x, $y_0 + t\,b$ for y, *etc.*), then solving for t. Since these were lengthy equations, we used mathematical software (Maple V Release 3, Brooks/Cole Publishing, Pacific Grove, CA) to obtain analytical solutions. Below, t is expressed as a function of x_0, y_0, z_0, u, v, w, cr, cl, h_{lc} and h_t. There are always two

solutions for t, corresponding to the two intersection points. If t is a complex number (i.e. m is negative), the light ray does not intersect the shape. Substituting t back into the light ray equation (Equation 2A-1) yields the x, y, z coordinates of each intersection point. Cylinders were described by Equation A2 and their intersection with the light ray by Equation 2A-3.

[2A-2] $(x-u)^2+(y-v)^2=cr^2$

[2A-3] $$t=\frac{-x_o a+au-y_o b+bv\pm\sqrt{m}}{a^2+b^2}$$

$$m=2x_o a\,y_o b-2x_o ab\,v-2au\,y_o b+2au\,bv-a^2{y_o}^2+2a^2y_o v$$
$$-a^2v^2+a^2cr^2-b^2{x_o}^2+2b^2x_o u-b^2u^2+b^2cr^2$$

Cones were described by Equation 2A-4 and their intersection with the light ray by Equation 2A-5.

[2A-4] $$(x-u)^2+(y-v)^2=\left[cr-\frac{cr}{cl}(z-h_{lc})\right]^2$$

[2A-5] $$t=\frac{-x_o a+au-y_o b+bv-\frac{cr^2c}{cl}+\frac{cr^2z_o c}{cl^2}-\frac{cr^2c\,h_{lc}}{cl^2}\pm\frac{\sqrt{m}}{cl}}{a^2+b^2-\frac{cr^2c}{cl^2}}$$

$$m=a^2cr^2{z_o}^2-2a^2cr^2z_o h_{lc}+a^2cr^2{h_{lc}}^2+2b^2cl^2x_o u-2b^2cl\,cr^2z_o+2b^2cl\,cr^2h_{lc}+b^2cr^2{z_o}^2$$
$$-2b^2cr^2z_o h_{lc}+b^2cr^2{h_{lc}}^2+cr^2c^2{x_o}^2-2cr^2c^2x_o u+cr^2c^2u^2+cr^2c^2{y_o}^2v-2cr^2c^2y_o v$$
$$+2x_o a\,cl\,cr^2c-2x_o a\,cr^2z_o c+2x_o a\,cr^2c\,h_{lc}-2au\,cl^2y_o b+2au\,cl^2bv-2au\,cl\,cr^2c$$
$$+2au\,cr^2z_o c-2au\,cr^2c\,h_{lc}+2y_o b\,cl\,cr^2c-2y_o b\,cr^2z_o c+2y_o b\,cr^2c\,h_{lc}-2bv\,cl\,cr^2c$$
$$+2bv\,cr^2z_o c-2bv\,cr^2c\,h_{lc}+2a^2cl^2y_o v-2a^2cl\,cr^2z_o+2a^2cl\,cr^2h_{lc}+2x_o a\,cl^2y_o b$$
$$-2x_o a\,cl^2bv-a^2cl^2{y_o}^2-a^2cl^2v^2+a^2cl^2cr^2-b^2cl^2{x_o}^2-b^2cl^2u^2+b^2cl^2cr^2+cr^2c^2v^2$$

For rocket-shaped crowns we looked for intersection points with the cylinder equation between heights $z=(z_b+h_{lc})$ to $z=(z_b+h_{lc}+\frac{3}{4}cl)$. If one or both of the intersection points was higher than this, we looked for intersections with the cone equation from $z=(z_b+h_{lc}+\frac{3}{4}cl)$ to $z=(z_b+h_t)$.

Paraboloid stems and crowns were described by Equation 2A-6 and their intersection with the light ray by Equation 2A-7. For stems, r is the stem radius at the base, and l is the length of the stem ($=h_t$). For crowns, r is the crown radius (cr) and l is crown length (cl).

[2-A6] $$(x-u)^2+(y-v)^2=-\frac{r^2}{l}[z-(h_t+z_b)]$$

[2-A7] $$t=\frac{1}{2}\left(\frac{-cr^2c-2cl\,x_o a+2cl\,au-2cl\,y_o b+2cl\,bv\pm\sqrt{m}}{cl\,a^2+cl\,b^2}\right)$$

$$m=c^2r^4-4cr^2l\,au+4cr^2l\,y_o b-4cr^2l\,bv+8l^2x_o a\,y_o b-8l^2x_o abv-8l^2au\,y_o b$$
$$+8l^2au\,bv-4a^2l^2y_o{}^2-4a^2l^2v^2-4b^2l^2x_o{}^2-4b^2l^2u^2+8a^2l^2y_o v$$
$$+8b^2l^2x_o u-4la^2z_o r^2+4la^2h_t r^2-4lb^2z_o r^2+4lb^2h_t r^2+4cr^2l\,x_o a$$

Ellipsoidal crowns were described by Equation A8 and their intersection with the light ray by Equation 2A-9.

[2A-8] $$\frac{(x-u)^2}{cr^2}+\frac{(y-v)^2}{cr^2}+\frac{(z-w)^2}{(cl/2)^2}=1$$

[2A-9] $$t=\frac{\dfrac{-x_o a+au-y_o b+bv}{cr^2}-4\dfrac{z_o c-cw}{cl^2}\pm\dfrac{\sqrt{m}}{clcr^2}}{\dfrac{a^2+b^2}{cr^2}+4\dfrac{c^2}{cl^2}}$$

$$m=8c^2cr^2x_o u-4c^2cr^2u^2-4c^2cr^2y_o{}^2+8c^2cr^2y_o v-4c^2cr^2v^2-4a^2z_o{}^2cr^2+8a^2z_o wcr^2$$
$$+2x_o acl^2y_o b-2x_o acl^2bv+8x_o az_o ccr^2-8x_o acwcr^2-2aucl^2y_o b+2aucl^2bv$$
$$-8auz_o ccr^2+8aucwcr^2+8y_o bz_o ccr^2-8y_o bcwcr^2-8bvz_o ccr^2+8bvcwcr^2$$
$$+2a^2cl^2y_o v-4a^2w^2cr^2+8b^2z_o wcr^2-4b^2w^2cr^2-4c^2cr^2x_o{}^2-a^2cl^2y_o{}^2+2b^2cl^2x_o u$$
$$-4b^2z_o{}^2cr^2-a^2cl^2v^2+a^2cl^2cr^2-b^2cl^2xo^2-b^2cl^2u^2+b^2cl^2cr^2+4c^2cr^4$$

Chapter 3. A Comparison of Light Modeling Approaches Applied to Understory Vegetation in Boreal Forests of Western North America

Introduction

Forest regeneration is a complex process involving vegetation dynamics and resource availability. Models of the regeneration process are necessarily simplified and have conventionally focused on vegetation competition using empirical models (Burton 1993). Development of alternative silvicultural systems, such as partial-cut harvest practices or reliance on advanced regeneration, has required more complex models to deal with the resource demands and dynamics of the residual overstory as well the regenerating understory. With the aid of faster computers, it has been increasingly possible to model the physical and biological processes driving regeneration. Since light is often a limiting resource for understory trees, much of this work has focused on light resource modeling (Canham et al. 1994, 1999, Koop and Sterck 1994, Cescatti 1997, Ter-Mikaelian et al. 1997, Bartelink 1998, Brunner 1998, Comeau et al. 1998, Mizunaga 2000, Stadt and Lieffers 2000). These approaches have accounted for the effects of overstory tree structure on light transmission, but the effects of competing understory vegetation on light are also important, and may benefit from a similar modeling approach. The purpose of our study was to develop a predictive model for light transmission suitable for the understory species and data of the western North American boreal region.

There is a continuum of approaches for modeling light transmission through plant canopies, from empirical to theoretical. Shropshire et al. (2001) used an empirical linear regression model to predict light transmission with shrub and herb cover or projected leaf area index, the crown volume of tree saplings, and soil type. Beer's Law is often used as a quasi-theoretical model, where the extinction coefficient is related to the light source angle, leaf inclination and dispersion, but is estimated empirically from light transmission and leaf area index (LAI) measurements. Aubin et al. (2000) developed a set of extinction coefficients by this method, for understory species associated with particular forest types, life-forms and strata, to predict light transmission in boreal forests of western Quebec. Theoretical approaches attempt to explicitly model the effect on light transmission of relevant and independently measurable quantities, such as LAI, leaf inclination, light

source angular distribution, foliage spatial distribution, and foliage surface transmissivity and reflectivity. Norman and Jarvis (1975) developed such a model to predict light from measurements of these factors in single-species tree plantations. A theoretical model, with all components but surface transmission and reflection, was applied to jack pine (*Pinus banksiana* Lamb.) and competing shrubs and herbs in north-central Ontario by Ter-Mikaelian et al. (1997).

An important consideration is the type of data required to drive the model. Complex model parameters can be calibrated for a region, but subsequent local applications of the model should not require extensive inputs; i.e. if the model isn't easy to use, it won't be. Many overstory light models, and some understory models require mapped stem locations and crown dimensions. While tree mapping is tractable, mapping understory ramets at any scale larger than a small plot is tedious to the extreme. For this reason, all models tested here assume a horizontally "infinite" layer of homogeneous foliage surrounding the sampling location.

LAI is a common input variable for light transmission models. Destructive foliage sampling (Aubin et al. 2000), litter-fall traps (Vose et al. 1995), late autumn point sampling (DeLong et al. 1997), or optical instruments such as the plant canopy analyzer (LAI2000, LI-COR, Lincoln, Nebraska) or TRAC (Chen and Cihlar 1995) are common methods for determination of LAI. However, the most common vegetation data collected is percent cover. This is usually estimated visually, and can be highly subjective if the observers do not check themselves against standard plots. A point-frame (e.g. Barbour et al. 1999) provides an objective method of estimating percent cover or vertically-projected leaf area index (PLAI). Identifying species components in LAI, PLAI or cover estimates also adds considerably to the sampling time. A relevant modeling question is the cost *vs.* the benefit of collecting species-specific data.

Effective empirical models are often simplifications of theoretical models. In addition, cover, PLAI and LAI can be related, given the foliage spatial and inclination distributions. Outlining the correspondence between models and driving variables is

helpful for building and applying meaningful models, particularly when LAI data is not available.

In this study we compare theoretical and empirical models for predicting light transmission through understory vegetation and outline the relationships between them. We also present a set of calibrated parameters for models driven by LAI, PLAI and cover data for understory species typical of the western North American boreal forest.

Methods

Light and Foliage Measurements

Plots were selected in the understories of mature *Populus tremuloides* Michx., and mixed *P. tremuloides*/*Picea glauca* (Moench) Voss forest stands across west-central Alberta (53-54°N, 115-116°W). Ecosites were of the BMd, BMe, LFe, and LFf type (Beckingham and Archibald 1996, Beckingham et al. 1996,). Mean annual temperature in this region is 1 - 2°C with 465 -530 mm precipitation, most of it falling in summer (Anon. 1982a, b).

For calibrating the understory light models, pure single species plots were obtained by pruning and removing the other understory species in a 2×2 to 4×4 m area (taller understories had a wider area cleared). Removals were done with great care to minimize disturbance to the remaining species, and none of the target species was removed. Five to seven pure plots were prepared, encompassing the range of natural densities, for each of the nine most common understory species: *Alnus crispa* (Ait.) Pursh, *Corylus cornuta* Marsh., *Rosa acicularis* Lindl., *Calamagrostis canadensis* (Michx.) Beauv., *Epilobium angustifolium* L., *Viburnum edule* (Michx.) Raf., *Lonicera involucrata* (Richards.) Banks, *Aralia nudicaulis* L., and *Cornus canadensis* L. No more than two calibration plots were selected within the same stand.

Validation plots containing natural mixes of understory species were selected in three mature stands in which no calibration information had been obtained. One stand was *P. tremuloides* dominated, one was *P. glauca* dominated, and the other was a mixture of

these with a 15 m diameter gap in the center. Ten 1×1 m plots were placed randomly in each stand for light and point-frame measurements. No vegetation was removed in these plots.

Light (photosynthetically-active photon flux density, PPFD) measurements were taken on cloudy days (solar disc invisible) with an 80-sensor, 80 cm linear quantum radiometer (SF80, Decagon Devices, Pullman, WA) in both calibration and validation plots. Light was estimated by the average of eight readings of these 80 sensors, moving the radiometer ~10 cm horizontally for each reading, and thus covering a roughly 80×80 cm area. Measurements were first taken above the plot, then near ground level (5 cm), at 30, 100 and 200 cm height (to the height of the understory vegetation), then again above the plot. This entire light profile was re-measured if there was more than 10% change in the above-plot measurements. Light measurements at each level were expressed as a fraction of the above-plot (but below the tree canopy) light. A single PPFD sensor (LI190SA, LI-COR, Lincoln, NB) attached to a datalogger (CR21X, Campbell Scientific, Logan, UT) was also placed in a nearby clearing and configured to read every 10 seconds. Overstory transmission was estimated by dividing the above-plot light measurement by the datalogger reading averaged over ±3 minutes from the time of the plot measurement.

Two observers made independent visual estimates of the vertically-projected percentage of ground surface covered by foliage (total %cover), and the %cover of the woody shrub, herbaceous, and grass components. Visual estimates were made before point-frame measurements.

A 1×1 m square point frame, with 100 holes drilled on a 10×10 cm grid, was placed over the center of each plot, and a 3.175 mm (1/8-inch) diameter sharpened steel pin was lowered through 25 randomly-selected holes. For each pin drop, the number of leaf and stem hits of each species was recorded while the pin was lowered through the >200, 100-200, 30-100, and 0-30 cm height intervals. We attempted to record pin tip hits only, since the pin diameter can affect the estimation of cover and projected area (Goodall 1952). This sampling scheme was also used for the taller species (*Alnus, Corylus*), using long

legs and guy ropes to secure the point frame. The long pins required for this height were sheathed in a copper pipe above the point frame so the pin could be lowered and retracted without bending or shaking. The height of the tallest vegetation was also measured.

Percent cover was calculated as the proportion of the 25 pins that touched vegetation. Vertically projected leaf area index (PLAI) was calculated as the average number of vegetation hits among the 25 pins. We estimated horizontal foliage dispersion at this scale (10-100 cm) by the variance to mean ratio of the number of hits for the 25 pins. The theoretical 95% confidence limits associated with 25 pin-drops reach a maximum ±0.44 m^2m^{-2} PLAI at the highest PLAI measured (4.84 m^2m^{-2}), and ±20% cover at 50% cover (i.e. the 25-pin sample will give a cover estimate between 30 – 70% cover, 95% of the time), assuming a random spatial leaf arrangement. This was a compromise between precise estimation and measurement effort (a ±10% cover precision would require 100 pin drops), and was intended to be similar to visual estimation precision.

In an un-pruned area adjacent to each plot, 100 measurements were taken of the leaf inclination of the target species. A clinometer (PM-5, Suunto, Espoo, Finland) was aligned with the steepest gradient of each leaf and the inclination read to the nearest 5 degrees. Where leaf surfaces were curved (*Calamagrostis, Epilobium, Cornus*) or inclined differently on separate sides of the midrib (*Corylus*), we located the measurement randomly on each leaf, measuring the tangent on curved leaves.

Light Prediction Models and Analysis

To relate the structure of the light models, we present the more complex theoretical models first, show a number of simplifications possible within these, then present the empirical models and how they correspond to their theoretical counterparts.

Theoretical Models

Foliage (leaves and stems) absorb, transmit, or reflect incident light rays. Theoretical modeling approaches are thus concerned with the strength and angle of the incoming light as well as the amount, spatial distribution, angle, transmissive and reflective

properties of foliage surfaces. In the photosynthetic waveband, leaf surface transmissivity and reflectivity are relatively low (typically < 0.10, Knapp and Carter 1998) so foliage is often treated as a perfect absorber. With this "black leaf" assumption, light transmission (T), the ratio of measured (Q) to above-understory PPFD (Q_i), can be modeled using Equation 3-1.

$$[3\text{-}1a]\quad T = \frac{Q}{Q_i} = \frac{\sum_{a=1}^{n\alpha}\sum_{z=1}^{nZ} \omega(a,z)\, p(0;\alpha_a, Z_z) \sin Z_z \cos Z_z}{\sum_{a=1}^{n\alpha}\sum_{z=1}^{nZ} \omega(a,z) \sin Z_z \cos Z_z}$$

$$[3\text{-}1b]\quad \alpha_a = \frac{a}{n\alpha} 2\pi$$

$$[3\text{-}1c]\quad Z_z = \frac{z}{nZ} \frac{\pi}{2}$$

Equation 3-1 represents a simplified ray-tracing algorithm, which starts from many points on the overlying hemisphere and traces nα (number of azimuth angles) × nZ (number of zenith angles) rays to the forest floor, calculating the effect of intervening foliage on light transmission. Here, α is the azimuth of the light ray, Z is its zenith (angle from vertical), a and z are indexes for the azimuth and zenith, $\omega(a, z)$ is the "brightness" (relative quantum radiance) of the part of overlying hemisphere where the ray originated, and $p(0; \alpha_a, Z_z)$ is the probability this light ray will not hit any foliage. Each ray is weighted by the sine of the zenith angle, since incrementing over the zenith samples the vertical region of the sky more heavily than the area near the horizon. The cosine-zenith term adjusts the ray radiance to its value through a horizontal plane. We used 20 rays for these overcast-day simulations (1 azimuth and 20 zenith angles).

The angular radiance distribution, $\omega(a, z)$, is contained in a 2-dimensional matrix with rows and columns corresponding to the number of azimuth and zenith angles used. Values for each $\omega(a, z)$ cell can be generated using the start and end dates of the simulation period, the latitude of the site, the fraction of diffuse radiation received over the period, and the distribution of diffuse radiation across the sky (Stadt and Lieffers

2000, a similar approach is outlined in detail by Smolander and Stenberg 2001). However, for understory work, the fine-scale patchiness of the light transmitted through the overstory canopy on sunny days makes it difficult to compare above and below understory vegetation light measurements. The solar angle and sunfleck pattern is such that these may receive very different levels of incident light. We limited our measurements to fully overcast days when patchiness was much reduced, and the distribution of incoming light with respect to azimuth was more-or-less equal. We used the "standard overcast sky" radiance distribution of Steven and Unsworth (1980), with 2.23 times more light coming from the vertical compared to the horizon (first term of Equation 3-2). This distribution was close to our own measurements of overcast skies. Since there is no dependence on azimuth in this case, evaluation over the azimuth can be left out of these equations (Equations 3-1, 3-2 and 3-4). The effect of the overstory was also incorporated, assuming a homogeneous layer of overstory leaf area. The distance a light ray must travel to pass through this layer increases as 1/cosZ with the angle of the ray, and its extinction was modeled as a Poisson process (the second term of Equation 3-2). The LAI and inclination of the overstory foliage affects the distribution as well (Figure 3-1). We tested two extremes and an intermediate set of parameters representing the range expected in boreal mixedwood overstories: an LAI of 1 and inclination parameter (χ, see below) of 0.5, an LAI of 3 with χ=1, and an LAI of 6 with χ=2.

[3-2] $$\omega(a,z) = (1 + 1.23\cos Z_z)\exp\left(-G\left[Z_z;\chi_{overstory}\right]/\cos Z_z LAI_{overstory}\right)$$

To examine the effect leaf surface transmissivity and reflectivity could have on light transmission through understory vegetation, we simplified the multi-layer model of Norman and Jarvis (1975). This approach divides the total leaf area into many layers (we used 20), each with a small enough fraction of the total leaf area that the probability of a light ray hitting more than one leaf is small. For each layer (m), downward (T_m) and upward transmission (T'_m) are calculated as in Equation 3-1, with the LAI contained in layer m only and the incoming angular distribution specific to this layer and direction (see below). Then, ($1-T_m$) is the average probability the light rays will hit a single leaf. Above

each layer, the downward (Q_m) and upward (Q'_m) light fluxes are adjusted to include the light transmitted between leaves (T_m, T'_m) plus the light provided by the transmissivity (τ), or reflectivity (ρ), of leaf surfaces hit in the adjacent layers (Equation 3-3).

[3-3a] $$Q_m = Q_{m+1}T_{m+1} + Q'_{m+1}(1-T_{m+1})\rho + Q_m(1-T'_{m+1})\tau$$

[3-3b] $$Q'_m = Q'_{m-1}T'_m + Q_m(1-T_m)\rho + Q'_{m-1}(1-T'_m)\tau$$

Note that when τ and ρ are zero ("black-leaf" models), the light flux only depends on transmission through the overlying layers, so these can be collapsed into the single layer approach represented by Equation 3-1. The downward light flux above the canopy (Q_{20}) was set to 1, so that the downward flux at any level (Q_m) represents the overall transmission through overlying vegetation. There was no direct-beam sunlight, so this component of Norman and Jarvis' (1975) model was omitted.

Each layer alters the incoming radiance distribution as well. Norman and Jarvis' (1975) formulation (their equation 3-8) caused the distribution to skew toward wide zenith angles, which results in an undesirable decrease in cloudy-day ground-level light transmission when leaf transmissivity and reflectivity were added. Since light scattering by leaf surface transmissivity and reflectivity should only have a minor effect on a layer's angular radiance distribution, we removed these from their equation. A downward ($\omega_m[a, z]$) and upward ($\omega'_m[a, z]$) radiance distribution was calculated for each layer, using Equation 3-2 for the downward distribution above the understory, an isotropic upward distribution above the soil ($\omega'_0[a, z]=1$), and Equation 3-4 for intermediate layers.

[3-4a] $$\omega_m(a,z) = \omega_{m+1}(a,z)p_{m+1}(0;\alpha,Z)$$

[3-4b] $$\omega'_m(a,z) = \omega'_{m-1}(a,z)p_m(0;\alpha,Z)$$

The light fluxes were estimated sequentially from the top layer to the soil layer (with $\tau_0=0$ and $\rho_0=0.1$), and then back up again. This process was iterated until there is no substantial change in any of the upward or downward fluxes. Since our downward and upward radiance distributions are not affected by foliage scattering, there was no need to

recalculate them after each iteration as in Norman and Jarvis's (1975) original model. We tested the multi-layer model with our leaf area, clumping and inclination data, and the range of leaf PPFD transmissivity and reflectivity values reported by Knapp and Carter (1998) for 26 species of the midwestern USA.

Foliage was assumed to incline as if covering the surface of an ellipsoid (Campbell and Norman 1989). We assumed there was no preferred azimuth orientation of the foliage, so the distribution is controlled by one parameter, χ, the ratio of vertical to horizontal projections of the ellipsoid. The distribution function of the foliage surface inclination angle (θ), is $g(\theta,\chi)$ (Equation 3-5), and the projected area of a unit of foliage surface area in the given direction (Z), is $G(Z,\chi)$ (Equation 3-6).

[3-5a] $$g(\theta,\chi)=\begin{cases}\dfrac{2\chi^2\sin\theta}{A\left(\cos^2\theta+\chi^2\sin^2\theta\right)^2} & \text{if } \chi\neq 1\\ \sin Z & \text{if } \chi=1\end{cases}$$

[3-5b] if $\chi<1$, $$A=1+\frac{\ln[(1+\varepsilon)/(1-\varepsilon)]}{2\varepsilon\chi^2},\ \varepsilon=\sqrt{1-\chi^{-2}}$$

[3-5c] if $\chi>1$, $$A=1+\frac{\sin^{-1}\varepsilon}{\chi\varepsilon},\ \varepsilon=\sqrt{1-\chi^2}$$

[3-6] $$G[Z,\chi]=\begin{cases}\dfrac{\sqrt{\chi^2\cos^2 Z+\sin^2 Z}}{A} & \text{if } \chi\neq 1\\ \frac{1}{2} & \text{if } \chi=1\end{cases}$$

A is as in Equation 3-5

A frequent assumption, when inclination data are not available, is that the foliage inclines as if covering a sphere. In this case χ=1. To provide an easier visualization of the degree of inclination of the leaves, the mean tilt angle (MTA) of the distribution was also calculated using Wang and Jarvis' (1988) approximation.

The ellipsoidal distribution was fit to the leaf inclination angle data by a maximum likelihood approach. The distribution function given by Campbell and Norman (1989) (Equation 3-5 is not a probability density function (*pdf*), since the area under the distribution is not equal to one for all χ values. To normalize the function, we divided the predicted frequencies for each five-degree leaf angle class (θ_5) by the sum of the predicted frequencies of all 18 classes (from 0 to 90°; Equation 3-7).

[3-7] $$pdf(\theta_5,\chi) \approx \frac{g(\theta_5,\chi)}{\sum_1^{18} g(\theta_5,\chi)}$$

The ellipsoidal χ parameter was then estimated by maximizing the joint probability (the likelihood) of this pdf, given the data. This means finding χ where the log likelihood function (*ln L*, Equation 3-8) is maximized (Hogg and Craig 1995).

[3-8] $$\ln L = \sum_1^n \ln pdf(\theta_5,\chi)$$

To accomplish this, we started with an initial χ parameter guess of 1, then used Newton's method, embedded in Excel Solver (Microsoft Inc., Redmond, WA), to find the χ which maximized Equation 3-8, given each leaf angle measurement in the plot (n=100). One χ parameter was estimated in this fashion for each plot, and plot values were then averaged for the species. One-way analysis of variance (ANOVA) was used to detect differences in χ among species.

The probability of each ray penetrating the vegetation without hitting foliage, $p(0; \alpha, Z)$, can be estimated by a Markov process (Equation 3-9) (Nilson 1971).

[3-9] $$p(0;\alpha,Z) = \prod_{i=1}^{\#\ of\ species} \exp\left(-\Omega_i \frac{G[Z;\chi_i]}{\cos Z} LAI_i\right)$$

Equation 3-9 accounts for the degree of clumping of foliage (Ω), the projection of the foliage in the ray direction ($G[Z;\chi]$), the effect of the overlying foliage area (LAI), and adjusts for the increasing length the ray has to travel to pass through the vegetation at wider angles ($1/\cos Z$).

The degree of clumping is related to the variance:mean (σ^2/μ) ratio of the number of foliage layers which could be hit by a light ray. Since pin-drops act like light rays coming

straight down (i.e. Z=0), σ^2/μ can be estimated by the mean and variance of the number of hits made by the 25 pins. For a random horizontal distribution, the probability of hitting a leaf is Poisson distributed, with the variance equal to the mean. Therefore, σ^2/μ=1 for random foliage, σ^2/μ>1 for clumped foliage, and σ^2/μ<1 for repulsed foliage (Nilson 1971). Ω was calculated using Equation 3-10 (derived from Nilson 1971), which is suitable for random or clumped foliage distributions.

[3-10] $$\Omega = \frac{2}{\left(1+\sigma^2/\mu\right)}$$

Chen and Cihlar's (1995) "effective LAI" is the product of the clumping parameter and the LAI. Another frequent model assumption is that the foliage spatial distribution is random. In this case Ω=1, and Equation 3-9 becomes a Poisson process.

Recent work by Kucharik et al (1999) suggests that Ω for boreal overstory trees should depend on zenith angle since there is marked clumping of foliage into distinct crowns when the forest is viewed vertically (looking up), but a near-random distribution when viewed horizontally. The same argument is more difficult to make with the interlaced foliage of understory vegetation. For this study, we assumed that clumping does not change with viewing zenith. This can be visualized as leaf aggregation into randomly positioned, spherical clumps.

Equation 3-10 considers foliage clumping within a species, and is related to that species' ramet distribution and branching pattern. The response of each branch "module" to the local light resource is important (Sorrensen-Cothern et al. 1993). This could be theoretically extended to foliage dispersion interactions among species, but is difficult to estimate for all species combinations. We assumed a random dispersion among species (implicit in Equation 3-9), but examined the variance:mean ratios from pin-drop data in undisturbed, mixed-species validation plots to evaluate the importance of interspecific dispersion.

The probability of non-interception in the given direction, $p(0; \alpha, Z)$, is also called the gap fraction. A special case is when the ray is vertical: then $p(0; \alpha, Z=0)$ is the vertical

gap fraction, which is one minus the cover fraction. Thus, it is possible to convert measurements of PLAI or vegetation cover to LAI for computing light on a theoretical basis. Rearrangements of these equations to estimate LAI for use in Equation 3-9 are given below (Equations 3-11, 3-12).

[3-11] All spatial distributions: $$LAI = \frac{PLAI}{G(Z=0;\chi)}$$

[3-12] Random or clumped spatial distributions: $$LAI = \frac{-\ln\left(1-\frac{\%cover}{100}\right)}{\Omega G(Z=0;\chi)}$$

If light comes from only one direction, light transmission is the probability of not hitting foliage in this direction (Equation 3-13).

[3-13] $T = p(0;\ \alpha_a,\ Z_z)$

For instantaneous measurements on sunny days, a large proportion of the light does come from one direction, the sun, while, on cloudy days, more light comes from the upper sky than the horizon, particularly if a dense overstory removes much of the low-angle light (Figure 3-1).

Unidirectional light is a reasonable simplifying assumption to test. Since we had overcast day measurements, we tested a set of models with a vertical light source (Equations 3-9 and 3-13 for LAI, Equations 3-9, 3-11 and 3-13 for PLAI, with the zenith set to zero). For cover data, light coming only from the vertical means that transmission should be equal to the vertical gap fraction (simplifying Equations 3-9, 3-12, and 3-13). If the cover data are subdivided by species, and each component is spatially independent of the next, then transmission should be equal to the product of the component gap fractions (Equation 3-14).

[3-14] $$T = \prod_{i=1}^{\#\ of\ species}\left(1-\frac{\%cover_i}{100}\right)$$

Empirical Models

Beer's Law was also developed for modeling transmission of unidirectional light (Equation 3-15).

$$[3\text{-}15]\quad T = \prod_{i=1}^{\#\ of\ species} \exp\left(-\kappa_i LAI_i\right)$$

$$[3\text{-}16]\quad T = \prod_{i=1}^{\#\ of\ species} \exp\left(-\beta_i PLAI_i\right)$$

A common approach to fitting Beer's Law is by estimating the parameters using transmission and LAI data. We used iterative least-squares to do this, with PLAI (Equation 3-16) as well as LAI (Equation 3-15) as the independent variable. Since we had pure-species plots, we regressed each species separately, as well as fitting a single regression line to all species. A test for coincident regression lines (Zar 1999) was used to determine if there was a significant improvement in the residual mean square when coefficients were fit for each species.

Beer's Law extinction coefficients, κ_i and β_i, are a "catchall" adjustment for leaf spatial dispersion, leaf inclination and the light source zenith angle, as can be seen by comparing Equations 3-15 and 3-16 with Equation 3-9. The LAI κ_i coefficient should be equal to $\Omega_i G(Z,\chi_i)$, or $\Omega_i G(Z=0,\chi_i)$, if the light source is primarily from the vertical and foliage transmissivity and reflectivity are unimportant. With PLAI data, leaf inclination is partially accounted for since PLAI is the vertical projection of LAI (perfectly accounted for if the light is only coming from the vertical), so the coefficients derived from fitting transmission vs. PLAI data should primarily reflect the degree of clumping, i.e. $\beta_i=\Omega_i$.

For cover data, we constructed an empirical equation 3-to allow departures from a direct relationship between transmission and cover (Equation 3-17). At 0% cover, the light transmission fraction will always be 1 (100%), so the equation 3-was constrained to pass through this point. If the light source is indeed vertical and foliage transmissivity and reflectivity are unimportant, the parameter η_i should approach one. Equation 3-17 was fit to the calibration data for each species, as well as to all calibration data (ignoring species)

by linear regression with a restricted intercept. A test for coincident regressions was used to detect species effects (Zar 1999).

$$[3\text{-}17]\quad T = \prod_{i=1}^{\#\ of\ species} \left[1 - \eta_i \left(\frac{\%\ total\ cover}{100}\right)\right]$$

Height Profiles

The vertical distribution of foliage area and cover control the light transmission profile with height. To model this vertical profile, we expressed the PLAI of each species overlying the current height as a fraction of the species' total PLAI ($TPLAI_i$, the species' PLAI from the ground up). Measurement heights (h: 0, 30, 100 and 200 cm) were expressed as a fraction of the species top height (H_i). A single vertical leaf area distribution parameter (ν_i) was fit for each species by iterative least-squares, using the cumulative distribution function shown in Equation 3-18. This relative leaf area vs. relative height approach allowed us to develop standardized vertical leaf area distributions for each species, regardless of microsite effects on leaf area and height.

$$[3\text{-}18]\quad \frac{PLAI_i}{TPLAI_i} = \begin{Bmatrix} \dfrac{1 - h/H_i}{1 + \nu_i (h/H_i)} & if\ 0 \le h \le H_i \\ 0 & if\ h > H_i \end{Bmatrix}$$

The same distribution was used to characterize overlying understory LAI or cover. Equation 3-18 was rearranged to predict the overlying PLAI (or LAI or cover), and measured light profiles were compared to model predictions at the four measurement heights.

Summary and Model Evaluation

We evaluated three general types of light transmission models. The theoretical models' parameters were obtained entirely by measurement of foliage properties (although statistical methods were used to consolidate measurements) while the empirical models had coefficients fit by least-squares, using functions relating foliage area or cover measurements to measured light. The models were, in order of decreasing complexity,

1) theoretical multi-layer model for foliage transmissivity and reflectivity

2) theoretical single-layer models, "black" leaves
3) empirical models (Beer's Law and the cover model)

We tested the theoretical models initially with three overlying radiance distributions (SOC sky with three types of overstory). In addition, the black leaf models were tested with a vertical light source. We tested all models with three measures of foliage area or cover (LAI, PLAI, and %cover); with three types of ellipsoidal foliage inclination distirbutions: the inclination parameter (χ_i) determined for each species, a spherical inclination (χ_i=1), and the average inclination parameter for these species; and with three types of foliage spatial distribution information: the degree of clumping (Ω_i) measured for each species, a random distribution (Ω_i=1) and the average clumping measured for these species. There were fewer models than a fully factorial design would suggest. LAI was calculated from PLAI using the foliage inclination information (Equation 3-11), so the theoretical LAI and PLAI models give the same results. The "spherical" approach to clumping used here means %cover data implicitly account for foliage spatial distribution (substitute Equation 3-12 into Equation 3-9 and the Ω terms disappear). Also, for the vertical light source models, foliage inclination does not affect the results for cover data so fewer models are tested. Table 3-2 and 3-3 show the models and their associated equations.

For each model, the prediction accuracy (bias) and precision were calculated from the mean and standard deviation of the residuals (the measured transmission measurement subtracted from the model estimate). Empirical models should show no bias for predictions using their calibration data because least-squares fitting generally yields unbiased predictions, but the other models rely on measurements of foliage parameters rather than coefficient-fitting, and bias will indicate problems in the models' structure. Similarly, prediction bias and standard error were calculated using data from the 30 validation plots. The validation plots provide an additional check on model predictions, to ensure the results we obtained were not due to the calibration plot selection and preparation.

All models were evaluated with ground-level cover, PLAI, LAI and light transmission data. The most promising model was tested using the vertical distribution function at the other measurement heights (30, 100 and 200 cm).

Statistical analyses were performed using the correlation, regression, general linear models, and nonlinear regression procedures in SAS version 8e, (SAS Institute, Cary, NC). Significance was defined at the 5% level.

Results

Light and Foliage Measurements

There was almost no bias in our visual cover estimates compared to the pin drop method (Figure 3-2). A regression line fit to this data had an intercept equal to zero and a slope slightly less than one. Mean estimation error for the data (visual estimate minus pin estimate) was –3%, with a standard deviation of 14%. The 95% confidence limits of the visual cover estimates (±2 standard deviations = 28% cover) appear larger than the theoretical confidence limits for the 25-pin sample (max ±20% cover), but the error in the point-frame estimates will inflate the apparent visual estimation error, as the true cover is not known. Since there were no substantial differences between visual and point-frame cover, and since visual estimates are more commonly used, only the results using visual cover are presented throughout the following analysis.

The ground-level light transmission fraction decreased from 1.00 to 0.02 (100 – 2 % of above-understory light) as vertically-projected leaf area index (PLAI) increased from 0.08 to 4.84 m^2m^{-2}, leaf area index (LAI) from 0.09 to 6.31 m^2m^{-2}, and cover from 8 to 100% among the calibration plots for all species (Table 3-1, Figure 3-3). Transmission decreased in a log-linear fashion with increasing PLAI and LAI, and in a linear fashion with cover (Figure 3-3).

All species tended toward a planophile inclination and clumped foliage distribution but differed in their degree of these display characteristics (Table 3-1). There was a significant difference among species for the leaf inclination parameter (χ_l, one-way

analysis-of-variance (ANOVA) $p<0.0001$) and for the vertical projection of this inclination distribution ($G[Z=0,\chi_i]$, one-way ANOVA $p<0.0001$). The species with the shortest stature tended to have the most horizontal mean tilt angles (*Cornus, Aralia*), but inclination did not increase consistently with stature. The grass, *Calamagrostis*, had the most spherical leaf angle distribution, but the tallest species (*Alnus, Corylus*) had more horizontal leaves than mid-height *Lonicera, Viburnum* and *Calamagrostis*. All species exhibited PLAI variance:mean ratios (σ^2/μ) greater than one, indicating foliage clumping at the scale we measured (10-100cm) (Table 3-1). There were significant differences in σ^2/μ and Ω_i among species (one-way ANOVA $p<0.0001$ for both). The variance:mean ratio was least (most close to random) in the shortest species (*Aralia, Cornus*) and generally increased with species stature. However, *Epilobium* foliage was the most clumped, owing to its columnar growth form. In the mixed-species validation plots, the variance to mean ratio for all pin hits on all species' foliage varied from 0.56 to 1.95, with a mean of 1.04.

There were significant differences among species in Beer's Law extinction coefficients and cover model coefficients (*F* test for coincidental regressions: LAI $p=0.05$, PLAI $p=0.03$, cover $p=0.0004$). LAI and PLAI Beer's Law coefficients, generated for each calibration plot by inversion of Equations 3-15 and 3-16, were not significantly correlated with the vertical projection of the plot's inclination parameter ($G[Z=0,\chi_i]$) (LAI $r=-0.13$, PLAI $r=-0.20$), the plot clumping parameter (Ω_i) (LAI $r=0.10$, PLAI $r=0.17$) or the product of these two values ($\Omega_i G[Z=0,\chi_i]$) (LAI $r=-0.23$, PLAI $r=-0.25$) (the critical r value for $n=57$ is 0.26 at $\alpha=0.05$).

Overstory light transmission was well correlated with the total understory cover estimate (all species) in the undisturbed validation plots ($r=0.69$), as well as the total PLAI ($r=0.66$) and LAI ($r=0.64$). Overstory transmission was also weakly correlated with the variance to mean ratio ($r=0.29$), the inclination parameter ($r=-0.36$), and the PLAI and LAI Beer's Law coefficients ($r=0.31$, $r=0.28$), but not the empirical cover coefficients ($r=0.23$) calculated from individual calibration plots ($n=57$, critical $r=0.26$).

Light Prediction Models

The three above-understory angular radiance distributions tested (Figure 3-1) had very little effect on model predictions. The flattest distribution ($LAI_{overstory}$=1, $\chi_{overstory}$=0.5) worsened the transmission fraction underestimation for some of the models by 0.01 (1%) over the other angular distributions, and did not affect the precision. Results shown in Table 3-2 and Figure 3-4 are for the intermediate distribution ($LAI_{overstory}$=3, $\chi_{overstory}$=1).

For calibration data, the theoretical models underestimated the light transmission fraction by -0.06 to -0.26 (i.e. 6-26% transmission). The full, multi-layer, LAI or PLAI-based model, which accounted for the overlying radiance distribution, leaf transmissivity and reflectivity, and foliage clumping and inclination, gave the lowest prediction bias of the theoretical models (-0.06). If we assumed spherically inclined, randomly distributed foliage, the model underestimated transmission by -0.20. However, with the average inclination and clumping parameters, underestimation was better, at -0.07.

Treating the canopy as a single layer of black leaves caused a transmission underestimate of -0.11 for LAI and PLAI data with the SOC sky, intermediate overstory, and species-specific foliage display information, -0.05 worse than the equivalent multi-layer model. A spherical leaf inclination and random spatial distribution made the model underestimate transmission much worse (-0.24), but, with the average inclination and clumping values, the model's estimates were nearly identical to the species-specific model.

The black leaf models that used a vertical light source made very similar predictions as when the SOC sky with intermediate overstory was used. Also, the effect of using a random spatial distribution was to generate a large underestimate in transmission (the inclination distribution did not affect this model). Using average parameters for clumping gave nearly the same values as the species-specific model.

Theoretical cover-based models showed similar patterns as the PLAI/LAI models, except the underestimates tended to be 0.05 to 0.06 worse than their PLAI/LAI counterparts. Again, the species-specific models made nearly identical predictions as the species-

average models. The "default" assumption (spherical inclination) did not cause as poor underestimates as in the PLAI/LAI models. This is largely because this is the effect of the inclination distribution, not the effect of clumping, as here cover data already account for effects of spatial distribution (see Methods).

The empirical models all show negligible bias, and residual standard deviations of 0.09-0.15. The species-specific models had less variation than the models using average coefficients by 0.02-0.04. The LAI and PLAI models were similar in precision, as was the species-specific cover model. The species-average cover model showed the largest prediction error (0.15).

In the independent and undisturbed validation data, there were other species encountered other than the nine selected for calibration. Overall, the calibration species made up 72% of the total pin-hits in the validation data. However, there were three plots where other species made up more than 50% of the PLAI. These were not outliers in any of the model estimates. However, it is not surprising that the models yielded predictions with more bias in the validation plots than in the calibration plots. These were also nearly all underestimates (Table 3-2). Validation bias was smaller for the empirical models compared to the theoretical approaches.

The vertical distribution function (Equation 3-18) fit the relative leaf area vs. relative height data for each species well (Table 3-1, Figure 3-5), with residual standard errors of 0.04 to 0.13 (4-13% of the total PLAI). When this vertical distribution was applied with the species' top height, foliage area or cover, and a light transmission model, predicted light transmission at heights > 0 had only marginally greater bias and standard error as at ground-level (Figure 3-6).

Discussion

In terms of accuracy and precision, the best models for predicting light transmission through understory vegetation used empirically-fitted Beer's Law coefficients based on leaf area index (LAI) or projected leaf area index (PLAI). The predictions of an empirical

cover-based model were almost as effective (Table 3-3). The least squares fitting procedure ensured unbiased estimation; this was corroborated by the relatively small bias of these models in validation plots (Table 3-3, Figure 3-4). With these models, light could be predicted with little bias and with as little or less residual error as the theoretical models over a wide range of PLAI and species-specific leaf inclination and dispersion (Tables 1-3).

The "catchall" coefficients of the empirical approach (Table 3-3) appear to adequately absorb the effects of light source angular distribution and leaf inclination, clumping, transmissivity and reflectivity. Interestingly, the expected correspondence between the coefficients of the Beer's Law models and the foliage clumping parameter (Ω_i) or the product of clumping and vertical projection of the foliage inclination ($\Omega_i G[Z=0,\chi_i]$, see Methods) were not significant. In addition, the empirical cover model coefficients were less than one. This suggests that the above-canopy radiance distribution is not sufficiently skewed to the vertical for these relationships to hold, or that foliage surface transmissivity and reflectivity play a significant role in determining the size of these coefficients. Generally, the theoretical models did not perform as well as the empirical. They tended to underestimate light, with larger errors at mid to low light levels (Table 3-2, Figure 3-4). Residual variation was comparable or higher than the empirical models. Not surprisingly, simplifying the light penetration model tended to increase the prediction bias. The simplest PLAI or LAI-based theoretical model, which assumed a vertical light source, a spherical distribution of foliage inclination, a random spatial arrangement, and no transmission or reflection of light by foliage surfaces, underestimated transmission by 0.18. Including the species-specific information (only foliage clumping affected this model), or using the average clumping index (Ω) for these species brought the bias up to a more reasonable 0.10. No improvement was gained when the light source was distributed as a standard overcast sky with an intermediate overstory (Figure 3-1), although adding species-specific or species-average foliage information improved the black-leaf models using this radiance distribution. Lastly, modeling foliage transmissivity (τ) and reflectivity (ρ) improved the estimates further. We did not measure species-specific foliage transmissivity or reflectivity, but the highest values from the ranges

reported by Knapp and Carter (1998) ($\tau = 0.12$, $\rho = 0.14$) brought predicted transmission near the measured transmission values. Since our nine boreal understory species are relatively thin-leaved, high transmissivity values are reasonable. Reflectivity is less likely to be high, but the multi-layer model was considerably less sensitive to the reflectivity parameter (data not shown).

A limitation of Norman and Jarvis' (1975) multilayer scattering model is that each successive layer is independent of the others. Thus, although clumping can be modeled within a given layer, using the Markov approach (Equation 3-9), clumping that extends across several layers is not captured by this model. Clumping resulting from having fairly large leaves may thus be adequately modeled, but clumping of multiple leaves into branch units and ramets may not be captured.

Within the black-leaf models (τ, $\rho = 0$), the additional complexity of carrying out numerical integration of the light transmission equation (Equation 3-1) across a standard overcast sky with an intervening overstory canopy was not warranted for overcast conditions (Figure 3-4 A, B). This may be due to the above-understory radiance distribution being skewed toward the vertical (Figure 3-1). The near-horizontal foliage of many of these species also tends to make integration unnecessary, as Oker-Blom (1986) demonstrated theoretically. For foliage that is not horizontal, hemispherical integration may be important when more of the sky hemisphere is visible, as it would be in large gaps. Integration is also important for including the contribution of direct sunlight, since the solar transverse is low in the sky for these boreal sites (Stadt and Lieffers 2000, Smolander and Stenberg 2001).

An important modeling question is whether foliage display (inclination, clumping) characteristics or extinction coefficients change with species, with light availability, or both. We did find differences in leaf inclination, leaf clumping, and empirical coefficients among the nine understory species studied. If we disregarded the species, we also found significant correlations between overstory transmission and leaf inclination, leaf clumping, LAI and PLAI extinction coefficients, but not the cover coefficients. However,

within each species there was no evidence of changes in any parameters in response to overstory transmission. This suggests the nine understory species have foliage characteristics adapting them to microsites with different light environments. It also suggests that there may be benefit in discriminating among understory species for light modeling.

For the empirical Beer's Law and cover models, the benefit of species discrimination was a 0.02-0.04 decrease in the residual standard deviation for a prediction. For the theoretical models, there was a definite benefit to using a planophile inclination and clumped spatial distribution over the frequently used "default" spherical and random assumptions (e.g. Jarvis and Leverenz 1983). Estimation bias decreased between 0.04 and 0.14 when the more representative parameters were applied, although there was little change in precision. However, applying the average parameter values in these distributions yielded similar residual bias and standard deviations as when species-specific parameters were used. In these understory environments, it is not worthwhile to discriminate among species for theoretical modeling, but it is helpful to know the average conditions of the foliage display.

Understory foliage display characteristics appear to be affected by regional variation. The range of our species-specific LAI-based Beer's Law coefficients was lower than the range published by Aubin et al. (2000) for eastern North American boreal understory species (0.37-0.98 vs. our 0.28-0.65). This may be due to the eastern species, such as *Acer spicatum*, having a more horizontal leaf inclination and dispersed spatial distribution, with consequently higher extinction coefficients (Aubin et al. 2000). Lower light levels have also been measured in the understory of eastern boreal forests (Lieffers et al. 1999), which is likely related to precipitation. As we found that species' foliage display appeared to be adapted to particular overstory transmission levels, it may be that regional differences in foliage display parameters can be simply related to overstory transmission.

The pure-species calibration plots had significant intraspecific foliage clumping, which increased light transmission considerably over randomly positioned foliage. The degree of clumping appears to be specific to each species. In mixed-species validation plots, variance to mean ratios varied from fairly clumped to dispersed. We found no simple solution to the problem of interspecific clumping or dispersion. Likely, a considerable amount of data would be required to estimate these multiple interactions. Since the average variance to mean ratio for the 30 validation plots was nearly one, spatial independence of each species' foliage is the most reasonable assumption.

Our simple model for the vertical distribution of leaf area worked very well. Coupled with the empirical models, the predicted light transmission profile with height followed the measured transmission fraction with almost as little error as the ground level data (Figure 3-6). This approach permits continuous modeling of light availability with height through the understory strata.

Visual estimation of vertically-projected cover is the most rapid and widely-used method of assessing vegetation abundance. It is subjective, so it is critical that the observers continually check themselves against known or point-frame plots. The lack of bias between visual and point-frame cover in this study was likely due to regular comparison with the point-frame measurement following our visual assessment of the plot. Cover data can be converted into LAI (Equation 3-12), but requires an estimate of foliage inclination and clumping. Our empirical model for total cover data also provided reasonable predictions (Table 3-3). The speed and simplicity of this technique is such that visual cover should be considered as an input parameter for forest growth models.

Constabel and Lieffers (1997) noted how stand-average light transmission to the ground stays remarkably constant in natural boreal stands during succession from young to old aspen or to aspen-spruce or spruce-dominated seres. The overstory leaf area index varies considerably during this sequence (Lieffers et al. 2002), and the understory layer fills in to capture the light resource when it is available. Our study corroborates this equilibrium leaf area hypothesis, as the LAI, PLAI and cover in our undisturbed understory validation

plots was positively correlated to overstory light transmission. This equilibrium hypothesis may seem to make the need for estimation of understory transmission rather mundane as the understory is simply the complement of the overstory (Cannell and Grace 1993). However, the role for modeling light transmission through forest strata is predicting how the distribution of light changes with height (from the ground to the top of the overstory), and for determining the effect of treatments that temporarily disturb this equilibrium, such as vegetation control or partial overstory removal. The set of parameters presented here allow simulation of light through the understory with height, and prediction of light transmission after disturbance, with local cover or leaf area measurements.

Literature Cited

Anon. 1982a. Canadian Climate Normals, Vol.2, Temperature 1951-1980. Downsview, ON: Environment Canada, Atmospheric Environment Service.

Anon. 1982a. Canadian Climate Normals, Vol.3, Precipitation 1951-1980. Downsview, ON: Environment Canada, Atmospheric Environment Service.

Aubin, I., M. Beaudet, and C. Messier. 2000. Light extinction coefficients specific to the understory vegetation of the southern boreal forest, Quebec. Canadian Journal of Forest Research 30: 168-177.

Barbour, M.G,. J.H. Burk, W.D. Pitt, F.S. Gilliam, and M.W. Schwartz. 1999. Terrestrial Plant Ecology, 3rd edition. Menlo Park, CA: Benjamin Cummings.

Bartelink, H.H. 1998. Radiation interception by forest trees: a simulation study on effects of stand density and foliage clustering on absorption and transmission. Ecological Modelling 105: 213-225.

Beckingham, J.D. and J.H. Archibald. 1996. Field guide to ecosites of northern Alberta. Canadian Forest Service, Northwest Region, Northern Forestry Centre, Edmonton, Alberta.

Beckingham, J.D., I.G.W. Corns, and J.H. Archibald. 1996. Field guide to ecosites of west-central Alberta. Canadian Forest Service, Northwest Region, Northern Forestry Centre, Edmonton, Alberta.

Brunner, A. 1998. A light model for spatially explicit forest stand models. Forest Ecology and Management 107: 19-46.

Burton, P.J. 1993. Some limitations inherent to static indices of plant competition. Canadian Journal of Forest Research 23:2141-2152.

Campbell, G.S. and Norman, J.M. 1989. The description and measurement of plant community structure. In Plant canopies: their growth, form, and function (G. Russell, B. Marshall and P.G. Jarvis, eds) - Society for Experimental Biology Seminar Series 31, pp. 1-19.

Canham, C.D., Finzi, A.C., Pacala, S.W. and Burbank, D.H. 1994. Causes and consequences of resource heterogeneity in forests: interspecific variation in light transmission by canopy trees. Canadian Journal of Forest Research 24: 337-349..

Canham, C.D., Coates, K.D., Bartemucci, P. and Quaglia, S. 1999. Measurement and modeling of spatially explicit variation in light transmission through interior cedar-hemlock forests of British Columbia. Canadian Journal of Forest Research 29: 1775-1783.

Cannell, M.G.R. and Grace, J. 1993. Competition for light: detection, measurement, and quantification. Canadian Journal of Forest Research 23: 1969-1979.

Cescatti, A. 1997. Modelling the radiative transfer in discontinuous canopies of asymmetric crowns. I. Model structure and algorithms. Ecological Modelling 101: 263-274.

Chen, J.M. and J. Cihlar. 1995. Quantifying the effect of canopy architecture on optical measurements of leaf area index using two gap size analysis methods. IEEE Transactions on Geoscience and Remote Sensing 33: 777-787.

Constabel, A.J. and V.J. Lieffers. 1996. Seasonal patterns of light transmission through boreal forest canopies. Canadian Journal of Forest Research 26: 1008-1014.

Comeau, P., R. Macdonald, R. Bryce and B. Groves. 1998. Lite: a model for estimating light interception through forest canopies, users manual and program documentation. Research Branch, Ministry of Forests, Victoria, B.C. Working Paper 35.

DeLong, H.B., V.J. Lieffers, and P.V. Blenis. 1997. Microsite effects on first-year establishment and overwinter survival of white spruce in aspen-dominated boreal mixedwoods. Canadian Journal of Forest Research 27: 1452-1457.

Goodall, D.W. 1952. Some consideration in the use of point quadrats for the analysis of vegetation. Australian Journal of Scientific Research Series B 5:1-41.

Hogg, R.V., and A.T. Craig. 1995. Introduction to Mathematical Statistics, 5th edition. Upper Saddle River, NJ: Prentice Hall.

Jarvis, P.G. and J.W. Leverenz. 1983. Productivity of temperate deciduous and evergreen forests. In O.L. Lange, P.S. Nobel, C.B. Osmond and H. Ziegler, Eds. Physiological Plant Ecology IV. Ecosystem Processes: Mineral Cycling, Productivity and Man's Influence. Encyclopedia of Plant Physiology, New Series, Vol. 12D. Springer-Verlag, Berlin, pp. 233-280.

Knapp, A.K. and G.A. Carter. 1998. Variability in leaf optical properties among 26 species from a broad range of habitats. American Journal of Botany 85: 940-946.

Koop, H. and F.J. Sterck. 1994. Light penetration through structurally complex forest canopies: an example of a lowland tropical rainforest. Forest Ecology and Management 69: 111-122.

Kucharik, C.J., J.M. Norman, and S.T. Gower. 1999. Characterization of radiation regimes in nonrandom forest canopies: theory, measurements, and a simplified modeling approach. Tree Physiology 19: 695-706.

Lieffers, V.J., C.M. Messier, K.J. Stadt, F. Gendron, and P. Comeau. 1999. Predicting and managing light in the understory of boreal forests. Canadian Journal of Forest Research 29: 796-811.

Lieffers, V.J., B.D. Pinno, and K.J. Stadt. 2002. Light dynamics and free-to-grow standards in aspen-dominated mixedwood forests. Forestry Chronicle 78: 137-145.

Mizunaga, H. 2000. Prediction of PPFD variance at forest floor in a thinned Japanese cypress plantation. Forest Ecology and Management 126: 309-319.

Nilson, T. 1971. A theoretical analysis of the frequency of gaps in plant stands. Agricultural and Forest Meteorology 8: 25-38.

Norman, J.M. and G.S. Campbell. 1991. Canopy structure. In Plant Physiological Ecology: Field Methods and Instrumentation R.W. Pearcy, J. Ehleringer, H.A. Mooney, P.W. Rundel, eds.). London: Chapman and Hall.

Norman, J.M. and P.G. Jarvis. 1975. Photosynthesis in Sitka spruce (Picea sitchensis (Bong.) Carr.) V. Radiation penetration theory and a test case. Journal of Applied Ecology 12: 839-878.

Oker-Blom, P. 1986. Photosynthetic radiation regime and canopy structure in modeled forest stands. Acta Forestalia Fennica 197: 1-44.

Shropshire, C., Wagner, R.G., Bell, F.W., and Swanton, C.J. 2001. Light attenuation by early successional plants of the boreal forest. Canadian Journal of Forest Research 31: 812-823. .

Smolander, S., and Stenberg, P. 2001. A method for estimating light interception by a conifer shoot. Tree Physiology 21: 797-803.

Sorrensen-Cothern, K.A., E.D. Ford, D.G. Sprugel. 1993. A model of competition incorporating plasticity through modular foliage and crown development. Ecological Monographs 63: 277-304.

Stadt, K.J. and V.J. Lieffers. 2000. MIXLIGHT: A flexible light transmission model for mixed-species forest stands. Agricultural and Forest Meteorology 102:235-252. .

Steven, M.D. and M.H. Unsworth. 1980. The angular distribution and interception of diffuse solar radiation below overcast skies. Quarterly Journal of the Royal Meteorological Society 106: 57-61. .

Ter Mikaelian, M.T., R.G. Wagner, C. Shropshire, F.W. Bell, and C.J. Swanton. 1997. Using a mechanistic model to evaluate sampling designs for light transmission through forest canopies. Canadian Journal of Forest Research 27: 117-126.

Vose, J.M., Sullivan, N.H., Clinton, B.D., Bolstad, P.V. 1995. Vertical leaf area distribution, light transmittance, and application of the Beer-Lambert Law in four mature hardwood stands in the southern Appalachians. Canadian Journal of Forest Research 25:1036-1043.

Wang, Y.P. and P.G. Jarvis. 1988. Mean leaf angles for the ellipsoidal inclination angle distribution. Agricultural and Forest Meteorology 43: 319-321.

Zar, J. 1999. Biostatistical Analysis, 4th ed. Upper Saddle River, N.J.: Prentice Hall.

Table 3-1. Foliage measurements and parameters for western North American boreal understory species. SE are parameter standard errors, SD are standard deviations.

Species	Range of %cover, PLAI and LAI min – max	Ellipsoidal inclination parameter, χ_l (SE) and MTA [1]	Variance: mean ratio for PLAI, (SE) and clumping, Ω [2]	Vertical distribution of foliage area or cover, ν_k (SE), [RSE] [3]	Top height of species, H_i (SD) [4]	Beer's Law extinction coefficient, κ_k for LAI (SE) [5]	Beer's Law extinction coefficient, β_k for PLAI (SE) [6]	Empirical extinction coefficient, η_k for cover (SE) [7]
Alnus crispa	52 – 100 1.0 – 4.4 1.1 – 5.1	3.32 (0.22) 25°	1.62 (0.20) 0.76	-0.85 (0.01) [0.05]	198 (40)	0.40 (0.05)	0.47 (0.06)	0.76 (0.06)
Aralia nudicaulis	20 – 88 0.2 – 1.0 0.3 – 1.1	4.23 (0.28) 20°	1.11 (0.10) 0.95	-0.82 (0.01) [0.04]	41 (9)	0.32 (0.05)	0.36 (0.04)	0.38 (0.09)
Calamagrostis canadensis	80 – 100 1.7 – 4.3 2.5 – 6.3	1.72 (0.08) 43°	1.43 (0.15) 0.82	0.66 (0.25) [0.09]	83 (26)	0.28 (0.06)	0.41 (0.09)	0.69 (0.05)
Cornus canadensis	8 – 68 0.1 - 0.9 0.1 – 1.0	5.24 (0.33) 17°	1.23 (0.13) 0.90	0	15 (5)	0.43 (0.08)	0.46 (0.06)	0.50 (0.13)
Corylus cornuta	44 – 100 0.9 – 4.8 1.0 – 5.8	3.15 (0.26) 27°	2.02 (0.21) 0.66	-0.21 (0.07) [0.06]	126 (31)	0.46 (0.10)	0.55 (0.07)	0.86 (0.05)
Epilobium angustifolium	8 – 100 0.2 – 4.4 0.3 – 5.1	3.51 (0.24) 24°	2.69 (0.13) 0.54	0.09 (0.19) [0.11]	98 (28)	0.41 (0.07)	0.47 (0.06)	0.85 (0.07)
Lonicera involucrata	64 – 100 1.1 – 3.6 1.3 – 4.3	2.92 (0.34) 28°	1.46 (0.10) 0.81	0.48 (0.20) [0.08]	87 (45)	0.48 (0.04)	0.58 (0.05)	0.82 (0.06)
Rosa acicularis	28 – 100 0.3 – 4.6 0.4 – 5.5	3.17 (0.23) 26°	2.08 (0.18) 0.65	0.24 (0.18) [0.09]	98 (27)	0.51 (0.03)	0.61 (0.07)	0.89 (0.10)
Viburnum edule	28 – 80 0.4 – 1.6 0.5 – 2.0	2.92 (0.19) 28°	1.71 (0.24) 0.74	0.06 (0.23) [0.13]	100 (22)	0.65 (0.08)	0.79 (0.09)	0.94 (0.09)

[1]Mean tilt angles are computed from χ_l using Wang and Jarvis' (1988) approximation

[2]Equation 3-10

[3]Equation 3-18 (note that no parameter could be fit for *Cornus* because of its short stature); SE is the parameter standard error, RSE is the regression standard error

[4]Equation 3-18

[5]Equation 3-14

[6]Equation 3-15

[7]Equation 3-16

Table 3-2. Theoretical light transmission models, parameters, and fit statistics for understory vegetation.

Model type	Above-understory radiance distribution[1]	Foliage area data	Foliage spatial distribution[2]	Foliage inclination	Model Equations (3-X)	Parameter Estimates	Calibration data		Validation data	
							Residual bias	Residual SD	Residual bias	Residual SD
Multi-layer	SOC+OS	PLAI or LAI	Clumped, by species	Ellipsoidal, by species	1, 2, 3, 4, 6, 9, 10, 11	χ, Ω = Table 3-1, τ = 0.12, ρ = 0.14	-0.06	0.13	-0.13	0.10
			Random	Spherical	1, 2, 3, 4, 6, 9, 11	χ = 1, Ω = 1, τ = 0.12, ρ = 0.14	-0.20	0.13	-0.24	0.10
			Clumped, average	Ellipsoidal, average	1, 2, 3, 4, 6, 9-11	χ = 3.35, Ω = 0.76, τ = 0.12, ρ = 0.14	-0.07	0.11	-0.12	0.09
		COVER	Random or clumped	Ellipsoidal, by species	1, 2, 3, 4, 6, 9, 12	χ = Table 3-1, τ = 0.12, ρ = 0.14	-0.11	0.15	-0.19	0.09
			Random or clumped	Spherical	1, 2, 3, 4, 6, 9, 12	χ = 1, τ = 0.12, ρ = 0.14	-0.18	0.15	-0.23	0.10
			Random or clumped	Ellipsoidal, average	1, 2, 3, 4, 6, 9, 12	χ = 3.35, τ = 0.12, ρ = 0.14	-0.11	0.15	-0.19	0.09
Black-leaf	SOC+OS	PLAI or LAI	Clumped, by species	Ellipsoidal, by species	1, 2, 6, 9, 10, 11	χ, Ω = Table 3-1	-0.11	0.13	-0.22	0.11
			Random	Spherical	1, 2, 6, 9, 11	χ = 1, Ω = 1	-0.24	0.14	-0.27	0.11
			Clumped, average	Ellipsoidal, average	1, 2, 6, 9, 10, 11	χ = 3.35, Ω = 0.76	-0.11	0.12	-0.16	0.09
		COVER	Random or clumped	Ellipsoidal, by species	1, 2, 6, 9, 12	χ = Table 3-1	-0.17	0.16	-0.24	0.10
			Random or clumped	Spherical	1, 2, 6, 9, 12	χ = 1	-0.21	0.16	-0.26	0.11
			Random or clumped	Ellipsoidal, average	1, 2, 6, 9, 12	χ = 3.35	-0.16	0.15	-0.22	0.10
	Vertical	PLAI or LAI	Clumped, by species	Any	6, 9, 10, 11, 13	Ω = Table 3-1	-0.10	0.13	-0.19	0.10
			Random	Any	6, 9, 11, 13	Ω = 1	-0.18	0.13	-0.22	0.10
			Clumped, average	Any	6, 9-11, 13	Ω = 0.76	-0.10	0.12	-0.15	0.09
		COVER	Random or clumped	Any	14		-0.16	0.16	-0.22	0.13

[1]SOC+OS=standard overcast sky with an overstory of LAI=3, leaf inclination parameter (χ)=1, Vertical=all light coming from the vertical

Table 3-3. Empirical light transmission models, parameters, and fit statistics for understory vegetation.

Model type	Foliage area data	Model Equations	Parameter Estimates (SE)	Calibration data		Validation data	
				Residual bias	Residual SD	Residual bias	Residual SD
Beer's Law	LAI	3-15	κ_i=Table 3-1	-0.00	0.09	-0.03	0.08
Beer's Law	LAI, all species combined	3-15	κ_i=0.43(0.02)	-0.01	0.12	-0.05	0.10
Beer's Law	PLAI	3-16	β_i=Table 3-1	-0.00	0.09	-0.04	0.08
Beer's Law	PLAI, all species combined	3-16	β_i=0.52(0.03)	-0.01	0.11	-0.04	0.09
Linear, intercept = 1	COVER	3-17	η_k=Table 3-1	-0.00	0.11	-0.06	0.08
Linear, intercept = 1	COVER, all species combined	3-17	η_k=0.77(0.03)	-0.00	0.15	-0.04	0.11

Figure 3-1. The angular distribution of light above the understory, assuming a standard overcast sky with 2.23 times as much radiance from the vertical as the horizontal (Steven and Unsworth 1980), and three different overstories: (—) an overstory LAI of 1 and overstory inclination parameter (χ) of 0.5, (-o-) an LAI of 3 and χ=1, or (---) an LAI of 6 and χ=2.

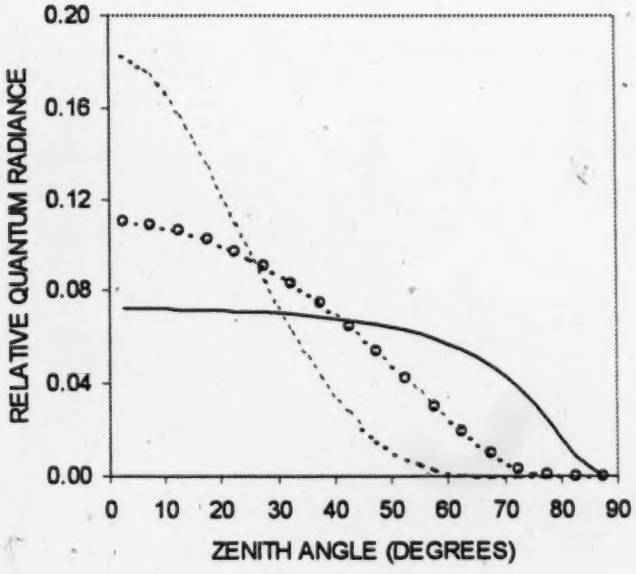

Figure 3-2. Comparison of visual percent cover estimates with the percentage of vertical pins which contacted vegetation. ◇Observer 1, △Observer 2, —1:1 relationship and theoretical 95% confidence limits for 25 pin-drops.

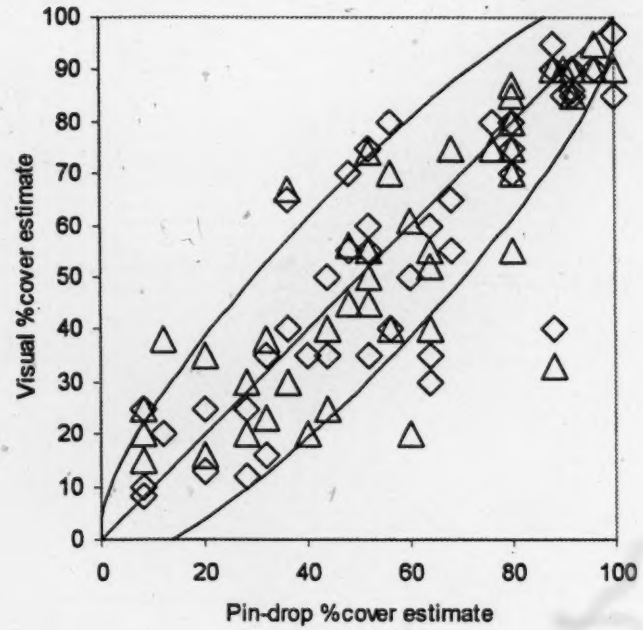

Figure 3-3. Ground-level light transmission (fraction of above-understory light) as a function of (A) percent cover, (B) projected leaf area index (PLAI) and (C) leaf area index (LAI) for weeded calibration plots of nine common species of the western boreal forest: ◇*Almus*, □*Aralia*, △*Calamagrostis*, ○*Cornus*, ×*Corylus*, +*Epilobium*, ✶*Lonicera*, ■*Rosa*, ◆*Viburnum*. Graphs B and C have light transmission on a logarithmic scale.

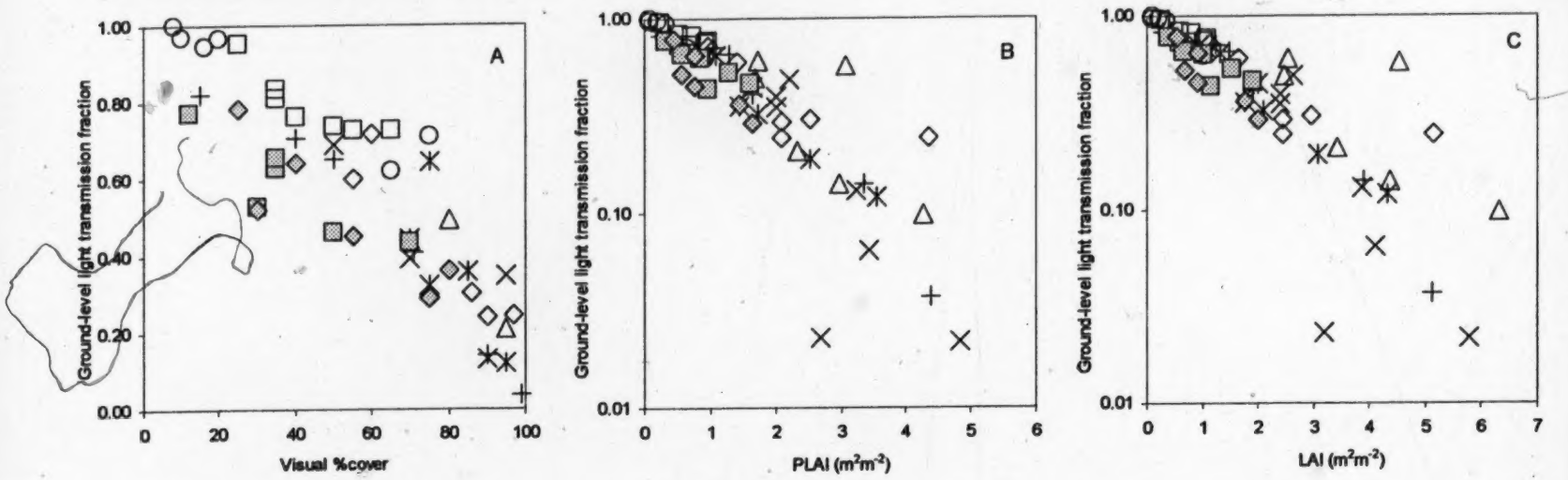

Figure 3-4. Predicted light transmission (fraction of above-understory light) at ground-level *vs.* transmission measurements in undisturbed validation plots. (A) Theoretical models, SOC sky, $LAI_{overstory}$=3 and $\chi_{overstory}$=1: ●Multi-layer model with leaf transmissivity = 0.12, reflectivity = 0.14, using PLAI or LAI data and the ellipsoidal inclination and clumping parameters measured for each species, □PLAI or LAI data and the ellipsoidal leaf inclination and foliage clumping parameters measured for each species, ◇cover data and the ellipsoidal leaf inclination measured for each species (foliage distribution irrelevant). (B) Theoretical models, vertical light source: □PLAI or LAI data and the foliage clumping parameter measured for each species, ◆cover data and the foliage clumping parameter measured for each species. (C) Empirical models: △LAI-based Beer's Law, □PLAI-based Beer's Law, ◆cover-based linear model. The ideal 1:1 relationship is shown as a straight line in all three graphs.

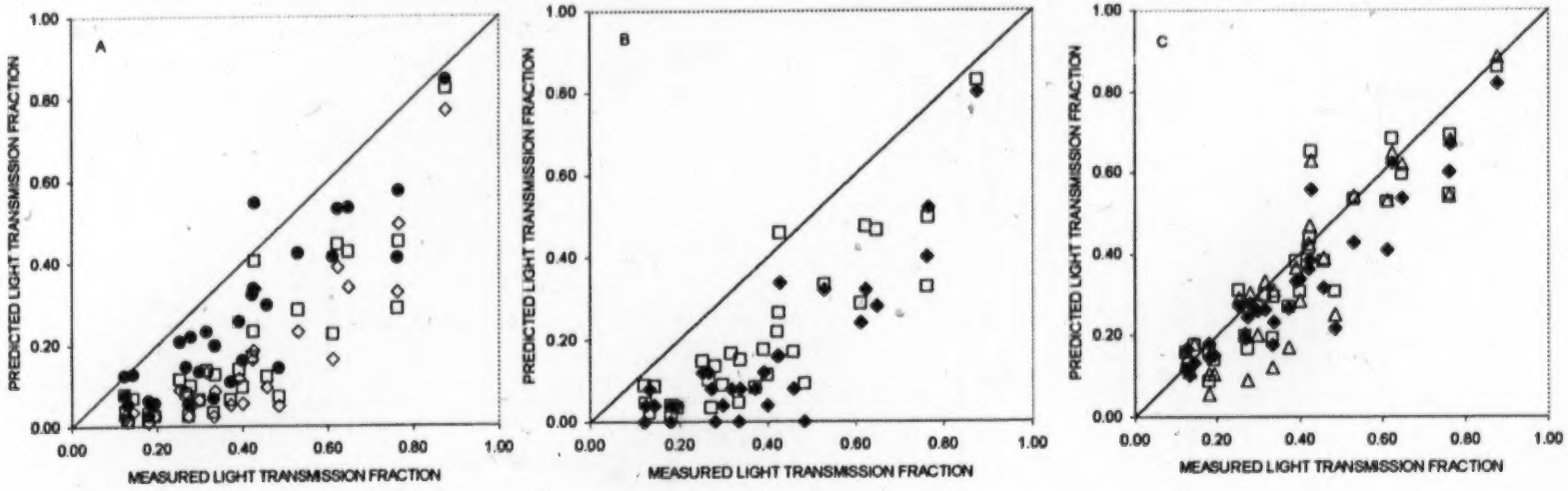

Figure 3-5. Vertical distribution of relative understory PLAI (PLAI above the current height / total ground-level PLAI) with relative height (measurement height / species' top height) for the nine understory species. ◆ measured relative PLAI, — predicted relative PLAI (Equation 3-18 and ν_l, H_l parameters in Table 3-1).

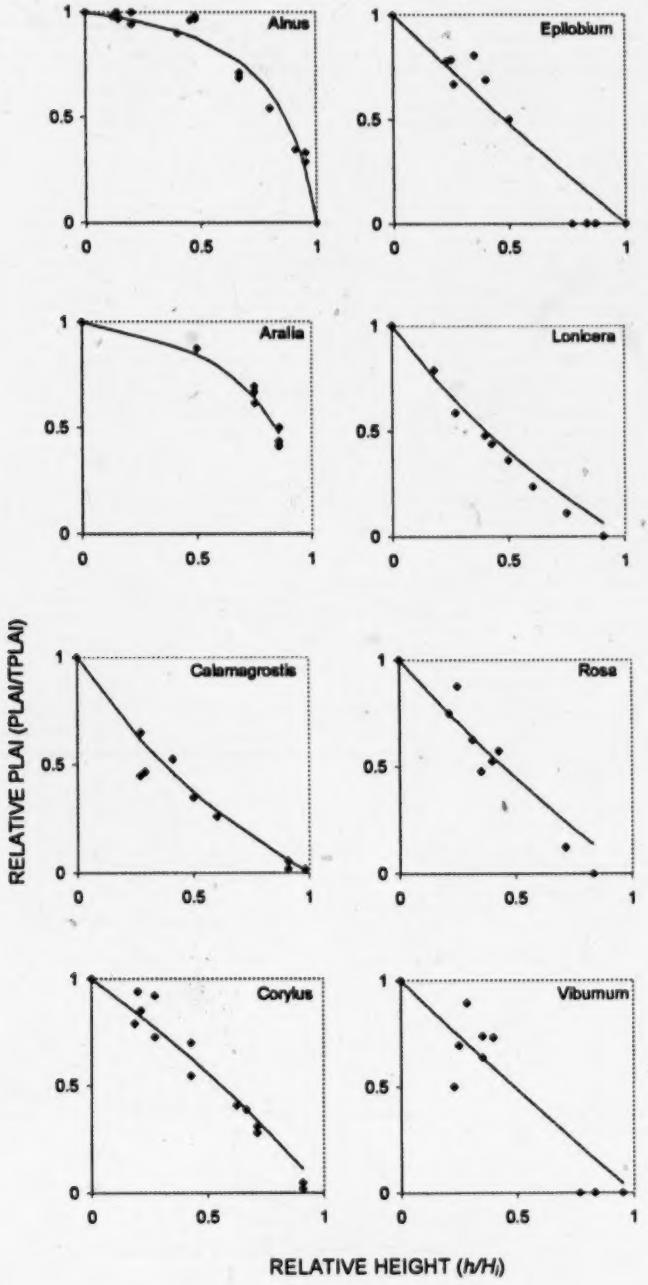

Figure 3-6. Light transmission fraction predicted using the point-frame estimate of total PLAI, vertical foliage area distribution functions for each species (Equation 3-18) and average species' top heights, *vs.* measured light transmission at (◇) 30 and (△) 100 cm. The transmission fraction was calculated with PLAI-based Beer's Law and species-specific coefficients (Equation 3-16, Table 3-1). Data are from undisturbed validation plots

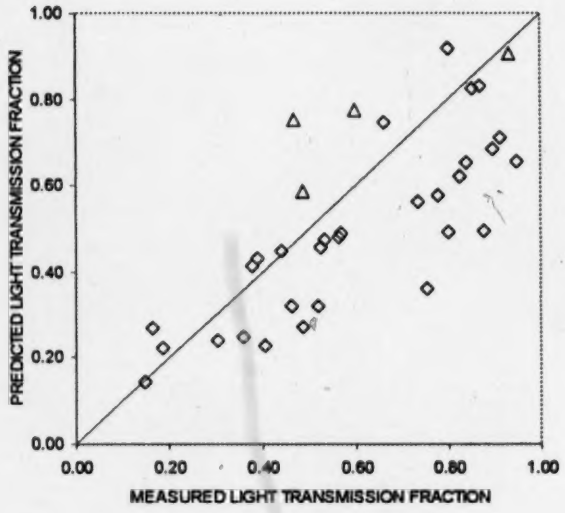

Chapter 4. Spatial modeling of light transmission and growth of *Picea glauca* and *Abies balsamea* in boreal forests of Alberta and Quebec

Introduction

The complexity of mixed-species forest dynamics, coupled with interest in partial-cut silvicultural systems for managing these forests, has stimulated the development of spatially explicit, process driven models of forest regeneration (Pacala et al. 1993, Canham et al. 1999, Bartelink 2000). These models grow trees by the local availability of resources, which depends on the spatial configuration, attributes, and size of their neighbours. Light (photosynthetically-active radiation: PAR) is usually the critical resource modeled. Such a model would be helpful for evaluating silvicultural options in the mixedwood boreal forest as well. In an earlier paper we described a light transmission model, MIXLIGHT, its calibration and stand-scale validation for western Canadian boreal forests (Stadt and Lieffers 2000). The present study tests the ability of MIXLIGHT to predict microsite (~1m^2) variations in the light environment, and investigates its ability to predict the growth of regenerating trees in the understory in boreal stands from both western and eastern Canada.

The chief concern for users of any model is its validation. Will the model predict tree growth adequately? For a light-driven model, validation has two stages. First, does the light prediction module predict accurately the range of light conditions possible in a real forest? Secondly, does tree growth respond to modeled light conditions? While it is possible to skip the first stage and accept a model only on its ability to model forest growth; there is little justification for using relatively complex light calculations if they do not correspond to real light conditions.

The time scale for a light and growth calculations is also relevant. Monteith (1977) presented crop yield evidence that radiation use efficiency (RUE), the ratio of seasonal net primary productivity (NPP) to photosynthetically active radiation absorbed (APAR) by the crop, is constant when resources other than light are not limiting. Bartelink (2000) used this approach to model the annual growth of Douglas fir and beech mixtures in

plantations. Pacala et al. (1994) and Wright et al. (1999) also described juvenile tree growth as a function of seasonal light conditions. There is ample evidence in the boreal forest as well that tree growth is related to light transmission (Messier et al. 1989, Klinka et al. 1992, Lieffers and Stadt 1994, Wright et al. 1999, Duchesneau et al. 2001).

An ideal validation of the light component would therefore compare predictions of light transmission with measurements of light over the entire growing season. However, this is prohibitive as it ties up measurement and sampling equipment for a full season. A comparison of predicted and measured transmission over one day is nearly as effective (Gendron et al. 1998), since the sun makes a full traverse across the sky. The only advantages in a longer simulation period are that the elevation of the solar traverse changes and a greater range of direct and diffuse light proportions are sampled. If the model performs adequately for a day with partial cloud, it should also perform adequately over the growing season.

There are several approaches for relating light availability to tree growth. Bartelink et al. (1997) calculated APAR as the seasonal light (in energy units) transmitted to each tree, less the light energy transmitted through the tree. Allometric equations (Bartelink 1998) were used to partition the NPP generated by this absorbed radiation (NPP = APAR × RUE) among tree organs to model radial and volume growth. Pacala et al. (1994), Wright et al. (1999), and Duchesneau et al. (2001) took a more direct approach, relating the radial and height growth of saplings directly to estimates of seasonal light transmission, using nonlinear functions. We adopted this direct approach.

The objective of this study was to validate the microsite-prediction capability of the MIXLIGHT light availability model on a daily and seasonal basis for two boreal forest sites in western and eastern Canada, and to investigate the relationship between the height growth rates of regenerating trees in these sites with predicted seasonal light.

Methods

Site Information and Stem Mapping

One of the biggest limitations for testing a spatial light-driven model of forest growth is obtaining stem-mapped stands of sufficient size. The low solar elevation at the latitudes of the boreal forest compounds this problem, since trees far to the east, south and west of a microsite can remove a substantial portion of the direct-beam radiation. Typical forestry sample plots (~1000m^2) are too small for this purpose. We were fortunate to obtain a 1.2ha mapped stand in west-central Quebec, and used digital aerial photo techniques to map a 3ha stand in north-central Alberta.

The Quebec site was a 120×100m plot on the west shore of Lac Duparquet (48° 30' N, 79° 20' W) on glacial till parent material with a 12% slope and 110° aspect. The area receives 823mm annual precipitation and has a 0.6° mean annual temperature (Anon. 1982a, b). The stand was 130 years old and was dominated by trembling aspen, with numerous white spruce and jack pine in the overstory. The understory had mountain maple (*Acer spicatum* Lam.) above some microsites. Regenerating balsam fir were abundant throughout the stand. The site was mapped in 1996 with reference to surveyed 10×10m grid stakes. Stems of all trees >5cm DBH had been plotted by the bearing and distance from the stem to the nearest stake. Tree species and DBH had also been recorded (Colin Kelly and Ian Ritchie pers. comm.). Tree heights, crown lengths, and crown radii were generated from equations developed in the Lac Duparquet region (Paula Bartemucci, pers. comm.).

The Alberta site was a 100×225m plot near Calling Lake, Alberta (55° 30' N, 113° 40' W) on glacial till with negligible slope. The area receives 356 mm precipitation and has a mean annual temperature of 0.3° (Anon. 1982a, b). The north end of the plot was approximately 80 years old and dominated by trembling aspen. The south end was 140 years old and dominated by white spruce. A heterogeneous region of mixed spruce and aspen occurred in the centre of the plot. Some selective logging had occurred in this stand in the 1940's creating several gaps (Dan MacPherson, pers. comm.). Understory white spruce occurred throughout the stand.

The Calling Lake site was stem-mapped from large-scale (1:1200) aerial photographs. These photographs were obtained before leaf-out so trees below the overstory hardwoods would be visible. A 40×40m grid of ground control stakes were surveyed with a total station (SET5F, Sokkia, Tokyo, Japan) prior to photography, and a highly visible target placed over the stakes. The cameras had 100mm lenses suspended beneath a boom with 6.1m separation. The film was 70mm AGFA colour diapositive. The diapositives were scanned, aero-triangulated with edge and ground control, and paired into digital stereo models by Integrated Mapping Technologies, Vancouver, BC, Canada.

Mapping was done on a Pentium III PC computer with a 3D video system (video card, shuttered glasses and DiAP support software from International Systemap Corp., Vancouver, BC, Canada) operating within the Microstation mapping environment (Bentley Systems Inc., Exton, PA, USA). In this system, elevations can be measured as well as horizontal coordinates, using stereo parallax and the computer's cursor as the floating dot. We measured the easting, northing, and elevation (*i.e.* x, y, z) coordinates of the top of each tree's crown and the base of the stem. Tree height was calculated by the difference in these elevation coordinates. The lens used to acquire the photos was too wide-angle to make multiple measurements of crown radius around each crown: trees away from the centre of each stereo model leaned away too much, obscuring the distal side of the crown. To estimate crown radius, we chose two points on opposite sides of the crown at its widest elevation. We projected a horizontal circle around the crown, passing through these points. The radius of the circle was nudged larger or smaller until the operator was satisfied the circle represented the best fit to the horizontal crown area. This radius was recorded. The output from each tree measurement included the operator's best estimate as to the species (the only confusion was occasionally between aspen and balsam poplar), a visual assessment of the health of the tree (0 for a branchless snag to 5 for a healthy tree), the tree's height, crown radius, and crown apex coordinates. Tree DBH and crown length were estimated from species-specific equations based on tree height, developed from data collected in this site.

The accuracy of the photo measurements was confirmed with a ground survey. At the same time, the light measurement microsites were checked for smaller trees that were missed in the aerial mapping. Any trees within a 5m radius that could obscure the sensor's sky-view were added to the map.

A detailed explanation of the digital aerial photo mapping process and ground truthing is found in Appendix 4A.

Light measurements

For light measurements, we constructed our own photosynthetic photon flux density (PPFD) sensors. These used a gallium arsenide phosphide (GaAsP) photocell (G-2711-01, Hamamatsu, Bridgewater, NJ, USA) as the sensing element, mounted in a well in a 25mm ∅ opaque black polyethylene rod. A 9.5mm ∅ cylindrical diffuser was cut from 3mm thickness white translucent acrylic and mounted on a sill above the sensor. The depth of the sill was carefully set so that enough of the diffuser edge was exposed to yield a near cosine response to the incident light angle.

Five GaAsP sensors were configured as conventional photovoltaic PPFD sensors by shorting the terminal ends of the sensor wires across a 1kΩ precision resistor and measuring the voltage drop. The very low current generated by the photocells in this configuration (~0.4μA at a typical understory light level of 100 $\mu molm^{-2}s^{-1}$, to 8μA at full sunlight) required that the voltage (~0.4-8mV) be measured by a precision voltmeter, like most commercial PPFD sensors. We had two dataloggers (CR10X, Campbell Scientific Inc., Edmonton, AB, Canada) with sufficient precision and data storage capacity available for this.

The other 44 sensors were configured as photodiodes, which leak current in proportion to the PPFD striking them. They were reverse-biased with 3V (positive battery terminal attached to the positive side of the photocell), supplied by two AA batteries at the terminal end of the lead wires. The current leakage was measured as the voltage drop across a potentiometer. The photocell required 0.5V to maintain reverse bias, so the

potentiometer was trimmed to a 2V voltage drop at full mid-day sunlight (~2000 $\mu molm^{-2}s^{-1}$ in Quebec). The voltage response to PPFD was a linear 0-2V from dusk to full sunlight, and this high output voltage permitted us to use inexpensive miniature dataloggers (Hobo H8, Onset Computer Corporation, Pocasset, MA, USA) to record light levels. The precision of these dataloggers was ±10mV ±0.5% of the reading, which translated to a PPFD accuracy of ±10 to 20$\mu molm^{-2}s^{-1}$ (zero to full sunlight). Timing accuracy was ±1 minute/week. Four sensors were attached with 6m lead wires to each of 10 dataloggers, enabling us to spread up to 40 sensors across the sites for simultaneous measurements.

The sensor-datalogger configurations were checked against a commercial PPFD sensor (LICOR 190SA, LICOR, Lincoln, NB) for a full day on a rooftop before and after each growing season. Aside from the failure of two sensors, correlation between our sensors and the commercial one was very satisfactory, even at PPFD levels below 100 $\mu molm^{-2}s^{-1}$ ($r>0.99$).

At the Lac Duparquet site, photodiode sensors were placed at 36 microsites in the central region of the site. A minimum buffer of 25m was maintained from any edge of the mapped region. 25 of the sensors were placed near the terminal bud of a regenerating balsam fir. The other 11 were positioned in locations above the mountain maple understory. As some of these were as high as 6m, the sensors were placed on self-levelling mounts. Sensor positions were mapped by distance, bearing and slope from the nearest survey stake. Another miniature datalogger with four photodiode sensors was placed 500m northeast of the stand on a treeless island to estimate the total above-canopy PPFD. The sensors were left to sample and log every 20 seconds for one day (July 27, 1999 0900-1700h EDT).

At the Calling Lake site, the photodiode sensors were positioned at 36 microsites, a minimum 25m from the plot edge, for one day (August 24, 2000 0900-1800h MDT). Sampling and data storage frequency was once every 20 seconds. In addition, five of the photovoltaic sensors were mounted on permanent stakes, sampled once per minute, and

the average stored every hour by a precision datalogger (CR10X, Campbell Scientific, Edmonton, AB, Canada) to provide a seasonal estimate of the light at these microsites. One photovoltaic sensor and one photodiode sensor were attached to a similar precision datalogger and placed in a 1ha clearing 500m northeast of the site for estimating the above-canopy radiation. A recently developed commercial sensor, which measures direct and total PPFD without requiring adjustment of the shade band (BF2 Sunshine Sensor, Delta-T Devices Ltd., Cambridge, UK), was also attached to the outside datalogger. For most of the growing season, the outside datalogger sampled its sensors every minute and averaged and stored data ever hour. On the day when the 36 microsites were being measured, sampling and storage (no averaging was done) frequency was increased to every 20 seconds to match the frequency of the understory photodiode sensors and dataloggers. Unfortunately, the battery on the outside datalogger failed July 28, and was not replaced until August 22, so the incoming radiation data are missing for this period. Sensor locations were mapped using a total survey station (SET5F, Sokkia Corp., Olathe, KS).

Measurement data was summarized by averaging the light readings inside and outside the forest first, then dividing the inside average by the outside average to calculate the transmission fraction. This corresponds with the sequence MIXLIGHT uses to calculate light transmission.

At some microsites in both sites, shrub and herb vegetation also obscured the sensors' sky-view. For these, we made visual estimates of the total vertically projected cover, and used this, with a calibrated adjustment factor (Chapter 3), to further reduce the overstory light transmission calculated by MIXLIGHT.

Light Transmission Modeling

MIXLIGHT represents tree stems and crowns as three-dimensional geometric shapes, defined by their crown dimensions (height, length and radius) and crown position, then calculates light transmission by a simplified ray-tracing approach. A hemispherical sky radiance distribution is generated by tracking the sun's position and using the measured

or estimated fractions of direct and diffuse light for short intervals (e.g. hours or minutes) during the full simulation interval. Rays are traced from the sky hemisphere to the simulation location. Where a ray encounters a tree crown, the transmission along the ray is calculated by the Poisson probability of encountering no leaves, given the crown's leaf area density, leaf inclination distribution and the length of the ray through the crown. The ray transmission values are weighted by the radiance of the part of the sky where they originated, then averaged to give the overall transmission value to this microsite. The complete structure and calibration of MIXLIGHT is described in Stadt and Lieffers (2000).

For the Lac Duparquet site, and in most applications of a light transmission model, only the total outside canopy PPFD is available. The diffuse skylight fraction during these measurements was estimated from the clearness index (K = global irradiance ÷ extraterrestrial irradiance at the time of measurement) (Spitters et al. 1986, Roderick 1999). Spitters et al. (1986) recommended a set of equations for the hourly diffuse fraction. We tested these, but developed our own linear equation, following Roderick (1999), to fit this data. We estimated global irradiance (S_g) by dividing the total PPFD reading by 2.04μmol J^{-1} (Meek et al. 1984) and used the equations of Spitters et al. (1986) for determining extraterrestrial irradiance (S_0) for each hour. Clock time was corrected to local apparent (solar) time by adjusting for daylight savings, longitude, and the eccentricity of the earth's orbit (Oke 1987).

The input to MIXLIGHT consisted of the list of trees with their crown dimensions and positions, species-specific estimates of leaf area density and leaf inclination (calibration data of Stadt and Lieffers 2000), the site slope, aspect, latitude and longitude, the radiation data (total PPFD and diffuse fraction) during the simulation period, the type of collector (horizontal = most PPFD sensors, or hemispherical = normal incidence) and the microsite positions. The software output was an estimate of the light transmission to each microsite during this simulation period. We simulated transmission on an hourly, daily, and seasonal basis, and compared simulated values to measurements.

Tree Growth Measurements

At Lac Duparquet, most of the regenerating trees were balsam fir. We selected 25 trees of 0.5 - 4 m height and measured their total height and the past three years' height growth. At Calling Lake, white spruce was the dominant regenerating tree. We selected 40 trees of 0.2 - 7 m height and measured the same attributes as the fir. Tree coordinates were mapped by distance and bearing from the survey stakes.

Mean annual height growth (g_h = three year height growth ÷ 3) was compared with MIXLIGHT's seasonal light transmission predictions for microsites at the apexes of the trees. We calculated the seasonal estimate of light transmission both for a horizontal collector and a hemispherical collector. The difference is that a horizontal collector includes a cosine correction in averaging the contribution of light rays of many zenith angles to the overall transmission value (Lambert's cosine law). The needles of white spruce are nearly spherically inclined, so should be able to utilize light equally well from any incidence angle, i.e. spruce should behave as a hemispherical collector. Balsam fir needles, on the other hand, are nearly planophile, so should absorb vertically-incident light more effectively than light from near horizontal. Fir growth may be better correlated with light transmission to a horizontal collector.

Statistical Analysis

Statistical analysis was performed using the correlation, linear and nonlinear regression and general linear models procedures in SAS version 8e (SAS Institute, Cary, NC). Significance was defined at the 5% level.

Results

Partitioning of Total PPFD to Direct and Diffuse PPFD

There was an obvious linear relationship between the hourly diffuse fraction of total PPFD (P_d/P_t) and the clearness index (S_g/S_o) (Figure 4-1). Following Roderick (1999), we fitted a linear equation to the data, and then placed bounds of 0.96 diffuse fraction at low clearness and 0.05 diffuse at high clearness (Equation 4-1, R^2=0.84, n=738, p<0.0001).

[4-1] $P_d/P_t = 0.96$ for $S_g/S_o \leq 0.14$

$P_d/P_t = 1.12 - 1.10 \times S_g/S_o$ for $0.14 < S_g/S_o \leq 0.96$

$P_d/P_t = 0.05$ for $S_g/S_o \geq 0.96$

Light Predictions

Average seasonal PPFD transmission predictions in the Calling Lake site were very well correlated with measured values at the five microsites with permanent sensors ($r=0.93$, $n=5$, $p=0.024$), and a plot of predicted vs. measured values lay close to the ideal 1:1 line (Figure 4-2).

Average daily PPFD transmission predictions were well correlated with measured values (Figure 4-3). The correlation coefficient was 0.81 ($n=36$, $p<0.0001$) for the Lac Duparquet site, and 0.76 ($n=34$, $p<0.0001$) for Calling Lake. The relationship between predicted and measured values was very close to 1:1 for the Lac Duparquet site (Figure 4-3A). At Calling Lake, MIXLIGHT tended to overestimate light to the brightest microsites, which were located in a long, narrow gap. Since MIXLIGHT estimated crown length as a function of height only, and gap-edge trees tend to maintain a longer crown than their closed-canopy counterparts, it was not surprising light levels were overestimated for these microsites.

Tree Height Growth

At the Lac Duparquet site, understory balsam fir annual height growth was positively correlated with measured daily as well as predicted seasonal light transmission values. Correlation coefficients were 0.72 for height growth vs. measured %PPFD on July 27, and 0.63 for height growth vs. predicted seasonal PPFD transmission to a horizontal surface (critical r is 0.38 for $n=25$ and $\alpha=0.05$). The equation for this linear relationship between height growth and seasonal light is given in Figure 4-4. Height growth was not significantly correlated with tree height ($r=0.33$), nor was relative height growth correlated with measured daily %PPFD ($r=0$) or predicted seasonal %PPFD ($r=0$).

At Calling Lake, white spruce annual height growth was positively correlated with predicted seasonal light transmission values. The correlation coefficient was similar whether transmission was computed with respect to a horizontal surface or a hemispherical collector (both r=0.77, n=40, critical r=0.30) although the predicted transmission values were higher for the hemispherical collector. Height growth was also correlated with tree height (r=0.59). Multiple correlation of height growth with tree height and light transmission (r=0.81) explains more variation than transmission or height alone. Relative height growth (height growth/tree height) was also correlated with light transmission (r=0.31), though not as well as absolute growth. Inspection of the residuals suggested the best model for predicting annual leader growth from sapling height (H) and seasonal light transmission (T) was a power function (Figure 4-4).

Discussion

Light Simulations

MIXLIGHT was able to model the spatial variation in light transmission at the microsite level across two highly heterogeneous mixed-species boreal stands, one in eastern Canada, and one in the west. Excellent correspondence between predicted and measured %PPFD was shown in the site monitored for most of the growing season, and very good results were obtained for full-day %PPFD at both sites. This correspondence held for microsites with %PPFD values from 1 to 45%. Clearly, the incoming radiation and crown representation used by MIXLIGHT is sufficient for simulating light transmission at this time interval.

The solar path and clear-sky direct-beam PPFD were straightforward to model using sun-earth geometry (Oke 1987). However, the scattering of sunlight in the atmosphere, which gives rise to diffuse skylight radiation, is complex due to the patchiness and unpredictability of clouds. Ideally, the partitioning of radiation into direct-beam sunlight and diffuse skylight components can be directly measured using a shadow band or shadow grid device such as we used at the Calling Lake site. Alternatively, the empirical relationship between the diffuse proportion of global radiation and the clearness index (Roderick 1999) accounts for much of the variation in this partitioning. This approach,

which requires only measurements of total PPFD or global radiation and the local apparent time, was effective at Calling Lake and was applied at Lac Duparquet.

The distribution of diffuse light across the sky is also subject to debate. The zenith is generally several times brighter than the horizon on overcast days, but this may be reversed on clear days (Brunger and Hooper 1993). Some preliminary simulation tests showed that when there was a significant radiation contribution from direct sunlight, the diffuse light distribution had little effect on predicted %PPFD. For simulations on overcast days, however, the distribution was quite important (Pinno et al. 2001).

For the canopy representation, the amount of leaf area is the most important determinant of light transmission (Larsen and Kershaw 1996). After this, the inclination of the leaf area and how it is aggregated (i.e. clumped, random, dispersed) are next in importance in their effect on transmitted light. We estimated leaf area density for all canopy species (trembling aspen, white spruce, balsam fir, balsam poplar, and paper birch), and the leaf inclination distribution for the two most common canopy species, white spruce and trembling aspen, as input variables for MIXLIGHT (Stadt and Lieffers 2000). MIXLIGHT models leaf area aggregation by defining a geometric crown envelope (ellipsoid, paraboloid, cone, inverted cone, cylinder, or rocket (a cone on a cylinder)) for each tree species and placing the appropriate leaf area density within the envelope, assuming the within-envelope distribution is random. The size and position of these envelopes, their leaf area density and inclination, coupled with the distribution of incoming radiation determine the pattern of predicted light measured within the canopy.

Clearly the simplification of the tree crowns into regular geometric shapes and the simplifications in representing the sky mean that the model cannot capture all the temporal and spatial details of light availability. We expect that MIXLIGHT would be less effective in predicting light transmission for shorter simulation and measurement time intervals. This is due both to model simplifications and measurement practicalities. A rogue branch may occur outside the crown envelope or the crown may not be radially symmetric. The distance between the "above canopy" sensor and the within canopy

sensor (500 m) means one could be under clouds and another in the sun at the same time. These would not affect the transmission of diffuse skylight greatly, since this is coming from the entire sky hemisphere. All surrounding trees affect the diffuse radiation, and the differences between the real leaf area distribution and the distribution imposed by geometric crown structures, as well as the difference between real sky angular radiance and the standard overcast model, even out. However, since the sun is nearly a point source of approximately 50% of the horizontal flux on average, small deviations in crown structure and the timing of full sun vs. cloud (due to the spatial separation between the "above canopy" and within canopy sensors), may create considerable deviation from measured values. For longer integration periods, the sun traverses more of the sky, so both real and simulated sun rays encounter more tree crowns on their way to the simulation location. The more crowns are encountered the more the simplifications in crown structure and the value and direction of the solar flux start to "average out".

Since the model cannot reproduce the second-by-second and centimeter-by-centimeter variations in the light environment, a reasonable test is whether the mean light transmission over a longer integration period is reproduced for a number of spatial positions (microsites). Certainly this was the case for daily and seasonal simulations here.

This discussion illustrates the increasing importance of the distribution of leaf area and the representation of the tree crowns as the integration period decreases. Crown dimensions are controlled by site quality, tree age, neighbourhood stem density, light availability and quality (Gilbert et al. 2001), hydraulic constraints (Protz et al. 2000), wind sway (Rudnicki et al. 2001), winter temperatures (Lieffers et al. 2001), and snow loading. The simplified crown models used here, based on stem diameter or tree height, could be improved by adjusting for these factors.

Tree Growth

Light availability was a critical resource for the predominant regenerating species (balsam fir at Lac Duparquet and white spruce at Calling Lake). Height growth was positively correlated with the modeled seasonal light transmission. Similar correlations

were also found when light transmission was calculated with respect to a hemispherical or a horizontal collector. The needle inclination distribution of white spruce is closer to spherical than horizontal, and more horizontal for balsam fir, so, although one might expect hemispherical transmission would be a better predictor of growth for spruce and horizontal transmission better for fir, there was not enough difference between %PPFD calculated for these two types of collectors (cross-correlation was 0.99) to detect this. These differences may be clearer if interior trees and edge trees of different aspects were compared. Linking growth to absorbed radiation (APAR) would have the advantage of accounting for differences in leaf inclination as well.

The mean leader growth vs. predicted seasonal light transmission response for balsam fir was linear over the range of light transmission levels tested (Figure 4-4A), but the relationship is influenced most by one high growth, high light point. The relative height growth vs. overcast-day light transmission relationship developed by Duchesneau et al. (2001) fits the lower range of this data (Figure 4-4A), but we had too small a sample size and too limited a range of light conditions in this site to confirm this relationship.

For white spruce, the leader growth vs. light transmission relationship was nearly identical to the height growth vs. clear-day light transmission relationship reported in an earlier study (Lieffers and Stadt 1994, Figure 4-4B this paper). This relationship was also qualitatively similar to the white spruce leader growth vs. seasonal light data of Wright et al. (1998) for the boreal plains region of British Columbia, although our data showed higher growth at high light. Prediction of spruce height growth was improved by including tree height as a predictor of growth in a power function (Figure 4-4B). Tree height provides a surrogate for crown size; it is likely that the additional growth that larger trees exhibited was due to greater light capture by their larger crowns.

Conclusions

This work illustrates that daily to seasonal PPFD transmission to microsites within a stand can be closely modeled using a simple geometric representation for the overstory canopy, an empirical cover model for the understory and ray-tracing techniques to

compute the overstory gap fraction. Accurate predictions were obtained under a range of overstory and understory vegetation types, including microsites around gaps, beneath aspen, spruce or mixedwood forests, and with nonexistent to dense understory vegetation cover. These relationships held for both a western and an eastern Canadian boreal site. Seasonal PPFD transmission was weakly correlated with balsam fir growth in the eastern site, and better correlated with white spruce growth in the western site. These results show promise for constructing a light-resource based model for understory regeneration in these forests.

Literature Cited

Bartelink, H.H., Kramer, K., Mohren, G.M.J. 1997. Applicability of the radiation-use efficiency concept for simulating growth of forest stands. Agricultural and Forest Meteorology 88: 169-179.

Bartelink, H.H. 1998. A model of dry matter partitioning in trees. Tree Physiology 18: 91-101.

Bartelink, H.H. 1998. Radiation interception by forest trees: a simulation study on effects of stand density and foliage clustering on absorption and transmission. Ecological Modelling 105: 213-225.

Bartelink, H.H. 2000. A growth model for mixed forest stands. Forest Ecology and Management 134: 29-43.

Bartelink, H.H. 2000. Effects of stand composition and thinning in mixed-species forests: a modeling approach applied to Douglas-fir and beech. Tree Physiology 20: 399-406.qqq

Brunger, A.P. and F.C. Hooper. 1993. Anisotropic sky radiance model based on narrow field of view measurements of shortwave radiance. Solar Energy 51: 53-64.

Canham, C.D., A.C. Finzi, S.W. Pacala, and D.H. Burbank. 1994. Causes and consequences of resource heterogeneity in forests: interspecific variation in light transmission by canopy trees. Canadian Journal of Forest Research 24: 337-349.

Canham, C.D., K.D.Coates, P. Bartemucci, and S. Quaglia. 1999. Measurement and modeling of spatially explicit variation in light transmission through interior cedar-hemlock forests of British Columbia. Canadian Journal of Forest Research 29: 1775-1783.

Duchesneau, R., I. Lesage, C. Messier, and H. Morin. 2001. Effects of light and intraspecific competition on growth and crown morphology of two size classes of understory balsam fir saplings. Forest Ecology and Management 140: 215-225.

Gendron, F., C. Messier and P.G. Comeau. 1998. Comparison of various methods for estimating the mean growing season percent photon flux density in forests. Agricultural and Forest Meteorology 92: 55-70.

Gilbert, I.R., P.G. Jarvis, H. Smith. 2001 Proximity signal and shade avoidance differences between early and late successional trees. Nature 411: 792-795.

Larsen, D.R. and J.A. Kershaw, Jr. 1996. Influence of canopy structure assumptions on predictions from Beer's law. A comparison of deterministic and stochastic simulations. Agricultural and Forest Meteorology 81: 61-77.

Lieffers, S.M., V.J. Lieffers, U. Silins, and L. Bach. 2001. Effects of cold temperatures on breakage of lodgepole pine and white spruce twigs. Canadian Journal of Forest Research 31: 1650-1653.

Lieffers, V.J. and K.J. Stadt. 1994. Growth of understory Picea glauca, Calamagrostis canadensis, and Epilobium angustifolium in relation to overstory light transmission. Canadian Journal of Forest Research 24: 1193-1198.

Monteith, J.L. 1977. Climate and efficiency of crop production in Britain. Philosophical Transactions of the Royal Society of London, Series B, pp.277-294.

Oke, T.R. 1987. Boundary Layer Climates, 2nd edition. Routledge, London. 435 p.

Pacala, S.W., C.D. Canham and J.A. Silander. 1993. Forest models defined by field measurements: I. The design of a northeastern forest simulator. Canadian Journal of Forest Research 23: 1980-1988.

Pacala, S.W., C.D. Canham, J.A. Silander, Jr. and R.K Kobe. 1994. Sapling growth as a function of resources in a north temperate forest. Canadian Journal of Forest Research 24: 2172-2183.

Pinno, B.D., V.J. Lieffers, and K.J. Stadt. 2001. Measuring and modelling the crown and light transmission characteristics of juvenile aspen. Canadian Journal of Forest Research 31:1930-1939.

Protz, C., U. Silins, and V.J. Lieffers. 2000. Reduction in brach sapwood hydraulic permeability as a factor limiting survival of lower branches of lodgepole pine. Canadian Journal of Forest Research 30: 1088-1095.

Roderick, M.L. 1999. Estimating the diffuse component from daily and monthly measurements of global radiation. Agricultural and Forest Meteorology 95: 169-185.

Rudnicki, M., U. Silins, V.J. Lieffers, and G. Josi. 2001. Measure of simultaneous tree sways and estimation of crown interactions among a group of trees. Trees: Structure and Function 15: 83-90.

Stadt, K.J. and V.J. Lieffers. 2000. MIXLIGHT: A flexible light transmission model for mixed-species forest stands. Agricultural and Forest Meteorology 102:235-252.

Wright. E.F., K.D. Coates, C.D. Canham, and P. Bartemucci. 1998. Species variability in growth response to light across a climatic in northwestern British Columbia. Canadian Journal of Forest Research 28: 871-886.

Figure 4-1. Hourly diffuse fraction of total PPFD at Calling Lake, Alberta vs. the clearness index for June 27 to July 28, and August 22 to September 15, 2000. The solid line is our fitted equation (Equation 4-1). The dotted line is the equation given by Spitters et al. (1986) for hourly values.

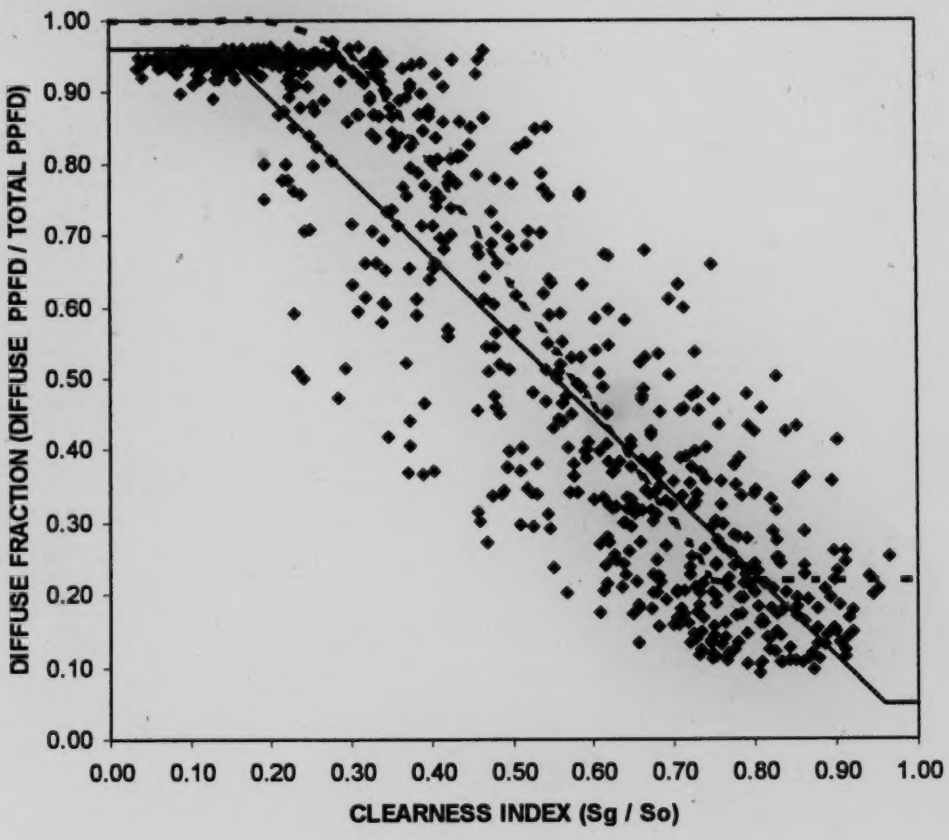

Figure 4-2. Simulated seasonal vs. measured PPFD transmission from June 27 to July 28 and August 22 to September 15, 2000 at five microsites at Calling Lake, Alberta (r=0.93). ◇horizontal collector, △hemispherical (normal incidence) collector, solid line shows the ideal 1:1 relationship.

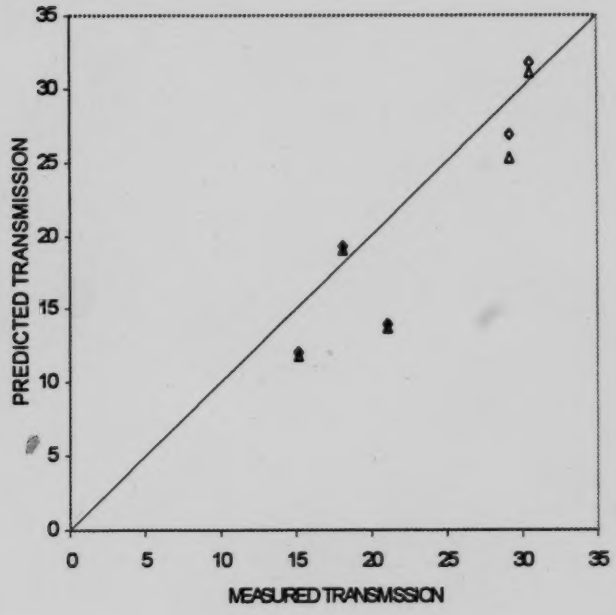

Figure 4-3. Simulated vs. measured daily PPFD transmission. A) Lac Duparquet, Quebec July 27, 1999, n=36 microsites, r=0.81. B) Calling Lake, Alberta August 24, 2000, n=34, r=0.76. Solid lines show the ideal 1:1 relationship.

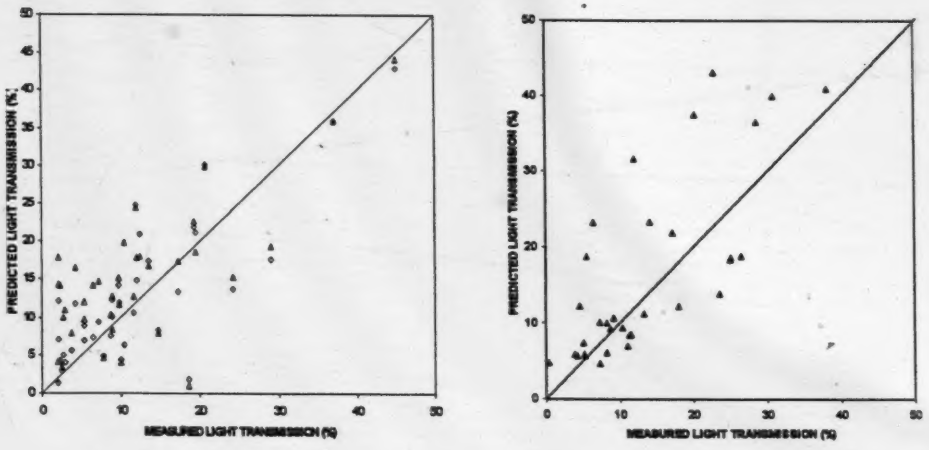

Figure 4-4. Annual leader growth (g) as a function of predicted seasonal light transmission (%PPFD from May 15 to Sept. 15, 2000) and tree height (H).
(A) Lac Duparquet, Quebec. Closed triangles, ▲, are data for balsam fir saplings 0.5 - 4 m tall. The solid line shows the linear regression for this data: $g = 0.88 + 0.75 \times \%PPFD$ (R^2=0.42, n=25, p<0.0001). There was no effect of height in this study. Open triangles, △, show values calculated with the relative height growth equation developed by Duchesneau et al. (2001) for each of the measured trees.
(B) Calling Lake, Alberta. Closed triangles show white spruce saplings in proportion to their size, ▲<1 m tall, ▲=1-3 m tall, ▲= 3-7 m tall. There was an effect of height, so open triangles, △, show the values predicted by the power function $g = 0.69 \times H^{0.56} \times (\%PPFD/100)^{0.80}$ (R^2=0.77, p<0.0001) for each of the measured trees. The lines show height growth *vs.* %PPFD relationships from other studies: the solid line is from Lieffers and Stadt (1994), the dashed curve is from Wright et al. (1998).

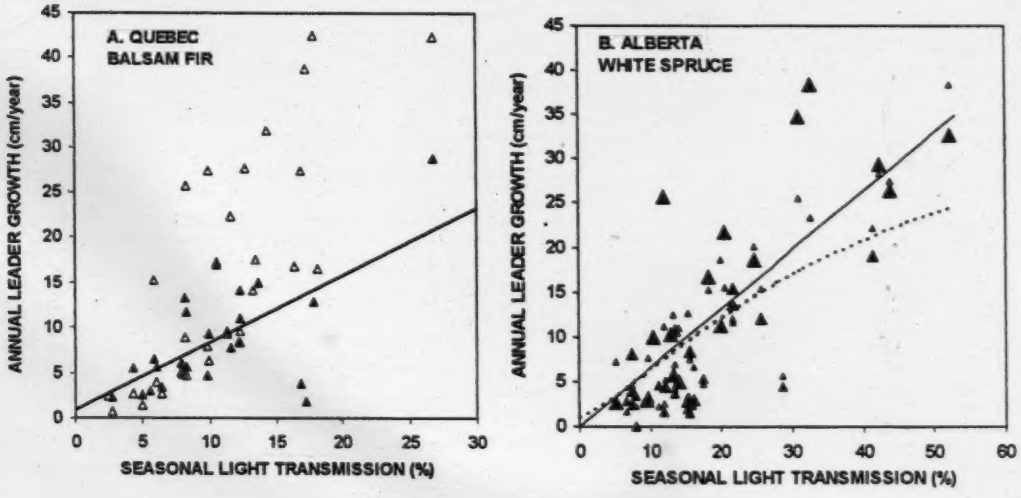

Appendix 4A. Tree Crown Mapping with Large Scale Digital Stereo Aerial Photography

Mapping the position and crown dimensions of a stand of trees in anything larger than a small plot is an onerous task from the ground. A logical alternative is to map trees from large-scale aerial photographs (LSP). If these are obtained as stereo pairs, tree height can be obtained as well as crown radius and position. The measurement of positions and dimensions from stereo photography is by no means a new concept. However, emerging digital mapping technology is now making this process much easier. This appendix describes crown mapping using large-scale photos and a digital mapping system.

The site was near Calling Lake, Alberta (55° 30' N, 113° 40' W). Access was from the Alberta-Pacific Forest Industries Calling Lake Connector Road, following a cut-line 0.6 km south of the Calling River bridge. The northeast corner of the site was located on this cut-line, 0.8 km west of the connector road. The site was a 100 x 225 m plot with the long axis oriented north-south and had negligible slope. It was dominated by 24 m tall aspen at the north end, and 25 m tall spruce at the south. Between these two different overstories, there was a region of mixed aspen-spruce composition. Smaller regenerating spruce trees occurred throughout the site, but were most abundant beneath the aspen and mixedwood overstories. Stand density varied from 1000-1500 overstory trees per hectare.

Prior to photography, a 40 × 40 m grid of ground control stakes were set out across the site with a surveyor's total station (SET5F, Sokkia, Tokyo, Japan), and a highly visible target (1 x 1 m heavy paper sheet with a day-glow orange "X" and a 60 cm high bright blue ID number) placed over the stakes. A geographic positioning system unit (GPS) was placed above each of the corner stakes for 30 minutes to translate the grid coordinates to UTM.

Aerial photos were flown by Timberline Forest Inventory Consultants of Edmonton, Alberta on March 26, 1999 from 9-10 am. There was still snow covering the ground (~30 cm deep), and the aspen were leafless, so spruce beneath the aspen were visible in the photos. The helicopter was fitted with a two-camera, fixed base system with simultaneous

shutter release. Both cameras were 70 mm Hasselblad MK70 with Hasselblad Planar100 lenses (Hasselblad, Fairfield, NJ) of a calibrated focal length of 100.555 mm. The film was 200 ASA Agfa color diapositive (Avichrome 200 PE1, Agfa, Mortsel, Belgium). Camera separation (photobase) was 6.1 mm. Flying altitude was about 120 m above-ground, giving a nominal photo scale of approximately 1:1200. Each photo covered about 60 x 60 m of ground area. Photos were flown in 3 lines, with 9-10 stereo exposures per line. Endlap was about 40% for sequential exposures of the same camera. Sidelap was a little low, at about 5-15%. The overlap between simultaneous exposures of the two cameras (stereo overlap) is ~90%, with the camera boom aligned along the flight line.

Integrated Mapping Technologies Ltd., of Vancouver, B.C. digitized the diapositives and performed the aero triangulation. On each image, ground control points were identified where visible and assigned their UTM coordinates. Pass points were also identified on overlapping regions of each block of adjacent photos. Aero triangulation was performed on the entire set of photos using block bundle adjustment software (PATB-NT, Klein and Ackermann 1998). Stereo models were set using the simultaneous exposures from the fore and aft cameras.

The digital images, stereo models and photo parameters (rotation, translation and scale) were input into Microstation mapping software (Bentley Systems, Inc., Exton, PA). Three-dimensional digital display was supported by additional software, a three-dimensional video card, and shuttered glasses (DiAP, International Systemap Corp., Vancouver, B.C.). Digital mapping was done on a Pentium III 500 MHz PC.

In this digital system, elevations can be measured as well as horizontal coordinates, using stereo parallax and the computer's cursor as the floating dot. Easting, northing, and elevation (*i.e.* x, y, z) coordinates of the top of each tree's crown and the base of the stem were measured. Tree height was calculated by the difference in these elevation coordinates. The lens used to acquire the photos was too wide-angle to make multiple measurements of crown radius around each crown: trees away from the centre of each stereo model leaned away too much, obscuring the distal side of the crown. To estimate

crown radius, two points were chosen on opposite sides of the crown at its widest elevation. A horizontal circle was projected around the crown, passing through these points. The radius of the circle was nudged larger or smaller until the operator was satisfied the circle represented the best fit to the horizontal crown area. This radius was recorded. The output from each tree measurement included the operator's best estimate as to the species (the only confusion was occasionally between aspen and balsam poplar), a visual assessment of the health of the tree (0 for a branchless snag to 5 for a healthy tree), the tree's height, crown radius, and crown apex coordinates. Tree DBH and crown length were estimated from species-specific equations based on tree height, developed from data collected in this site.

The accuracy of the photo measurements was confirmed with a ground survey. At three regions within the site (aspen region, mixedwood region, and spruce region) a number of trembling aspen and white spruce trees were selected, representing the range of height, crown radius and crown diameter that could be found. The location of the tree base was plotted with a surveyor's total station, using the nearest ground control stake as a reference. Tree height and crown length were measured using an automated laser range-finder – clinometer (Impulse). Crown radius was measured in the four cardinal directions using a "moosehorn" device. This device contains a bull's-eye level, a mirror and sighting lenses, and assists in making a ground measurement of the distance from the edge of a tree crown to the stem. To compare these four radii to the single radius estimated with the DiAP system, the geometric average of the four ground-measured radii was calculated.

Estimates of tree height and crown diameter measured with the digital system agreed closely with the same measurements made on the ground (Figure 4A-1). Aspen was the more difficult species to measure, both for height and crown radius, since its gray-brown branches provided little contrast against the snow. This was reflected in a less-precise relationship between photo and ground measurements.

Figure 4A-1. Comparison of stereo digital aerial photographs and ground measurements for A) tree height, and B) crown radius, for △white spruce, and ○ trembling aspen. The straight line indicates the ideal 1:1 relationship.).

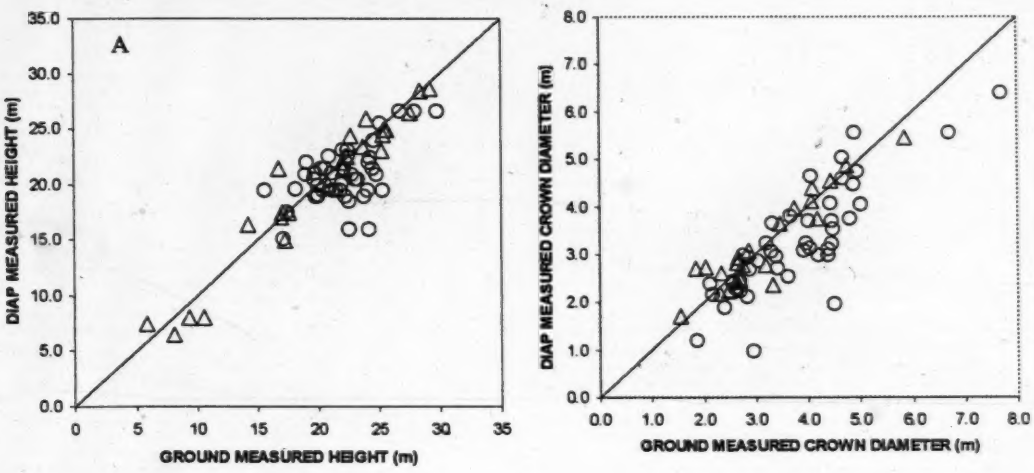

Chapter 5. Modeling the Red:Far-Red Ratio in Boreal Forests

Introduction

Leaves absorb photosynthetically active radiation (PAR: 400-700 nm) strongly but transmit and reflect most of the near-infrared radiation (NIR: 700-1300 nm), creating a spectral signal for underlying vegetation. This signal is detected by the pigment phytochrome, which inter-converts between active (P_r) and inactive (P_{fr}) forms in response to red (600-700 nm) and far-red light (700-800 nm) (Smith 2000). The spectral quality of light with respect to phytochrome is often summarized by the ratio of the quantum flux densities at peak absorption for P_r in the red (660 nm) and for P_{fr} in far-red (730 nm) wavelengths (R:FR) (Monteith 1976).

There is considerable evidence for phytochrome-mediated morphogenesis in forest plants. In an experiment where the R:FR ratio of artificial light was decreased with the overall photosynthetic photon flux density (PPFD) remaining constant, *Pinus radiata* D. Don cuttings showed increased shoot elongation, fascicle development and apical dominance (Morgan et al. 1983). *Pinus sylvestris* L. seedlings with non-shading conspecific neighbours or black screens to the north developed more needles on the south side of their stems presumably because of the reflected R:FR signal from their neighbours (Galinski 1994). When increasing tree density decreased R:FR, a *Populus* L. hybrid developed taller stems while maintaining the same leaf area. This relationship held even when the trees were too small to shade each other (Gilbert et al. 1995). The same response has also been observed for *Pseudotsuga menziesii* (Mirb.) Franco (Ritchie 1997), *Acer pseudoplatamus* and *Betula pendula* (Gilbert et al. 2001). Indeed, Gilbert et al. (1995, 2001) found that the variation in height growth was very closely correlated with the R:FR ratio.

A model for determining the R:FR ratio in stands would be helpful for predicting and managing the growth response of trees and understory vegetation in stands. A number of studies have attempted to model the quality of light in forests using the physical properties of leaves. Endler (1993) outlined an approach for determining light quality in

forest microsites, which lends itself well to hemispherical photo analysis. Combes et al. (2000) presented a voxel-space model that was able to roughly approximate the irradiance of red and far-red light within a single *Juglans regia* L. crown. Norman and Jarvis (1975) developed a model to predict the average horizontal PAR and NIR irradiance in a closed *Picea sitchensis* (Bong.) Carr. forest plantation with a heterogeneous distribution of leaf area. This approximated the change in measured light values in these wavebands with height reasonably well. Norman and Welles (1983) developed a spatially-explicit version of this model which was later shown to approximate the hourly change in PAR transmission at several microsites on the forest floor of a *P. sitchensis* and a *Pinus radiata* plantation (Wang and Jarvis 1990). We developed a spatially-explicit model, MIXLIGHT, which was similar in approach to Norman and Welles (1983), but with more diverse crown shapes and an incoming radiation averaging algorithm, to rapidly predict light levels in stands (Stadt and Lieffers, 2000). We also tested this model's predictions on PAR in a wide range of age classes and forest compositions (Stadt and Lieffers 2000, Pinno et al. 2001, Chapter 4).

The objective of this paper was to develop a model to predict the red:far-red ratio at microsites within a mixed-species, heterogeneous forest canopy. We combined elements of previous work by Norman and Jarvis (1975), Norman and Welles (1983) and Stadt and Lieffers (2000), to develop a model driven by the physical attributes of light penetration and scattering through forest canopies.

Methods

Physical Models

Norman and Welles (1983) and Stadt and Lieffers (2000) developed spatial models for calculating light transmission through a stand of tree crowns represented as three-dimensional geometric objects. These models trace rays from a microsite to sectors of the sky hemisphere and detect intervening crowns by analytical solutions to the equations describing the ray and the ellipsoidal crowns in three-dimensional space. Rays that do not intersect crowns represent the between-crown gap fraction. For the rays that pass through

the crowns, within-crown gap fraction is calculated assuming a random (Poisson) distribution of leaf area within the crown (Equation 5-1).

[5-1] $$p(0;\alpha,Z) = \prod_{i=1}^{n} \exp\left(-G_i[Z]F_iS_i\right)$$

Here, $p(0;\alpha,Z)$ is the gap fraction for the ray extending from the simulation point to the sky in the direction given by the ray's azimuth (α) and zenith (Z), n is the number of crowns intersected by the ray, $G_i(Z)$ is the projection of a unit leaf area in crown i viewed from zenith angle Z (we assumed azimuthal symmetry of leaf inclination and used the ellipsoidal distribution (Campbell 1986) to describe each species mean inclination), F_i is the one-sided leaf, bole, and branch area density (m^2m^{-3}) in the crown, and S_i is the length the ray passes through the tree crown.

Norman and Welles (1983) assumed a uniform angular distribution of light across the sky hemisphere, and sampled the surrounding tree crowns with many rays from each simulation point. Tracing a single ray from the sun to the simulation location incorporated the solar flux. MIXLIGHT (Stadt and Lieffers 2000) used the same approach, but with a greater variety of crown shapes and a ray-weighting method which incorporates direct and diffuse sky radiation into the same incoming angular distribution, $\omega(a, z)$ (Equation 5-2). This reduces computation to one set of rays for any simulation interval, from an instantaneous to a seasonal simulation.

[5-2] $$T = \frac{Q}{Q_i} = \frac{\sum_{a=1}^{na}\sum_{z=1}^{nz} \omega(a,z)\cos Z_z \; p(0;\alpha_a,Z_z)}{\sum_{a=1}^{na}\sum_{z=1}^{nz} \omega(a,z)\cos Z_z}$$

$$\alpha_a = \frac{a}{na}2\pi, \qquad Z_z = \cos^{-1}\left(\frac{z}{nz}\right)$$

Equation 5-2 is a numerical integration over the upper or lower hemisphere, with na azimuth and nz zenith angles; a and z are the azimuth and zenith indexes. Integration is over the cosine of the zenith to sample the sky with sectors of equal solid angle.

This simulation approach is driven by the canopy gap fraction only, and ignores radiation that is reflected or transmitted from foliage surfaces. In the PAR waveband, transmissivity and reflectivity are low, so predictions of a model considering gap fraction only approach measured PAR values fairly closely (Stadt and Lieffers 2000, Pinno et al. 2001, Chapter 4). However, in the NIR waveband, transmissivity and reflectivity may be quite high, so it is essential that these light scattering components be included in the model.

Iterative methods are necessary to model the multiple scattering of light that takes place as light is reflected and transmitted from leaf surfaces. Norman and Jarvis (1975) developed a technique where the canopy is divided into a number of layers, each with a small enough fraction of the total leaf area that the probability of a ray hitting more than one leaf per layer was very low. Each layer had an average hemispherical gap transmission (T, Equation 5-2) based on the angular distribution of the incoming radiation and the layer's projected foliage area, and an average non-gap fraction ($1-T$) consisting of one leaf-thickness surfaces. The downward light flux above each layer was then modeled as the sum of three components: the flux passing through the overlying layer's gaps, the flux transmitted through the overlying layer's leaf surfaces, and the flux reflected from the leaves in the overlying layer. The upward light flux was calculated similarly, based on the gap transmission, transmissive and reflective properties of the underlying layer. The upward and downward light flux calculations above each layer were iterated until the fluxes were stable, to account for the light transmitted and reflected multiple times among the layers.

In this layer model, the angular distribution of radiation changes with depth in the canopy. Norman and Jarvis (1975) included surface reflectivity and transmissivity in calculating these angular distributions, but our own work in forest understory vegetation using this approach (Chapter 3) revealed that the distributions become unreasonably skewed toward wide zenith angles with depth, causing an undesirable decrease in the flux passing through the canopy when reflectivity and transmissivity were added. Since the non-gap fraction in each layer is also quite small (<0.03), we ignored the contribution of

surface transmission and reflection to the angular distribution (though not to the layer's overall flux), which yielded satisfactory results.

Norman and Jarvis' (1975) model was applied in a closed, single-species Sitka spruce plantation with clumping of leaf area into trees and branch whorls. The model calculates the average light flux available at a given depth in the canopy, but does not distinguish among microsites. We call this a stand-level layer model to distinguish it from the microsite-level geometric model.

Norman and Welles (1983), coupled this stand-level layer model with their geometric model to allow semi-spatial modeling of reflected and transmitted light within very heterogeneous stands. Their approach was to calculate the upward and downward-looking hemispherical gap transmission at each microsite using the geometric approach, then place enough leaf area above and below the microsite in the stand-level layer model to obtain the same upward and downward hemispherical gap transmission. This puts the effective leaf area (*sensu* Chen and Cihlar 1995) around the microsite, which allows the stand-level layer model to account for the clumping of leaf area into discrete crowns. The layer model is then run with the appropriate reflectivity and transmissivity information to compute the overall radiation fluxes. The model is semi-spatial, since the reflected and transmitted contributions are calculated with non-spatial methods, but using effective leaf area estimates derived from a spatial model.

We modified Norman and Jarvis' (1975) stand-level layer model to use the same integrated angular radiation distribution as MIXLIGHT. This approach generates the sky hemisphere angular radiation distribution, $\alpha(a, z)$, by tracking the sun across the sky for the daylight hours of the simulation interval. The sky is divided into a matrix of azimuth (a) and zenith (z) segments, 48 azimuths and 40 zeniths in this study. The zenith segments are cosine-weighted so that the zenith intervals are larger at the top of the sky (the zenith) than at the horizon, compensating for the narrowing of the azimuth segments at the top of the sky. An input list of date, time, total and diffuse radiation is read and the direct (total – diffuse) radiation assigned to the segment where the sun would be at that

time. The diffuse radiation is distributed across the sky using the standard overcast sky approximation (Equation 5-3), with 2.23 times as much radiation incident from the zenith as from the horizon (Steven and Unsworth 1980).

[5-3] $$\omega(a,z) = (1 + 1.23\cos Z)$$

If the time interval in the input list is not less than a tenth of the time it would take the sun to transverse one segment from boundary azimuth to azimuth, linear interpolation is used to step the diffuse and direct fractions through the interval. In this fashion, at least ten estimates of diffuse and direct radiation per simulation day are used to build each segment of the angular distribution matrix. The distribution was normalized so that all cell values of the matrix sum to one. We assumed the foliage was symmetrically inclined with respect to the azimuth, so, for the stand-level layer model, we were able to simplify the above-canopy angular distribution by summing over the azimuth, and compute the gap fractions considering only the zenith. This approach also eliminated the need to include separate terms for direct and diffuse light for calculating layer fluxes within the canopy (Norman and Jarvis 1975).

With this integrated angular sky distribution approach, we were able to improve on Norman and Welles' (1983) strategy of using hemispherical transmission to determine how much leaf area to place above and below the microsite. The geometric approach of MIXLIGHT (Stadt and Lieffers 2000, Chapter 2) measures the intersected LAI projected along each sampling ray before calculating gap fraction (Equation 5-1), and weighting this by the corresponding sky segment. The effective canopy LAI can also be calculated with the leaf area encountered in each intersected crown on each ray (Equation 5-4).

[5-4] $$LAI_i = \sum_{z=1}^{nz}\sum_{a=1}^{na}\left\{\omega(a,z)\cos Z\sum_{j}^{n_{ij}} S_{ij}F_{ij}\right\}$$

The product of the crown leaf area density (F) and ray length through each crown's interior (S) is the LAI with respect to the ray direction (a, z). This is corrected to the LAI

viewed from above by the cosine of the zenith. In addition, the leaf area in some crowns will be more important than others in terms of light transmission if they are positioned between the sun's traverse and the simulation microsite. We accordingly weighted the estimates of each species' LAI by the angular radiance of the sky segment where they originated. Rays that did not intersect crowns returned zero LAI. Thus the stand-level estimate of LAI for each canopy species accounts for the relative importance of each tree's leaf area in terms of the region of sky it covers. We calculated the radiation-weighted LAI by this method separately for each canopy species.

Since LAI is often determined from litter fall, sapwood area, or optical methods (Welles and Cohen 1996), we also included a more direct estimate of LAI. We generated estimates of each species' LAI derived from the trees in a 40m × 40m plot surrounding each microsite, by adding the leaf area contained in the crowns (the product of crown volume, V_{ij}, and foliage area density, F_{ij}) of all n_j trees of each species (j) within the plot and dividing by the plot area, A (Equation 5-5). This latter value will approach the LAI calculated by the ray-tracing technique for canopies with a random horizontal distribution of foliage.

$$[5\text{-}5] \quad LAI_j = \frac{\sum_{i}^{n_j} V_{ij} F_{ij}}{A}$$

These two estimates of LAI were used in separate simulations with the stand-level layer model. Inputs to the model were each species' LAI, leaf inclination distribution, leaf reflectivity and transmissivity. Each species' LAI was divided into 20 layers. The height and rank of each single-species layer in the canopy was assigned by the mean height of the species' crown centres.

Leaf Data

Leaf transmissivity and reflectivity are properly measured with an integrating sphere to capture the radiation scattered in all directions (Daughtry et al. 1989). However, estimates of transmissivity can also be obtained for broadleaves with a horizontal sensor,

since a leaf lamina presents an effectively infinite horizontal surface when it covers the sensor. Transmissivity measurements were obtained this way for leaves of each broadleaf species present in the test sites, with the exception of *Acer spicatum*, which was unavailable. Leaves were collected from sites near Edmonton, Alberta (53° 30' N, 113° 30' W) in midsummer. One leaf sample was removed from each of at least five trees, and samples were taken from several sites with different light conditions to capture the range of variation in leaf characteristics. Previous work suggests that leaf transmissivity and reflectivity show little variation (Knapp and Carter 1998), so this should provide adequate sampling.

Quantum flux density measurements were made with a two-channel red/far-red sensor (SKR110 Skye Instruments Ltd., Llandrindod Wells, Powys, UK) with peak response at 660nm and 730nm and ~95% response between 625 and 670nm, and 705 to 750 nm. The sensor channels were attached to a precision microvolt datalogger (CR21X, Campbell Scientific Ltd., Edmonton, Alberta Canada). All measurements were taken in bright sun with no visible haze (<15% diffuse PPFD), and the sensor surface horizontal. For each wavelength, we measured the flux density attributable to dark current (Q_0) with the sensor completely covered with an opaque object, the flux density of full sunlight (Q_I), and the flux density passing through a leaf draped over the sensor with its upper (Q) and lower (Q') surface facing upwards.

[5-6] $$\tau = \frac{Q - Q_0}{Q_I - Q_0} \qquad \tau' = \frac{Q' - Q_0}{Q_I - Q_0}$$

Downward and upward transmissivity (τ, τ') were calculated using Equation 5-6. Since there was little difference between transmission through a leaf from the top down or bottom up, leaf transmissivity was taken to be the average of τ and τ'. The internal cellular structure of the leaf scatters light in a near Lambertian fashion, so that transmissivity and reflectivity tend to be similar (Walter-Shea and Norman 1991, Knapp and Carter 1998). Leaf cuticles can cause specular (mirror-like) reflections and increase reflectivity at the expense of transmissivity, but for the purposes of this study, we assumed that leaf-level reflectivity was equal to transmissivity. In a few cases, far red transmissivity exceeded 0.5. Since this suggests near zero absorption, we assumed $\rho = 1 - \tau$.

Transmissivity and reflectivity data for conifers was obtained from literature values (Table 5-1).

Williams (1991) observed how the reflectivity of three conifers (*Picea abies*, *Pinus strobus* and *Pinus resinosa*) decreased from 0.50-0.55 when viewed at the needle level to 0.20-0.25 at the canopy level. A broadleaf species (*Acer saccharum*) showed a much smaller decrease (0.45 to 0.40). He attributed this to the three-dimensional structure of the branches and crowns, where depth and overlap cause shadowing and trapping of radiation, as well as the absorption of radiation by the woody structure of the trees.

The change in reflectivity and transmissivity when scaling from the needle or leaf to the tree crown is key to the effective functioning of this R:FR model. The assumption of the geometric model is that leaf and wood area are randomly arranged within the crown shells. Leaf or needle clustering into branches and whorls and the tight association between needles and twigs are not explicitly accounted for. The direct-beam transmission technique used to estimate foliage (leaf + wood) area density for the MIXLIGHT model (Stadt and Lieffers 2000) measures the crown-average effective area density. Reflectivity and transmissivity data for this model should then reflect crown-average effective reflectivity and transmissivity rather than leaf-level values as well.

Spruce and fir trees contain a large bole and a tremendous amount of branch wood relative to the leaf area volume of their crown, which effectively blocks transmission of most PAR and NIR within the tree. These conifers also retain dead branch wood for years. Broadleaf tree crowns, on the other hand, have considerably less wood area per unit crown volume and do not retain dead wood for long. Unfortunately, no studies have been done of the change in transmissivity from the needle to the crown or canopy level. We have estimates of wood area density (projected area ÷ crown volume) in deciduous broadleaf species, obtained during leaf-off by optical methods (Stadt and Lieffers 2000), but since conifers retain several years of needles, we can only subjectively estimate the wood area in these species from recently dead trees.

We found four white spruce trees that had died in the past few years and shed their needles, photographed these, and compared them to adjacent live trees of similar size. A typical example is shown in Figure 5-1. In these cases, wood area covered nearly as much of the background as in the live trees' crowns. Based on this evidence, we estimated that non-gap fraction transmission through these crowns is essentially zero.

Before entering transmissivity and reflectivity data into the physical model, we adjusted the values to reflect these scaling issues. Broadleaf transmissivity and reflectivity for both PAR and NIR were reduced by 10%, conifer reflectivities were reduced by 50%, and conifer transmissivities set to zero (Table 5-1).

Field Sites

To test the spatial light quality model and calibrate the empirical model, we used two previously mapped mixed-species boreal forest plots, one near Calling Lake, Alberta (55° 10' N, 113° 10' W) and one near Lac Duparquet, Quebec (48° 30' N, 79° 19' W). Each plot had a tree list consisting of each tree's species, diameter at breast-height (DBH), height, crown length, crown radius, and horizontal (x, y) coordinates. A shape (cylinder, cone, rocket (i.e. a cone perched on a cylinder), paraboloid or ellipsoid), foliage area density, and ellipsoidal leaf inclination distribution were assigned to each crown according to its species (Stadt and Lieffers 2000).

The Quebec site was a 120×100m plot on glacial till parent material with a 12% slope and 110° aspect. The region receives 823mm annual precipitation and has a 0.6° mean annual temperature (Anon. 1982a, b). The plot was 130 years old and was dominated by trembling aspen (*Populus tremuloides* Michx.), with some paper birch (*Betula papyrifera* Marsh.), white spruce (*Picea glauca* (Moench) Voss, black spruce (*Picea mariana* (Mill.) BSP.) and balsam fir (*Abies balsamea* (L.) Mill.) in the overstory. The understory had a significant layer of mountain maple (*Acer spicatum* Lam.) and hazel (*Corylus cornuta* Marsh.) above some microsites. Tree position and DBH had been plotted by a ground survey in 1996. Tree height, crown length, and crown radii had been generated from equations developed in the Lac Duparquet region (Paula Bartemucci pers. comm.).

The Alberta site was a 100×225m plot on glacial till with negligible slope. This region receives 356 mm annual precipitation and has a mean annual temperature of 0.3° (Anon. 1982a, b). The north end of the plot was approximately 80 years old and dominated by trembling aspen while the south end was 140 years old and dominated by white spruce. A heterogeneous region of mixed spruce and aspen with some balsam poplar (*Populus balsamifera* L.) occurred in the centre of the plot. Some selective logging had occurred in this stand in the 1940's creating several narrow gaps. The plot was mapped for tree species, position, height and crown radius from large-scale stereo aerial photographs. Crown length was determined by linear regressions developed from a sample of trees in the site. More details on stem and crown mapping are found in Chapter 4.

Light Measurements

To determine if there were changes in the incoming R:FR ratio in response to cloudiness or solar angle, a red/far-red sensor (SKR110, Skye Instruments Ltd., Llandrindod Wells, Powys, UK) was attached to a datalogger (CR10X, Campbell Scientific Ltd., Edmonton, Alberta) and placed in a 1 ha clearing near the Calling Lake site. A total and diffuse PPFD sensor (Model BF2, Delta-T Devices Ltd., Cambridge, UK) was attached to the same datalogger. Total and diffuse PPFD, and red and far-red flux density were sampled every minute and averaged once per hour from June 27 to July 28, and August 22 to September 15, 2000.

At the Quebec site, within-canopy measurements of red and far-red light were made at 40 microsites, chosen to encompass a wide range of light transmission values. Some were positioned below clumps of mountain maple. The position and aboveground height of each microsite was measured with reference to survey grid stakes within the plot. The same sensor and datalogger were used as for the leaf measurements. On a fully overcast day, a single instantaneous reading was taken outside the plot, then at each microsite, then once again outside the plot.

At the Alberta site, fully overcast days in midsummer were rare. We sampled 11 microsites across the site, from the spruce-dominated area to the aspen region including some gap positions. The horizontal and vertical location of the microsites was also plotted with respect to grid stakes. At each microsite, we set the R:FR sensor and datalogger to sample every minute and average every ten minutes for at least a half-day to smooth out any variability due to sunflecks. When red and far-red measurements were being taken within the site, the outside canopy light sensor measurements were also averaged every 10 minutes.

The R:FR ratio was calculated as the simple ratio of the 660 nm and 730 nm instantaneous sensor readings for the Quebec site. The outside canopy readings were used to adjust the modeled red and far red transmission predictions before calculating the predicted R:FR ratio (*i.e.* predicted R:FR = measured outside R:FR × predicted red transmission to the microsite / predicted far red transmission to the microsite). For the Alberta site, measured and predicted R:FR ratios were calculated similarly, though these time-integrated measurements were obtained by averaging the red and far red flux density measurements first, before taking the ratio.

Results and Discussion

The outside canopy R:FR ratio remained remarkably constant at about 1.2 over the two month measurement period. There was no relationship between outside R:FR and the solar angle or the amount of diffuse radiation relative to the total PPFD (Figure 5-2). The relationship was most variable at sunrise and sunset (solar zenith near 90, diffuse fraction near 1). Gilbert et al. 1995) observed similarly stable relationships regardless of the cloudiness of the atmosphere or time of day. This makes modeling the R:FR ratio a simpler task.

Leaf and crown level effective transmissivity and reflectivity data are compiled in Table 5-1. Leaf level parameters are similar to other values reported in the literature (Knapp and Carter 1998) with low transmissivity and reflectivity in the PAR region but very high

values in the NIR. There were few differences between broadleaf species and conifers at the leaf level in either the red or far red wavelengths. The major differences between broadleaf and conifer species are in the crown level effective transmissivity and reflectivity. We assigned zero transmissivity to the conifers and reduced their reflectivity by 50% while we reduced broadleaf parameters by only 10% after Williams' (1991) observations. As a result, a unit of broadleaf leaf area will reduce R:FR ratio much more than spruce-fir leaf area.

Modeled R:FR ratios using these parameters and either the radiation-weighted effective LAI for each species or the plot-based LAI estimates are plotted against the measured values in Figure 5-3. Modeled R:FR followed measured R:FR ratios closely from 0.25 to 0.93. Good predictions were obtained for both instantaneous measurements under overcast conditions at the Quebec site and for integrated half-day measurements under mainly sunny conditions in Alberta. These modeling approaches very effectively predict the R:FR ratio at the microsite level in heterogeneous canopies.

The small differences between the model using the plot-based LAI calculation and the radiation-weighted effective LAI suggests that the horizontal distribution of leaf area is not important for modeling R:FR. For overcast day measurements this is not surprising since the angular distribution of radiance is evenly weighted across the sky, although with bias toward the zenith. The radiation-weighted approach therefore samples a large circular plot in determining effective LAI. Sunny-day R:FR predictions for microsites along the edge of a narrow gap, which were the situations where we expected to see the radiation-weighted approach function the best were not appreciably more variable. However, under these conditions, the radiation measurements were integrated for several hours, while the sun traversed at least 45 degrees of azimuth. The sun's rays would have passed through numerous crowns during this time, even for the gap-edge microsites, so perhaps it is not surprising the radiation-weighted LAI approached the plot-weighted LAI. Morgan et al. (1985) likewise found no differences in R:FR between two *Pinus radiata* canopies of similar leaf area index, but very different density. Spatial modeling may only be necessary for extreme cases, such as instantaneous R:FR predictions on

sunny days, or for gap edges, patch and strip cuts. It appears that in relatively closed forest canopies, the simpler stand-level layer model is as effective at predicting R:FR as the geometric semi-spatial approach.

Lieffers et al. (1999) compiled evidence that the R:FR ratio beneath stands decreases with decreasing PAR availability more rapidly for broadleaf than coniferous canopies. Clearly, it is the clumping of leaf area and amount of wood area carried within the crown that causes this effect. Broadleaf crowns are relatively large, with lower, dispersed densities of both leaf area and wood area. Petioles and longer leaves disperse the leaf area away from the branches. Dead branches on broadleaf trees self-prune rapidly as well. Their crowns are open structures allowing radiation exchange by both transmission and reflection from the leaf lamina which readily lowers the R:FR ratio in their proximity.

On spruce and fir, the clumping of needles into twigs and the compact, dense crown traps much of the radiation, resulting in a sequential decrease in needle level *vs.* branch *vs.* level canopy level reflectivity (Williams 1991). Transmissivity would be reduced similarly. However, the needles are borne at the outer fringe of the crown, so while outward reflections from shoots are not affected, inward reflections and nearly all radiation transmitted through needles is absorbed by the wood area. The close association between needles and twigs prevent these from being considered statistically independent components for modeling radiation interaction. Indeed, the shoot (needle + twig) is usually considered the random unit for LAI determination by optical methods (Stenberg et al. 1994). The twig absorbs a significant proportion of the radiation that would otherwise be transmitted through the needle cluster. Spruce and fir have a large silhouette area in bole and structural branches relative to their crown silhouette. They are also slow to self-prune their dead branches and twigs. Transmission of both PAR and NIR through spruce and fir, other than penetration through within-crown gaps is consequently extremely low. Since reflection is the sole factor affecting light quality near spruce and fir, the effect of these species on the R:FR ratio is much reduced.

There are considerable ecological implications in this difference in R:FR signaling between broadleaf and spruce/fir species. Phytochrome is present in all green plants, cyanobacteria and some other bacteria, so all plants have some degree of R:FR-regulated morphogenesis (Smith 2001). Gilbert et al. (2001) presented evidence for broadleaf trees that early successional species respond by accelerated height growth more strongly to the R:FR signal than late successional species. They concluded that R:FR sensitivity may be the mechanism for shade avoidance by early successional species, while shade tolerant late successionals do not need this mechanism. However, our results show the R:FR signal developed in spruce/fir dominated forests is much weaker than the signal in broadleaf forests. We expect pine forests would be intermediate, owing to their high degree of needle clumping into shoots, but relatively open crown structure and rapid self-pruning. For shade avoiders, growth in spruce/fir shade creates a problem since there is very little signal to accelerate height growth. These light-demanding species are less likely to reach the upper canopy, and will not persist in these forests for long. Thus, the lack of a strong R:FR signal in these canopies may be part of the reason early successional trees are excluded from these stands.

This study has shown that the R:FR ratio can be readily predicted at the microsite level using local estimates of species' LAI and crown-average transmissivity and reflectivity. A semi-spatial model was no more effective at predicting R:FR than the model based on local LAI, but should be more precise for microsites near larger gaps. The difference between wood area density in spruce and fir vs. broadleaf species was the key factor in this model's function. The weak R:FR signaling from spruce and fir may contribute to the exclusion of early successional species from these forests.

Literature Cited

Campbell, G.S. 1986. Extinction coefficients for radiation in plant canopies calculated using an ellipsoidal inclination angle distribution. Agricultural and Forest Meteorology 36: 317-321.

Daughtry, C.S.T., K.J. Ranson, and L.L. Biehl. 1989. A new technique to measure the spectral properties of conifer needles. Remote Sensing of Environment 27: 81-91.

Endler, J.A. 1993. The color of light in forests and its applications. Ecological Monographs 63: 1-27.

Galinski, W. 1994. Non-random needle orientation in 1-year-old Scots pine (*Pinus sylvestris* L.) seedlings when adjacent to non-shading vegetation. Trees 8: 160-164.

Gilbert, I.R., G.P. Seavers, P.G. Jarvis, and H. Smith. 1995. Photomorphogenesis and canopy dynamics. Phytochrome-mediated proximity perception accounts for the growth dynamics of canopies of *Populus trichocarpa x deltoides* 'Beaupre'. Plant, Cell and Environment 18: 475-497.

Gilbert, I.R., P.G. Jarvis, H. Smith. 2001 Proximity signal and shade avoidance differences between early and late successional trees. Nature 411: 792-795.

Knapp, A.K. and G.A. Carter. 1998. Variability in leaf optical properties among 26 species from a broad range of habitats. American Journal of Botany 85: 940-946.

Leckie, D.G., P.M. Teillet, D.P. Ostaff, and G. Fedosejevs. Sensor band selection for detecting current defoliation caused by the spruce budworm. Remote Sensing of Environment 26: 31-50.

Lieffers, V.J., C.M. Messier, K.J. Stadt, F. Gendron, and P. Comeau. 1999. Predicting and managing light in the understory of boreal forests. Canadian Journal of Forest Research 29: 796-811.

Messier, C. and P. Bellefleur. 1988. Light quantity and quality on the forest floor of pioneer and climax stages in a birch – beech – sugar maple stand. Canadian Journal of Forest Research 18: 615-622.

Monteith, J.L. 1976. Spectral distribution of light in leaves and foliage. *In* Smith, H. (Ed.) Light and Plant Development. Butterworth, London, UK pp. 447-460.

Morgan, D.C., D.A. Rook, I.J. Warrington and H.L. Turnbull. 1983. Growth and development of Pinus radiata D. Don: the effect of light quality. Plant, Cell and Environment 6: 691-701.

Ritchie, G.A. 1997. Evidence for red:far red signaling and photomorphogenic growth response in Douglas-fir (*Pseudotsuga menziesii*) seedlings. Tree Physiology 17: 161-168.

Smith, H. 2000. Phytochromes and light signal perception by plants – an emerging synthesis. Nature 407: 585-591.

Stenberg, P., S. Linder, H. Smolander, and J. Flower-Ellis. 1994. Performance of the LAI-2000 plant canopy analyzer in estimating leaf area index of some Scots pine stands. Tree Physiology 14: 981-995.

Welles, J.M and S. Cohen. 1996. Canopy structure measurement by gap fraction analysis using commercial instrumentation. Journal of Experimental Botany 47: 1335-1342.

Williams, D.L. 1991. A comparison of spectral reflectance properties at the needle, branch, and canopy level for selected conifer species. Remote Sensing of Environment 35: 79-93.

Table 5-1. Leaf level and crown level reflectivity (ρ) and transmissivity (τ) data for boreal forest species at red (660 nm) and far red (730 nm) wavelengths.

Species	Leaf level parameters				Data source	Crown level parameters**			
	660nm		730nm			660nm		730nm	
	ρ	τ	ρ	τ		ρ	τ	ρ	τ
Aspen	0.05	0.05*	0.47	0.47*	This study	0.05	0.05	0.42	0.42
Balsam poplar	0.05	0.05*	0.44	0.44*	This study	0.05	0.05	0.40	0.40
Paper birch	0.05	0.05*	0.49	0.51*	This study	0.05	0.05	0.44	0.46
Hazel	0.04	0.04*	0.42	0.58*	This study	0.04	0.04	0.38	0.52
Mountain maple	0.05	0.05	0.50	0.50	Estimate	0.05	0.05	0.45	0.45
White spruce	0.06	0.04	0.45	0.40	Daughtry et al. 1989 (based on black spruce measurements)	0.03	0	0.23	0
Black Spruce	0.06*	0.04*	0.45*	0.40*	Daughtry et al. 1989	0.03	0	0.23	0
Balsam fir	0.12*	0.12	0.55*	0.45	Leckie et al. 1988	0.06	0	0.28	0

*Quantity measured. Other leaf-level parameters are estimated assuming $\rho=\tau$, or $\rho=1-\tau$ (see Methods).

**Adjusted from leaf level measurements using proportions derived from Williams (1991).

Figure 5-1. A recently dead white spruce crown that has shed its needles (left) next to two healthy crowns (right).

Figure 5-2. Outside canopy R:FR ratio vs. (A) solar zenith angle and (B) the diffuse fraction of total PPFD

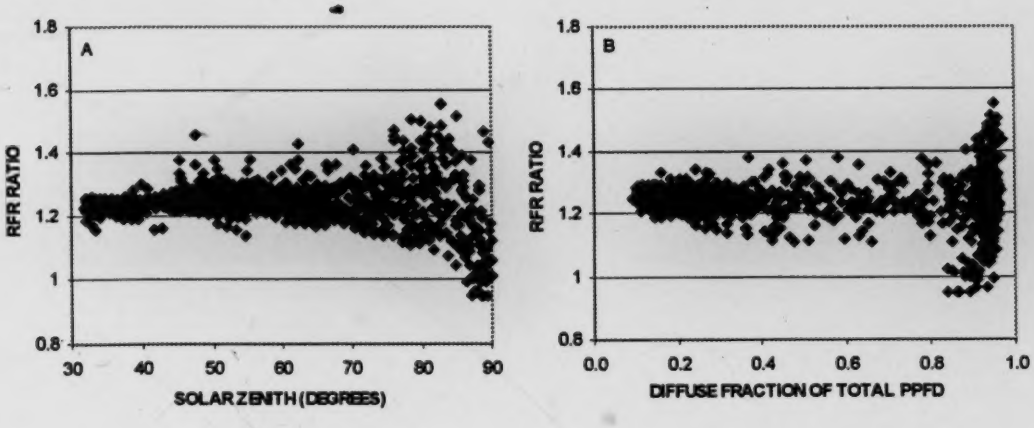

Figure 5-3. Predicted vs. measured R:FR ratio (◇) at 40 microsites in an aspen – black spruce – balsam fir – mountain maple stand on Lac Duparquet, Quebec (instantaneous measurements and predictions under overcast conditions), (△) at 11 microsites in an aspen – white spruce transition site near Calling Lake, Alberta (integrated measurements and predictions over half a mainly sunny day). The solid line shows the ideal (1:1) relationship. (A) Predictions using the radiation-weighted, effective LAI for each species determined while ray-tracing for gap-fraction. (B) Predictions using the LAI for each species contained in a 40 × 40 m plot surrounding the microsite.

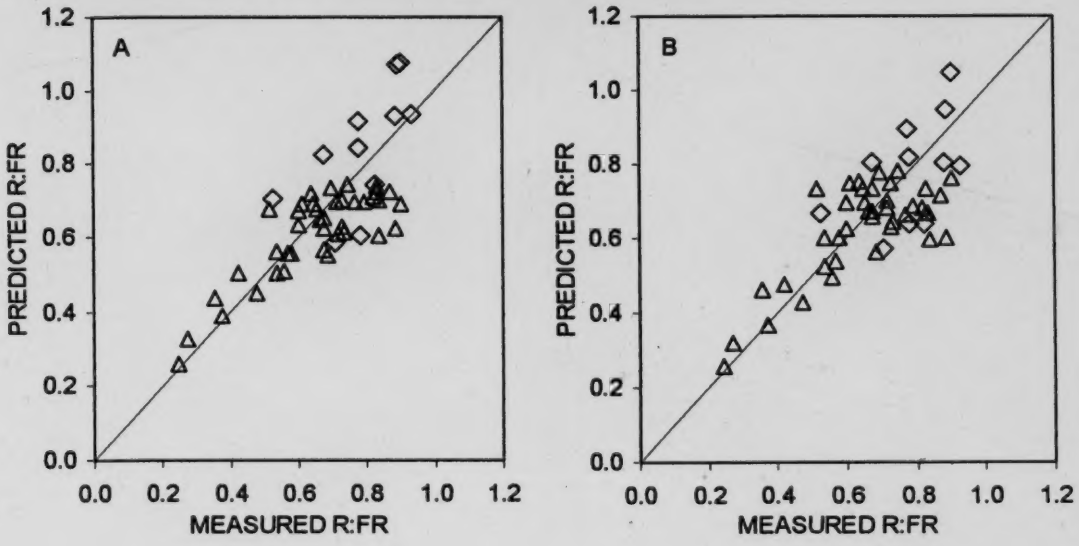

Chapter 6. General Discussion

The overall objective of this dissertation was to develop and evaluate light resource models for applications in modeling mixed-species boreal forest dynamics. A ray tracing software for determining photosynthetically-active radiation (PAR) transmission through overstory canopy gaps was developed. This software, MIXLIGHT, functions at either the stand or microsite level and was described, calibrated and tested (first at the stand level only) in Chapter 2. In Chapter 3, a series of models, from theoretical to empirical, was evaluated for simulating the additional effect of forest understory vegetation on PAR transmission. In Chapter 4, the microsite level predictions of the geometric crown overstory model coupled with a simple empirical cover-based understory light model were tested in two large heterogeneous sites, one in eastern Canada and one in the west. This chapter also examined the relationship between sapling height growth and seasonal light transmission. Lastly, in Chapter 5, a semi-spatial approach for determining the shift in light quality, specifically in the red:far red (R:FR) ratio, at microsites with different local species compositions and leaf area was tested in the same eastern and western Canadian sites used in Chapter 4.

The ray tracing approach for canopy gap fraction used in MIXLIGHT was quite effective, both for instantaneous PAR measurements on the stand level (Chapter 2), and for daily and seasonal PAR measurements at the microsite level (Chapter 4). The stand level simulation represented the canopy as a single volume with randomly distributed leaf area, while the microsite level approach represented individual crown as regular geometric shapes (cylinders, cones, paraboloids, ellipsoids, or combinations of these) containing species-specific leaf area density, randomly distributed within each crown. There was no apparent bias in predicting PAR on either scale. However, the understory model suggested that ray-tracing without considering light scattered by leaf surfaces would result in underestimation of the overall PAR transmitted by the canopy (Chapter 3). Why the gap fraction approach underestimates understory canopy transmission, but not the overstory or combined overstory and understory canopy transmission, is not entirely clear. It may be that the direct-beam transmission inversion method used for determining

mature trees' leaf area density (LAD) captured enough of the scattering effect, since scattering in the direction of the sun's rays would increase the direct-beam measurement. This would underestimate each species' LAD, and perhaps this was enough to compensate for scattering when the model was run in closed forest conditions. Understory leaf area index (LAI), on the other hand, was more sampled by a point-frame and leaf inclination measurements which would not have the same bias as the transmission technique. Any additional light provided by scattering would cause the measured light transmission to be higher than the prediction based on this unbiased understory LAI.

The R:FR modeling approach tested in Chapter 5 also illustrates scaling and estimation issues. When the transmissivity and reflectivity of single broadleaf and coniferous leaves were compared there were few differences. However, species differences in leaf clumping, leaf association with their twigs, and structural branch and bole density meant that transmissivity and reflectivity at the crown scale were very different. When appropriate crown level values were used for each species, the semi-spatial R:FR model functioned very well.

Considerable research effort has been (and continues to be) expended on these scaling issues. The high degree of organization of conifer needles, twigs, whorls and crowns is of particular interest (Norman and Jarvis 1975, Oker-Blom et al. 1991, Chen and Cihlar 1995, Kucharik 1999, Smolander and Stenberg 2001) as this is important for estimating true LAI from canopy transmission measurements and critical for calculating light levels for leaf level processes such as photosynthesis.

There is considerable interest in developing physiological, or functional-structural models (e.g. Perttunen et al. 1996, Grote and Erhard 1999) to grow trees according to linked physiological and structural principles. These models typically function on hourly time steps. Photosynthetic irradiance (PI) or photon flux density (PPFD) is simulated for each hour under measured atmospheric conditions. The studies in this dissertation have focused primarily on simulating light conditions over the long-term, under conditions

where spatial and temporal variation are low (overcast days), or for stand-level spatial average conditions. I did not test any models under hourly conditions, but this would be an appropriate test and application for MIXLIGHT as well. To do this, more flexible crown shapes such as quarter ellipsoids (Koop and Sterck 1994, Cescatti 1997) may be more appropriate. These would also allow for more realistic crown to crown interactions, such as the development of crown shyness. Additionally, penumbra, the "gray" shade cast when the sun is partially obscured by foliage, becomes an issue for short-term simulations. Penumbra has been dealt with by describing the light components (direct, diffuse, penumbra) beneath the canopy with statistical distributions (Ross et al. 1998). The link between real tree structures and the distribution parameters in this approach has yet to be developed.

The problem with building models which accurately scale leaf level processes to the tree and stand is their complexity for calibration and testing, and a penalty in terms of either processing speed or computer power. This is the tension between these models and those for simulating stand and landscape level forest dynamics over long periods. The adage that you can have it fast and inexpensive, inexpensive and flexible, or fast and flexible, but not all three of these, applies here.

One of the immediate applications of this work will be to form part of a process-driven forest dynamics model for the Canadian boreal forest. This scheme has been developed after the SORTIE model, which has been applied in New England hardwood forests (Pacala et al. 1993) and British Columbia interior cedar-hemlock forests (Wright et al. 1998). In this model, full descriptions are maintained of every tree in terms of its species, location, stem and crown size. The time step is 1-5 years. Starting with an existing or typical spatially-mapped forest structure, each time step has a spatially-explicit regeneration event (seed dispersal, vegetative suckering, or planting of nursery stock), a growth event where the trees grow according to the available light resource and possibly some other resource or competition index, and a mortality event which kills individual trees by a stochastic process related to their current growth rate. The light models and

supporting parameters (e.g. mature tree species' LAD) developed here are intended for use in the light resource modeling component of this larger process model.

The MIXLIGHT model has also been an effective tool for evaluating the competition status, the "free-to-grow" standards, for regenerating white spruce in juvenile stands (Lieffers et al 2002). These light models have other promising applications: designing partial cuts for control of competing vegetation (Lieffers and Stadt 1994), identifying hardwood stands suitable for under-planting spruce (Stewart et al. 2000), as well as numerous other forest management and research questions related to forest light conditions. A harvest simulator is also provided to aid forest managers in manipulating stand structures to achieve target light levels. Our informational brochure, "An Overview of the MIXLIGHT Forest Light Simulator", outlines some of the features of the MIXLIGHT software, and is attached as Appendix 6A.

Literature Cited

Cescatti, A. 1997. Modelling the radiative transfer in discontinuous canopies of asymmetric crowns. I. Model structure and algorithms. Ecological Modelling 101: 263-274.

Chen, J.M. and J. Cihlar. 1995. Quantifying the effect of canopy architecture on optical measurements of leaf area index using two gap size analysis methods. IEEE Transactions on Geoscience and Remote Sensing 33: 777-787.

Grote, R. and M. Erhard. 1999. Simulation of tree and stand development under different environmental conditions with a physiologically based model. Forest Ecology and Mangement 120: 59-76.

Koop, H. and F.J. Sterck. 1994. Light penetration through structurally complex forest canopies: an example of a lowland tropical rainforest. Forest Ecology and Management 69: 111-122.

Kucharik, C.J., J.M. Norman, S.T. Gower. 1999. Characterization of radiation regimes in nonrandom forest canopies: theory, measurements, and a simplified modeling approach. Tree Physiology 19: 695-706.

Lieffers, V.J., B.D. Pinno, and K.J. Stadt. 2002. Light dynamics and free-to-grow standards in aspen-dominated mixedwood forests. Forestry Chronicle 78: 137-145.

Lieffers, V.J. and K.J. Stadt. 1994. Growth of understory Picea glauca, Calamagrostis canadensis, and Epilobium angustifolium in relation to understory light transmission. Canadian Journal of Forest Research 24: 1193-1198.

Norman, J.M. and P.G. Jarvis. 1975. Photosynthesis in Sitka spruce (Picea sitchensis (Bong.) Carr.) V. Radiation penetration theory and a test case. Journal of Applied Ecology 12: 839-878.

Oker-Blom, P., M.R. Kaufmann, and M.G. Ryan. 1991. Performance of a canopy light interception model for conifer shoots, trees and stands. Tree Physiology 9: 227-243.

Pacala, S.W., C.D. Canham and J.A. Silander. 1993. Forest models defined by field measurements: I. The design of a northeastern forest simulator. Canadian Journal of Forest Research 23: 1980-1988.

Perttunen, J., R. Sievanen, E. Nikinmaa, H. Salminen, H. Saarenmaa, J. Varkeva. 1996. LIGNUM: a tree model based on simple structural units. Annals of Botany 77: 87-98.

Ross, J., M. Sulev and P. Saarelaid. 1998. Statstical treatment of the PAR variability and its application to willow coppice. Agricultural and Forest Meteorology 91: 1-21.

Smolander, S., and P. Stenberg. 2001. A method for estimating light interception by a conifer shoot. Tree Physiology 21: 797-803.

Stewart, J.D., S.M. Landhäusser, K.J. Stadt, and V.J. Lieffers. 2000. Regeneration of white spruce under aspen canopies: seeding, planting and site preparation. Western Journal of Applied Forestry 15: 177-182.

Wright. E.F., K.D. Coates, C.D. Canham, and P. Bartemucci. 1998. Species variability in growth response to light across a climatic in northwestern British Columbia. Canadian Journal of Forest Research 28: 871-886.

Appendix 6A:An Overview of the MIXLIGHT Forest Light Simulator

Developed by Ken Stadt and Vic Lieffers, Department of Renewable Resources, University of Alberta
http://www.rr.ualberta.ca/research/EFM/Mixlight.htm, kstadt@ualberta.ca

What is MIXLIGHT?

- Software for simulating light levels in forest stands.
- 3-dimensional spatial model with capacity to handle non-spatial data.
- Simulates light to any position within a stand of any species composition (currently calibrated for aspen, balsam poplar, birch, white spruce, lodgepole pine, balsam fir).

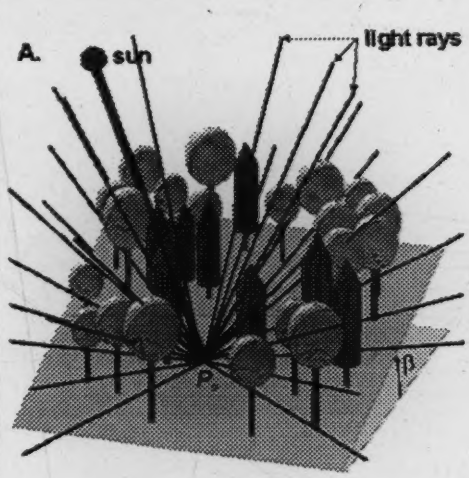

Why simulate light levels in the forest?

- In understory environments, light is the often the limiting resource for tree growth.
- Identify stands suitable for underplanting spruce.
- Planning partial cuts to achieve target light levels which promote spruce growth while suppressing competitors.
- Our work suggests that white spruce height growth reaches a maximum at 30% of above-canopy light (see adjacent graph). Stands or partial cuts with light levels of 20-40% should show adequate spruce height growth with few competition problems.

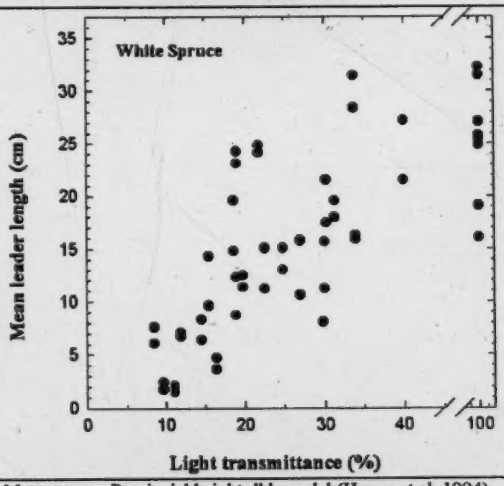

What data does MIXLIGHT require?

Tree list (required):

- Plot code - allows sequential simulation of more than one plot
- Species - any text as long as it matches the species identifier in the species curves file.
- Crown class - Dominant (D), Codominant (C), Intermediate (I), Supressed (S) to place the tree in the appropriate canopy layer
- DBH - stem diameter; "breast height" is adjustable from zero to any height

Tree list (estimable):

- Tree height
- Crown base height (or crown length or live-crown ratio)

Mature trees: Provincial height-dbh model (Huang et al. 1994)
Ht = 1.3+a*(1-exp(-b*dbh))^c (Richards function; y0=1.3)

species	a	b	c
aspen	25.6614	0.06834	1.1394
birch	27.9727	0.03522	0.8695
balsam/alpine fir	24.7532	0.06615	1.5695
douglas fir	21.3299	0.0609	1.5973
tamarack	26.3266	0.05375	1.4026
balsam poplar	25.57	0.0505	0.9865
jack pine	31.4263	0.03888	1.1279
lodgepole pine	29.0075	0.04859	1.1782
black spruce	24.5751	0.05432	1.2243
engelmann spruce	36.3184	0.02604	1.093
white spruce	32.1261	0.04633	1.3032

Juvenile aspen: (Pinno 2000)
Ht = 0.3 + a*(1-exp(-b*d30))^c (Richards function; y0=0.3)
d30 is stem diameter (dbh) at 30cm above ground

species	a	b	c
aspen	14.4686	0.1891	1.5928

- Crown radius

Tree list data (continued):

- Leaf area density or leaf area per tree - Mature trees appear to have constant leaf area density - as the crowns get bigger they have more leaf area but don't have any more leaves per cubic meter of crown volume. In juvenile aspen, leaf are density decreases as the trees get larger - Brad Pinno has modeled this where leaf area per tree increases with stem diameter, but the increase in crown length and radius cause crown volume to increase more rapidly.
- Leaf Inclination - horizontal leaves block light more effectively than vertical leaves. Experimentally determined ratios of vertical/horizontal leaves are given (default is 1).
- Position - (x, y) or (easting, northing) coordinates from mapped stands. Trees can also be put in rows, placed randomly or placed randomly with restrictions on the amount of crown overlap allowed.

Plot and Sky attributes (affect the sun angle):

- Location (approximate latitude and longitude)
- Start/end dates of growing season
- Slope and aspect
- Plot size and orientation (only important if the trees are stem-mapped or strip cuts imposed in a particular direction).
- Diffuse light fraction and distribution across the sky – our data suggest ~50% of the light comes from the sun, 50% from sky illumination (scattered sunlight). The upper part of the sky hemisphere contributes more light than near the horizon. We suggest a ratio of 2.23 times more from the vertical part of the sky vs. the horizon.

Other Features of MIXLIGHT

- Harvesting functions – currently strip cuts, species and diameter limits available.
- Reset Default Button – resets the program to standard simulation format.
- Help – explains the functions of MIXLIGHT features, otherwise email us.

Mature trees Crown length - dbh equations (Stadt, unpubl.)
CL = y0 + a*dbh (Polynomial)

species	y0	a
aspen	3.12	0.1161
birch	1.07	0.3277
balsam fir	1.67	0.4389
tamarack	3.87	0.1339
balsam poplar	2.91	0.1816
jack pine	1.15	0.3070
lodgepole pine	0.76	0.2371
white spruce	3.12	0.3410

Juvenile aspen Crown length (Pinno 2000)
CL=a*d_{30}^b (Power function), d_{30} is stem diameter at 30cm

species	a	b
aspen (codominant)	0.9936	0.6846
aspen (intermediate)	0.8346	0.6845

Mature trees Crown radius - dbh equations (Stadt, unpubl.)
CR=a*dbh (Polynomial)

species	a
aspen	0.087265
birch	0.083222
balsam fir	0.069843
tamarack	0.06589
balsam poplar	0.085283
lodgepole pine	0.069152
black spruce	0.073279
white spruce	0.066413

Juvenile aspen Crown radius (Pinno 2000)
CR = a*d_{30}^b (Power function), d_{30} is stem diameter at 30cm

species	a	b
aspen (codominant)	0.3122	0.5958
aspen (intermediate)	0.3027	0.5692

Mature trees Leaf area density and Leaf inclination ratio (Stadt and Lieffers 2000); LAD=y01; LIR=y02 (constant)

species	y01	y02
balsam fir	1.98	1.00
white spruce	1.88	0.10
lodgepole pine	1.39	1.00
aspen	0.44	0.82
birch	0.80	1.00
balsam poplar	0.30	1.00

Juvenile aspen Leaf area per tree and leaf inclination (Pinno 2000)
LA = a*d_{30}^b (Power function); LIR = 0.82 (constants), d_{30} is stem diameter at 30cm

species	a	b
aspen (codominant)	0.137	1.9535
aspen (intermediate)	0.1295	1.6773

Further Information

Pinno, B. 2000. MSc. Thesis. Crown Characteristics and Understory Light in Young Aspen Stands. University of Alberta, Edmonton, Alberta, 85pp.

Huang, S., S.J. Titus, T.W. Lakusta, R.J. Held. 1994. Ecologically-based individual tree height-diameter models for major Alberta tree species. Alberta Environmental Protection Land and Forest Services Forest Management Division, Edmonton, Alberta, 27pp.

Stadt, K.J. and V.J. Lieffers. 2000. MIXLIGHT: A flexible light transmission model for mixed-species forest stands. Agricultural and Forest Meteorology 102: 235-252.